OULU 2015
C 533

ACTA UNIVERSITATIS OULUENSIS

Tiina Leppäjärvi

PERVAPORATION OF ALCOHOL/WATER MIXTURES USING ULTRA-THIN ZEOLITE MEMBRANES

MEMBRANE PERFORMANCE AND MODELING

UNIVERSITY OF OULU GRADUATE SCHOOL;
UNIVERSITY OF OULU,
FACULTY OF TECHNOLOGY

ACTA UNIVERSITATIS OULUENSIS
C Technica 533

TIINA LEPPÄJÄRVI

PERVAPORATION OF ALCOHOL/ WATER MIXTURES USING ULTRA-THIN ZEOLITE MEMBRANES

Membrane performance and modeling

Academic dissertation to be presented with the assent of the Doctoral Training Committee of Technology and Natural Sciences of the University of Oulu for public defence in Kuusamonsali (YB210), Linnanmaa, on 26 June 2015, at 12 noon

UNIVERSITY OF OULU, OULU 2015

Acta Univ. Oul. C 533, 2015

Supervised by
Professor Juha Tanskanen
Doctor Jani Kangas
Doctor Ilkka Malinen

Reviewed by
Professor Joan Llorens
Professor Mika Mänttäri

Opponent
Associate Professor Marc Pera-Titus

ISBN 978-952-62-0841-1 (Paperback)
ISBN 978-952-62-0842-8 (PDF)

ISSN 0355-3213 (Printed)
ISSN 1796-2226 (Online)

Cover Design
Raimo Ahonen

JUVENES PRINT
TAMPERE 2015

Leppäjärvi, Tiina, Pervaporation of alcohol/water mixtures using ultra-thin zeolite membranes. Membrane performance and modeling
University of Oulu Graduate School; University of Oulu, Faculty of Technology
Acta Univ. Oul. C 533, 2015
University of Oulu, P.O. Box 8000, FI-90014 University of Oulu, Finland

Abstract

The production of liquid transportation fuels such as bioethanol and more recently also biobutanol from renewable resources has received considerable attention. In the production of bio-based alcohols, the separation steps are expensive as the mixtures to be separated are dilute. As an energy-efficient separation technology, pervaporation is considered to be a potential process in biofuel purification.

One of the main constraints in the commercialization of pervaporation has been low membrane fluxes, and the consequent high costs due to the high membrane area needed. In order to obtain high fluxes, the membranes should be as thin as possible. In this thesis, the performance of ultra-thin zeolite membranes in pervaporation was investigated. Binary ethanol/water and *n*-butanol/water mixtures were studied using both hydrophobic and hydrophilic zeolite membranes for alcohol concentration, as well as dehydration.

The development of pervaporation membranes and processes has been mainly empirical. Process modeling, however, is an indispensable tool in process design. In this work, the pervaporation performance of the studied membranes was evaluated on the basis of experimental results in combination with mathematical modeling. Due to the low film thickness of the studied membranes, the fluxes were generally higher than reported earlier. Nevertheless, the evaluation in this work showed that the pervaporation performance of the ultra-thin membranes decreased due to flux limitation by membrane support.

In this work, pervaporation was modeled by applying both a semi-empirical and a detailed Maxwell-Stefan based mass transfer model. The latter model considers explicitly both adsorption and diffusion, i.e. the phenomena involved in separation by pervaporation. The description of the support behavior was included in the models. Maxwell-Stefan formalism was applied in unary pervaporation for the determination of diffusivities in zeolite membranes. The models performed well within the range of experimental data.

Additionally, a practical modeling approach was developed in this work to predict the temperature dependency of adsorption on zeolites. The developed approach can be utilized, e.g., in pervaporation modeling. Thus, this thesis provides knowledge of using ultra-thin zeolite membranes in the pervaporation of alcohol/water mixtures, and offers tools for pervaporation modeling.

Keywords: adsorption, Maxwell-Stefan, membrane separation, pervaporation, vapor pressure, zeolite membranes

Leppäjärvi, Tiina, Alkoholi/vesiseosten erotus pervaporaatiolla ultraohuita zeoliittimembraaneja käyttäen. Membraanien suorituskyky ja mallinnus
Oulun yliopiston tutkijakoulu; Oulun yliopisto, Teknillinen tiedekunta
Acta Univ. Oul. C 533, 2015
Oulun yliopisto, PL 8000, 90014 Oulun yliopisto

Tiivistelmä

Kiinnostus uusiutuvista raaka-aineista valmistettavia liikennepolttoaineita, kuten bioetanolia ja -butanolia, kohtaan lisääntyy koko ajan. Biopohjaisten alkoholien tuotannossa etenkin erotusvaiheet ovat kalliita, koska erotettavat liuokset ovat laimeita. Pervaporaatio on energiatehokas kalvoerotusmenetelmä ja sen vuoksi potentiaalinen osaprosessi biopolttoaineiden tuotantoon.

Pervaporaation kaupallistamisen merkittävimpiä rajoitteita ovat olleet alhaiset ainevuot, jotka johtavat suureen kalvopinta-alan tarpeeseen ja näin ollen korkeisiin kustannuksiin. Korkean ainevuon saavuttamiseksi kalvojen tulisi olla mahdollisimman ohuita. Tässä väitöstyössä tutkittiin hyvin ohuiden zeoliittimembraanien suorituskykyä pervaporaatiossa. Kohteena olivat binääriset etanoli/vesi- ja *n*-butanoli/vesiseokset, joista väkevöitiin alkoholeja tai poistettiin vettä hydrofobisia ja hydrofiilisiä zeoliittimembraaneja käyttäen.

Pervaporaatiossa käytettävien kalvojen ja pervaporaatiota hyödyntävien prosessien kehitystyö on ollut pääasiassa kokeellista. Prosessimallinnus on kuitenkin tärkeä työkalu prosessisuunnittelussa. Tässä työssä membraanien suorituskykyä pervaporaatiossa arvioitiin sekä kokeellisesti että mallinnuksen keinoin. Käytettyjen kalvojen ohuuden ansiosta tässä työssä saavutetut ainevuot olivat yleisesti ottaen korkeampia kuin aiemmin raportoiduilla membraaneilla. Ohuilla kalvoilla tukimateriaalin aiheuttama aineensiirron vastus oli kuitenkin merkittävä, alentaen membraanien suorituskykyä.

Tässä työssä pervaporaatiota mallinnettiin käyttäen sekä puoliempiiristä että yksityiskohtaisempaa Maxwell-Stefan -pohjaista mallia. Jälkimmäisessä mallissa adsorptio ja diffuusio, eli ilmiöt joihin erotus pervaporaatiossa perustuu, otetaan eksplisiittisesti huomioon. Myös tukimateriaalin vaikutukset huomioitiin käytetyissä malleissa. Maxwell-Stefan -mallinnusta käytettiin puhtaiden komponenttien pervaporaatiossa zeoliittimembraanin diffuusiokertoimien määrittämiseksi. Käytettyjen mallien suorituskyky kokeellisella alueella oli hyvä.

Tässä työssä kehitettiin lisäksi helppokäyttöinen menetelmä aineiden adsorptiokäyttäytymisen ennustamiseen zeoliiteissa eri lämpötiloissa. Kehitettyä menetelmää voidaan hyödyntää esimerkiksi pervaporaation mallinnuksessa. Kokonaisuudessaan väitöstyöstä saadaan tietoa ultraohuiden membraanien käytöstä pervaporaatiossa sekä työkaluja pervaporaation mallinnukseen.

Asiasanat: adsorptio, höyrynpaine, kalvoerotus, Maxwell-Stefan, pervaporaatio, zeoliittimembraanit

Dedicated to Liia, Venla and Luukas

Acknowledgements

This study was carried out in the Chemical Process Engineering research group of Faculty of Technology at the University of Oulu during 2007–2015.

I am grateful to all the people who have supported me in one way or another during this work and without whom this work would not have been possible. First of all, I would like to express my gratitude to my supervisor Prof. Juha Tanskanen for his encouragement, and for making the research work possible. In addition, I would like to thank my advisor Dr. Ilkka Malinen who came to the project in a critical phase, and contributed enormously to it's progress. I am also grateful to my advisor Dr. Jani Kangas for all the valuable advice, which was crucial for the completion of this thesis. I wish to express my sincere thanks also to the project partners at the Luleå University of Technology, especially to Prof. Jonas Hedlund for welcoming me to visit their research group, and the co-authors of my publications Dr. Danil Korelskiy, Dr. Han Zhou and Dr. Mattias Grahn. Further, I would like to thank Mr. Jorma Penttinen for all the help in the laboratory.

I would like to express my sincere gratitude to Prof. Joan Llorens from the University of Barcelona and Prof. Mika Mänttäri from the Lappeenranta University of Technology for reviewing the manuscript of this thesis. Sue Pearson and Mike Jones from Pelc Southbank Languages are acknowledged for the linguistic corrections of this thesis, and several papers included in this thesis.

I am very grateful to the Graduate School in Chemical Engineering (GSCE) for funding the majority of this work, including a conference trip to the Netherlands, the research exchange in Luleå, and attendance of various post-graduate courses, all of which have provided me valuable knowledge and experience. The GSCE also gave me the opportunity to meet fellow researchers in the broad field of chemical engineering. The financial support for the finalization of the thesis from Emil Aaltonen Foundation and University of Oulu Graduate School (UniOGS) are also appreciated.

My colleagues in Chemical Process Engineering research group deserve special thanks: I have truly enjoyed working with you! Thank you for all the refreshing discussions, research related and otherwise! I want to thank all my other friends, I am very lucky to be surrounded by the best people in the world!

Finally, I want to thank my parents Aila and Urho, and my sister Jenni and her kids, for their constant and unwavering support, both professionally and personally. Above all, I want to thank my husband Janne for his patience, support, love, encouragement and understanding - as promised, for better or for worse. The

biggest hugs to our kids: Liia, Venla and Luukas, who came along during the thesis project and made me the happiest person in the world. Your laughter is my driving force! Kiitos!

Oulu, May 2015 Tiina Leppäjärvi

List of symbols and abbreviations

A	Specific area of adsorbent (m^2)/effective membrane area (m^2)
b	Adsorption equilibrium parameter (Pa^{-1})
B	Permeability (m^2)
c	BET adsorption parameter
C	Number of data points
d	Diameter (m)
D	Diffusivity ($m^2\ s^{-1}$)
E	Energy ($J\ mol^{-1}$)
f	Fugacity (Pa)/function
H	Enthalpy ($J\ mol^{-1}$)
J	Flux ($kg\ m^{-2}\ h^{-1}$ or $mol\ m^{-2}\ s^{-1}$)
K	Knudsen structural parameter (m)
l	Thickness (m)
n	Dimensionless adsorption parameter
m	Sample amount (kg)
M	Molar mass ($g\ mol^{-1}$)
P	Pressure (Pa)
R	Gas constant ($8.314\ J\ mol^{-1}\ K^{-1}$)
t	Sampling time (h)
T	Temperature (K)
w	Weight fraction
x	Mole fraction in adsorbed or liquid phase
y	Mole fraction in gas phase
q	Adsorption loading ($mol\ kg^{-1}$)

Greek symbols

γ	Activity coefficient
Γ	Thermodynamic factor
ε	Adsorption potential
θ	Fractional surface coverage
λ	Mean free path (m)
μ	Chemical potential
π	Spreading pressure (Pa)
ρ	Density ($kg\ m^{-3}$)

Subscripts

ads	Adsorption
dif	Diffusion
f	Feed
F	Freundlich
H	Henry's law
i,j	Components
Kn	Knudsen
perm	Permeate
pore	Pore
s	Support layer
vis	Viscous
tot	Total
SL1	Support layer 1
SL2	Support layer 2
Z	Zeolite film

Superscripts

0	Reference state
eff	Effective
exp	Experimental
f	Feed side
mod	Model
p	Permeate side
pred	Predicted
sat	Saturated

Abbreviations

ABE	Acetone Butanol Ethanol
BET	Brunauer-Emmet-Teller
BuOH	Butanol
EtOH	Ethanol
FAU	Faujasite (zeolite framework type)
GC	Gas Chromatography
IAST	Ideal Adsorbed Solution Theory
IUPAC	International Union of Pure and Applied Chemistry
LLE	Liquid-Liquid Equilibrium
LTA	Linde Type A (zeolite framework type)
MD	Molecular Dynamics
MFI	Mordenite Framework Inverted (zeolite framework type)
MS	Maxwell-Stefan
NRTL	Non-Random Two Liquid
NMR	Nuclear Magnetic Resonance
PDMS	Poly(dimethyl siloxane)
PFG	Pulsed Field Gradient
PSI	Pervaporation Separation Index
PVA	Poly(vinyl alcohol)
QENS	Quasi-Elastic Neutron Scattering
RAST	Real Adsorbed Solution Theory
SEM	Scanning Electron Microscopy
SSR	Sum of Squared Residuals
XRD	X-ray Diffraction
ZSM-5	Zeolite Socony Mobil-5 (zeolite framework type)

List of original papers

This thesis is based on the following publications, which are referred to throughout the text by their Roman numerals:

I Korelskiy D, Leppäjärvi T, Zhou H, Grahn M, Tanskanen J & Hedlund J (2013) High flux MFI membranes for pervaporation. Journal of Membrane Science 427: 381–389.

II Leppäjärvi T, Malinen I, Korelskiy D, Kangas J, Hedlund J & Tanskanen J (2015) Pervaporation of ethanol/water mixtures through a high-silica MFI membrane: Comparison of different semi-empirical mass transfer models. Periodica Polytechnica: Chemical Engineering 59(2): 111–123.

III Leppäjärvi T, Malinen I, Kangas J & Tanskanen J (2012) Utilization of P_i^{sat} temperature-dependency in modelling adsorption on zeolites. Chemical Engineering Science 69: 503–513.

IV Leppäjärvi T, Kangas J, Malinen I & Tanskanen J (2013) Mixture adsorption on zeolites applying the P_i^{sat} temperature-dependency approach. Chemical Engineering Science 89: 89–101.

V Leppäjärvi T, Malinen I, Korelskiy D, Hedlund J & Tanskanen J (2014) Maxwell-Stefan modeling of ethanol and water unary pervaporation through a high-silica MFI zeolite membrane. Industrial & Engineering Chemistry Research 53: 323–332.

VI Zhou H, Korelskiy D, Leppäjärvi T, Grahn M, Tanskanen J & Hedlund J (2012) Ultrathin zeolite X membranes for pervaporation dehydration of ethanol. Journal of Membrane Science 399–400: 106–111.

In Paper I the author planned and performed the pervaporation experiments together with the first author. The author also modeled the mass transfer resistance of the support and took intensively part in writing the article. In Papers III and IV the author collected all the data and did the modeling work using the models created in collaboration with the other authors, in addition to the writing of the papers. In Papers II and V, the author planned and performed the experiments and analysis as well as the modeling work and writing. In Paper VI, the author participated on performing the pervaporation experiments, and in the modeling and writing the paper.

Contents

1 Introduction

During the past decades, the production of chemicals and fuels from renewable resources has received growing attention due to limited oil resources, the increasing oil price, and environmental concerns. The primary focus on liquid transportation biofuels has centered on bioethanol and biodiesel. Commercial bioethanol is mainly produced from starch/sugar-based crops, and also the production of bioethanol from lignocellulosic materials has started (Guo *et al.* 2015). More recently, the production of *n*-butanol from biomass feedstocks (namely biobutanol) has also received considerable attention (Abdehagh *et al.* 2014, Bankar *et al.* 2013). Biobutanol is mostly produced by ABE (acetone butanol ethanol) fermentation, an old industrial process. Butanol is an attractive biofuel as it has several advantages over ethanol: higher energy content, lower vapor pressure and higher flash point (safety), less hygroscopic (less corrosion) and better miscibility with gasoline. However, the production of biobutanol is still in the development stage.

Fermentation is a process typically inhibited by the products. In the production of fermented bio-based alcohols, the separation steps are expensive due to the low concentration of the desired products. Micro-organisms start to experience ethanol inhibition above 5–8 wt.% ethanol (Vane 2005), and the fermentation process stops at ethanol concentrations near 15 wt.% (Caro & Noack 2008). Similarly butanol inhibition is a severe problem in ABE fermentation, as normally the final product concentration is below 3 wt.% making the separation costs high (Huang *et al.* 2014).

Distillation is the leading separation process in the chemical industry, and also in ethanol enriching. Ethanol forms a homogeneous azeotrope with water with approximately 95 wt.% ethanol, at atmospheric pressure, and a temperature of 78 °C. The separation of mixtures forming azeotropes by distillation traditionally occurs through pressure-swing distillation, or by using a third component as an entrainer in extractive or azeotropic distillation; both alternatives being very energy intensive. Generally, concentrating ethanol by distillation for more than 85 wt.% concentration becomes very expensive (Huang *et al.* 2008).

The recovery of butanol from dilute ABE fermentation broth involves the removal of acetone and ethanol, and the separation of butanol from water. This can be carried out in a series of distillation columns (Mariano & Filho 2012). Separation of acetone due to its high volatility is easy, but separating the butanol-water system is more complicated since *n*-butanol forms a heterogeneous azeotrope with water with approximately 56 wt.% *n*-butanol, at atmospheric pressure, and at a temperature of 93 °C. As a whole, biobutanol recovery by distillation is too energy-

intensive for a large-scale industrial process (Schiel-Bengelsdorf *et al.* 2013). Thus, there is great interest in investigating other separation methods to concentrate ethanol or butanol from fermentation broths.

Pervaporation is recognized as an energy-efficient separation process with great potential in biofuel production (Huang *et al.* 2014, Oudshoorn *et al.* 2009, Vane 2005, Weyd *et al.* 2008). Pervaporation is a separation process in which a liquid mixture is fed to a membrane, and one or several of the mixture components are selectively transported through the membrane and evaporated on the other side of the membrane. The permeate is typically subsequently condensed back into liquid. Generally, a low partial or total pressure is maintained on the permeate side of the membrane. Preferably, the membrane should have both high permeation selectivity and high permeability. Thus, even a component with a low concentration in the feed can be enriched in the process.

Processes involving phase changes are generally energy-intensive. However, pervaporation is referred to as an energy-efficient and cost-effective process. In pervaporation, separation is based on membrane selectivity, not e.g. on vapor-liquid equilibrium. Pervaporation typically deals with components of less than 10 wt.% of the liquid mixtures, and only the permeating species is evaporated. Pervaporation is considered as a unit process alternative especially in cases where separation is difficult to achieve by conventional separation processes, such as in the separation of azeotropic or close-boiling mixtures, thermally sensitive compounds or isomers.

The core of the pervaporation process is the membrane. The first pervaporation plants were installed in the 1980s by GFT (now owned by Sulzer) for ethanol dehydration (Kujawski 2000). Most of the available commercial membranes are polymer based. A few hundred small pervaporation plants have been installed around the world mostly for the removal of water from ethanol and isopropyl alcohol streams produced in the pharmaceutical and fine chemicals industries (Baker 2012). Generally, the zeolite membranes exhibit a higher pervaporation performance in ethanol and isopropyl alcohol dehydration in terms of separation factor and flux when compared to polymeric membranes (see e.g. Chapman *et al.* 2008). However, the zeolite membranes are more expensive when compared to polymeric membranes (Wee *et al.* 2008), which has slowed down the commercialization of zeolite membranes in pervaporation applications.

At present, the majority of the existing ethanol plants use a combination of distillation and molecular sieve drying to separate the ethanol/water mixture. Nevertheless, the use of pervaporation in bioethanol production has a great

potential due to the fact that the worldwide production of fuel bioethanol in 2013 was 87.2 billion liters (REN21 2014) and is likely to increase in the future when cost-effective lignocellulose-to-ethanol technologies fully enter the market.

During the past decades, the development of inorganic membranes, especially zeolite membranes, has gained increasing interest due to their thermal and chemical stability (Bowen *et al.* 2004, Caro & Noack 2008, Wee *et al.* 2008). The increasing industrial use of zeolite membranes might broaden the application range of pervaporation. Zeolites are hydrophilic or hydrophobic by nature, enabling separation of water over organics as well as organics over water. So far, pervaporation using zeolite membranes has been more successful in dehydrating organic components than in separating organic components from aqueous mixtures (Wee *et al.* 2008).

In general, the development of pervaporation membranes and process concepts applying them has focused on empirical work. Process simulation software provides tools for process design and evaluation, but commercial simulation programs do not provide phenomenon-based models for membrane technology. Thus, users are forced to build the models themselves and integrate them into existing simulation programs to enable feasible process design and evaluation. In order to be able to do so, it is crucial to understand and model the behavior of permeating components in zeolite membranes in pervaporation. However, modeling of pervaporation through zeolite membranes has been somewhat neglected, especially in the case of membranes of hydrophobic character.

The steps in bioethanol or biobutanol production are shown in Fig. 1. Biomass has to be broken down into fermentable sugars by pre-treatment and hydrolysis. Then, in fermentation, yeast or bacteria is used to convert the sugars into valuable products, such as alcohols. Finally, the fermented alcohol is recovered and purified.

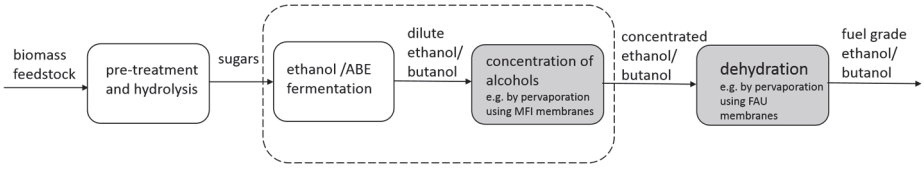

Fig. 1. Potential applications of pervaporation using zeolite membranes in biofuel (ethanol/butanol) production (colored gray).

Pervaporation is seen as a viable method to separate the fermentation products and thus surpass the product inhibitory effect (Liu *et al.* 2014). The alcohol-enriched

solution could be further dehydrated to produce anhydrous alcohols, as shown in Fig. 1. In this study, the focus is on pervaporation using both hydrophobic and hydrophilic zeolite membranes. The hydrophobic high-silica Mordenite Framework Inverted (MFI) -type zeolite membranes can be used, e.g., for the concentration of alcohols from fermentation broths, whereas the hydrophilic Faujasite (FAU) -type zeolite membranes can be used, e.g., for the dehydration of alcohol-rich solutions (see the colored gray zones in Fig. 1). The dashed line in Fig. 1 emphasizes the possibility of coupling fermentation with pervaporation (see e.g. Bankar *et al.* 2013 and Huang *et al*. 2014).

1.1 Objectives and scope

This study is focused on zeolite membranes due to their unique, defined microporous inorganic structure, making the application of zeolite membranes in pervaporation of great interest. Low membrane thickness is a desired membrane property in order to obtain high fluxes, which is essential for industrial applications. Thus, in this study, ultra-thin zeolite membranes are investigated in the selected applications. The importance of both the experimental and modeling work is realized in evaluating the pervaporation performance of zeolite membranes. The objectives of the thesis can be summarized as

- Increase the understanding of the pervaporation process using zeolite membranes;
- Evaluate the pervaporation performance of ultra-thin supported zeolite membranes (MFI/FAU) in the separation of aqueous ethanol and *n*-butanol solutions;
- Apply and modify available semi-empirical and detailed models to describe the pervaporation process behavior;
- Investigate the contribution of the support to mass transfer in the case of supported ultra-thin zeolite membranes, and apply the description of the support behavior in membrane mass transfer models;
- Formulate phenomenon-based tools to enable detailed modeling of the ultra-thin supported zeolite membranes.

In this work, pervaporation using zeolite membranes is studied in the separation of binary ethanol/water and *n*-butanol/water mixtures. Pervaporation through zeolite membranes is generally described phenomenologically by adsorption into the membrane pores and diffusion along the surface of the zeolite pores as a

consequence of the chemical potential gradient within the pores. Hence, the separation of the components is a result of the combined effect of adsorption and diffusion selectivity, and the driving force prevailing across the membrane. The different phenomena shown in Fig. 2 having an effect on the separation performance of the membranes are considered in this thesis.

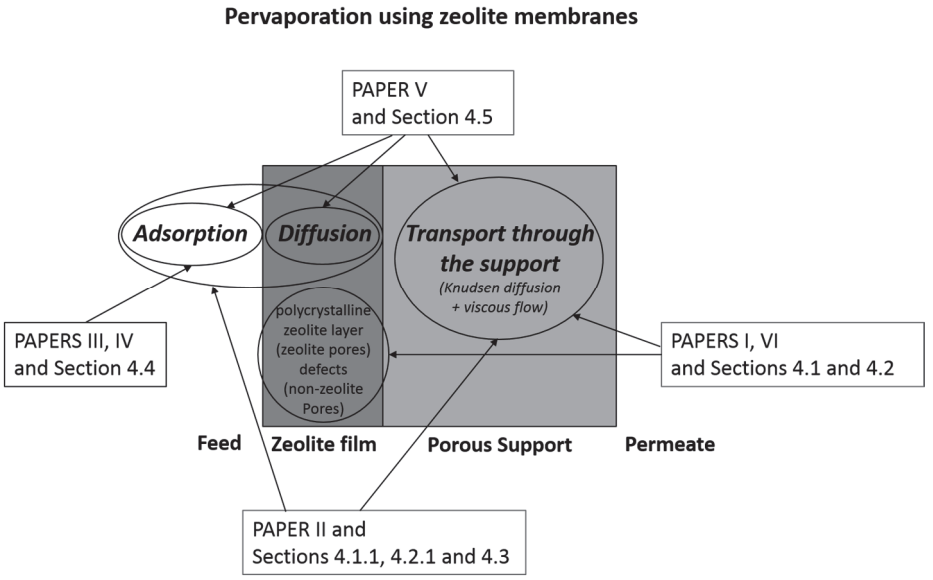

Fig. 2. Outline of the thesis.

The scope of each paper and its contribution to the thesis are shown in Fig 2. In Papers I and VI, the pervaporation performance of ultra-thin MFI and FAU membranes are evaluated for the first time for the separation of aqueous mixtures of ethanol and *n*-butanol. The zeolite film properties and defects are characterized and the effect of the mass transfer resistance is investigated.

In Paper II, pervaporation using hydrophobic high-silica MFI membranes in ethanol separation from aqueous mixtures is further studied and analyzed. The pervaporation process is modeled using a semi-empirical mass transfer model, also including a model for the membrane support. In the models of Paper II the driving force is well established whereas the permeation-related effects of adsorption and diffusion phenomena are combined into a single permeance term.

Papers III and IV deal with adsorption on zeolites. In Paper III, a new, easy, and relatively reliable approach is introduced to describe the temperature

dependency of pure component adsorption on zeolites with the temperature dependency of pure component saturated vapor pressure. In Paper IV, the approach introduced in Paper III is studied in the prediction of mixture adsorption on zeolites with a small amount of experimental adsorption data. The proposed approach can be used as a short-cut tool in the modeling and design of industrial processes exploiting adsorption, such as pervaporation using zeolite membranes where separation is based on both adsorption and diffusion phenomena.

In Paper V, unary ethanol and water pervaporation through a high-silica MFI zeolite membrane is modeled in more detail, considering various phenomena separately. Hence, Maxwell-Stefan modeling is applied to describe the membrane behavior in Paper V. The tool introduced in Paper III to describe adsorption is also exploited in Paper V.

1.2 Dissertation structure

Chapter 2 presents the theory closely related to this work. In order to be able to evaluate the pervaporation performance of supported zeolite membranes, it is important to know, for example, the zeolite membrane structure, synthesis and characterization methods, and to understand the effects of the membrane support. Process models are typically based on the mathematical description of phenomena occurring in the process. The separation in pervaporation is based on adsorption of the components in the zeolite pores and diffusion along the surface of the zeolite pores. Thus, the theory of adsorption and diffusion is also included in Chapter 2. The methods that have been used to achieve the objectives of this thesis are summarized in Chapter 3. The main results are shown in Chapter 4 (see Fig. 2). Conclusions are summarized in Chapter 5 and proposals for future research arising from this thesis are discussed in Chapter 6.

2 Theory

2.1 Zeolite membranes

Zeolites are naturally occurring inorganic crystalline aluminum-silicates, which can also be synthetically produced. Zeolites have a three-dimensional framework structure with uniform, molecular-sized pores. Their structure is composed of a framework of $[SiO_4]^{4-}$and $[AlO_4]^{5-}$ tetrahedra linked to each other at the corners, sharing the oxygen atoms. The framework exhibits a negative charge when aluminum is incorporated in the structure, which is balanced by cations such as Na^+, K^+, Ca^{2+} and H^+. The mobile cations are not part of the zeolite framework; instead, they are located in the channels. Nevertheless, cations affect the zeolite pore size and play an important role in determining the adsorption properties of zeolites (Ruthven 1984).

According to the International Zeolite Association, more than 200 different zeolite types have been recognized and assigned with a three letter code. Zeolite pores are made up of rings in the zeolite framework. The pores are categorized as micropores as their pore size range from about 0.3 to 1.3 nm, depending on the zeolite structure and cations present in the zeolite channels.

Silicalite-1, a pure siliceous zeolite, is hydrophobic. The inclusion of aluminum in the zeolite structure increases the net negative charge, and the material becomes hydrophilic. This is due to the fact that the localized electrostatic poles between the positively charged cations and the negatively charged zeolite framework preferentially attract polar molecules (Huang *et al.* 2006). Hence, the lower the Si/Al ratio of a zeolite, the more hydrophilic the zeolite, adsorbing polar molecules more strongly. The Si/Al ratio of a zeolite can be controlled in zeolite synthesis.

Due to the unique properties of zeolites, they have been used, for example, as catalysts and adsorbents. The unique properties of regular, molecular-sized pores, high thermal stability, acidic or basic properties, hydrophilic or organophilic properties, ion-exchange possibilities, dealumination and realumination possibilities, isomorphous substitution and insertion of catalytically active parts (Cot *et al.* 2000) also make zeolites very promising candidates for membrane material.

Zeolite membranes have the unique properties of zeolites in a film-like configuration. They are polycrystalline structures composed of well intergrown zeolite crystals. Zeolite membranes are typically supported, in order to provide

mechanical stability. The most common zeolite structures that have been prepared as membranes are MFI, Linde Type A (LTA), and FAU.

MFI zeolite membranes have a suitable pore size (~0.55 nm pore diameter) for the separation of many industrially important molecules (Vroon *et al.* 1998). The MFI structure includes silicalite-1, which is made up of pure silica, and ZSM-5, which has Al substituted for some of the Si atoms. In the literature, silicalite-1 and high-silica Zeolite Socony Mobil-5 (ZSM-5) are often referred to as hydrophobic. One potential application of high-silica MFI membranes is the concentration of alcohols from fermentation broths in the production of fuel grade alcohols (Vane 2005).

LTA-type zeolite membranes are very well suited for organic dehydration because they are highly hydrophilic and their pore diameter (~0.4 nm) is smaller than most organic molecules but larger than water. In fact, organic dehydration by pervaporation using hydrophilic zeolite membranes was demonstrated on a large scale more than 10 years ago (Morigami *et al.* 2001). Nowadays there are about 200 such units in operation around the world, as the only commercial application of zeolite membranes so far (Lin & Duke 2013).

FAU zeolite has relatively large pores of 0.74 nm. The Si/Al ratio, and thus the polarity of FAU zeolite can vary a lot. Low-silica FAU is denoted as zeolite X while high-silica FAU as zeolite Y. FAU zeolite membranes are considered to have potential in organic dehydration (Sato *et al.* 2008a, Zhu *et al.* 2009).

2.1.1 Synthesis

The aim in membrane preparation is to produce membranes that are as thin as possible in order to obtain high fluxes and to have a low defect concentration in order to obtain high selectivities, be reliably reproducible and be durable. Zeolite membrane thicknesses ranging from 0.5 μm (Hedlund *et al.* 2002, Kosinov *et al.* 2014) to several hundred micrometers (Nomura *et al.* 1998, Sano *et al.* 1995a) have been reported. Since zeolite membranes have to be very thin to reach high permeation fluxes, zeolite films are mostly prepared on porous inorganic supports to supply mechanical strength and durability to the membrane.

Zeolite membranes are usually prepared by hydrothermal synthesis. The synthesis mixture usually contains water, a silica source, an alumina source, a mineralizing agent, and an organic structure-directing template (Andersson 2007). The synthesis mixture is heated typically to 150–180°C, reaction time often being in the range of 16–24 hours (Gavalas 2006).

Supported zeolite membranes can be prepared either by *in situ* crystallization where zeolite crystals nucleate and grow directly on the support, or by secondary (seeded) growth where seed crystals are first well deposited onto the support followed by the hydrothermal growth of the seeds into a continuous layer (McLeary *et al.* 2006). Zeolite seeds are typically prepared as a colloidal solution by hydrothermal synthesis. By first seeding the support, a more uniform film can be obtained in addition to the better reproducibility of the membranes than in one step *in situ* hydrothermal synthesis (Hang Chau *et al.* 2000). After synthesis the membranes are dried to remove the solvent, and calcined i.e., heated in air (at ~500°C) in order to remove the organic template that blocks the pores.

2.1.2 Membrane support

The interaction between the synthesis solution and the support depends on the physical and chemical nature of the support. The quality of the underlying support determines largely the quality of the selective membrane layer on top of it (McLeary *et al.* 2006). Adhesion of the zeolite film to the support surface, for example, is very important. The support surface should be smooth, because if the surface is rough or has large pores, adhesion of a thin and continuous zeolite film is less likely. The most frequently used supports in the zeolite membrane literature are alumina and stainless steel. The typical pore diameter of alumina supports varies between 5 nm (γ-alumina) and 200 nm (α-alumina), and that of stainless steel in the range of 0.5–4 μm (Bowen *et al.* 2004).

Alumina supports have been used in the majority of the reported work due to the availability of high-quality ultrafiltration and microfiltration membranes with a smooth surface, also being suitable to be used as zeolite membrane supports. Instead, the stainless steel supports typically have a rougher surface and larger pores with respect to alumina supports (Algieri *et al.* 2011). The support surface roughness and pore size are important factors when synthesizing high-quality zeolite membranes. Basically, the optimum zeolite crystal size and film thickness for each support-zeolite combination can be defined on the basis of support roughness and film thickness (Hang Chau *et al.* 2000). It might be difficult to deposit a uniform seed layer on a rough stainless steel surface (Stoeger *et al.* 2011). Although, zeolite film formation can be also altered with, e.g., chemical modification of the support surface (Hang Chau *et al.* 2000, Ji *et al.* 2012). In addition, stainless steel supported zeolite membranes have a higher risk of cracking during calcination due to the thermal expansion mismatch between the steel support

and the zeolite layer (Caro *et al.* 2000). However, it is known that in the hydrothermal synthesis of zeolite membranes on alumina supports, aluminum can be leached into the zeolite film (Geus *et al.* 1992, Shu *et al.* 2012). As a result, the leached aluminum changes the zeolite framework so that it contains more aluminum and thus the framework becomes more hydrophilic.

Besides the fact that the support should allow the application of a thin and defect-free separation layer on top of it, the flow resistance of the support is also a concern when choosing the support material. As the composite membrane consists of both a selective layer and a porous support layer(s), all the layers contribute to the transport of a component through the membrane. Typically the main transport resistance is in the zeolite film (de Bruijn *et al.* 2003, Thomas *et al.* 2001). Thus, in order to increase the flux, the zeolite film should be very thin. However, as a consequence, the resistance over the thicker support becomes more significant.

In macroporous and mesoporous media, i.e., in the zeolite membrane support media, the nature of the transport is determined by the magnitude of the mean free path λ of the molecules and the pore diameter d_{pore}. When the ratio of the mean free path over the pore size is large ($\lambda >> d_{\text{pore}}$), collisions of molecules with the pore walls dominate. This transport regime is referred to as the Knudsen regime (Kärger & Ruthven 1992). Knudsen molar flux in low pressures can be defined as (de Bruijn *et al*. 2003)

$$J_{\text{Kn},i,\text{s}} = -\frac{1}{RT} D^{\text{eff}}_{\text{Kn},i,\text{s}} \nabla p_{i,\text{s}}, \tag{1}$$

where R is the gas constant, T is the temperature, $D^{eff}_{Kn,i,s}$ is the effective Knudsen diffusivity, and $\nabla p_{i,s}$ is the partial pressure gradient of component i through support layer s. In the Knudsen regime the diffusivity is controlled by the molecular weight rather than the molecule size. Knudsen diffusivity is given by

$$D^{\text{eff}}_{\text{Kn},i,\text{s}} = \frac{\varepsilon}{\tau}\frac{d_{\text{pore}}}{3}\sqrt{\frac{8000RT}{\pi M_i}} = 97K_{\text{s}}\sqrt{\frac{T}{M_i}}, \tag{2}$$

where ε is the porosity and τ is the tortuosity of the support (which considers deviations from a straight path), M_i is the molar mass of component i and K_s is the Knudsen structural parameter for support layer s.

As can be seen in Eq. (2), Knudsen diffusivity varies only weakly with temperature and is basically independent of pressure, since the mechanism does not depend on intermolecular collisions. The selectivity effect of Knudsen diffusion

originates from the ratio of molecular masses and the partial pressure gradient of the investigated components.

When the support pores are large, i.e. in the macropore scale, or the pressure is high, the relative number of molecule-molecule collisions increases compared to the number of collisions with the pore wall. In these conditions, viscous (Poiseuille) flow emerges as an important mechanism of mass transfer. Basically, viscous flow is a non-selective mass transfer mechanism. The viscous molar flux is induced by a pressure gradient of the fluid mixture as (de Bruijn *et al.* 2003)

$$J_{\mathrm{Vis},i,\mathrm{s}} = -\left(\frac{\overline{p_{i,s}}}{RT}\right)\frac{B_{0,\mathrm{s}}^{\mathrm{eff}}}{\eta}\nabla P_{\mathrm{s}}\,, \tag{3}$$

where $\overline{p_{i,s}}$ is the average arithmetic pressure of component *i* in the support layer *s*, η the viscosity, ∇P_s, is the pressure gradient through layer *s*, and $B_{o,s}^{eff}$ is the effective permeability for support layer *s* defined as

$$B_{0,\mathrm{s}}^{\mathrm{eff}} = \frac{\varepsilon}{\tau}\frac{d_{\mathrm{pore}}^{2}}{32}\,. \tag{4}$$

For materials with a broad pore size distribution, Eqs. (2) and (4) can only be used to approximate the average structural parameters. As the diffusion through the zeolite layer is typically assumed to be much lower compared to that of the support, the transport resistance through the porous support material is often neglected. However, the support can introduce a significant relative resistance to transport, especially in the case of thin membranes. Subsequently, in order to decrease the mass transfer resistance of the support, and hence increase the diffusivity of the support, the support layer characteristics should be affected. As it is seen in Eqs. (1)–(4), the important parameters are the support porosity and pore size, tortuosity and thickness. Thus, to minimize the transport resistance caused by the membrane support, the support should ideally be thin, have high porosity, large pores and straight diffusion paths to ensure high flux. Besides minimizing the resistance of the support, the support surface should be smooth to enable complete coating by a thin zeolite film.

2.1.3 Defects

Zeolite pores are defined by a crystal lattice. Due to the polycrystalline nature of zeolite membranes, membranes have transmembrane pathways larger than the

intracrystalline zeolite pores, called defects. Both the zeolite pores and defects, also referred to as non-zeolite pores, offer pathways for mass transfer. The adsorption and diffusion properties of molecules are different in zeolite pores and defects. According to IUPAC definitions, the defects in zeolite membranes can be classified into macrodefects (size > 50 nm), mesodefects (size 2–50 nm) and microdefects (size < 2 nm) (Tavolaro & Drioli 1999).

Pinholes, cracks, and open grain boundaries are typical examples of defects. Different types of mesodefects and microdefects are typically formed by non-perfect intergrowth between zeolite crystals in hydrothermal synthesis (Tavolaro & Drioli 1999).

Pinholes are holes that may propagate through the zeolite film, and may be formed due to non-uniform seeding in membrane synthesis, for example. Generally, the number of pinholes is dependent on the synthesis procedure (Hedlund *et al.* 2003). Cracks, on the other hand, may be formed during calcination, for example, if there is a mismatch between the thermal expansion between the zeolite and the support (Geus & van Bekkum 1995). Similarly, cracks typically extend from one side of the zeolite film to the other. A crack is typically characterized as a macrodefect.

Zeolite membranes consist of several crystals or grains, and the grain boundaries can be either intergrown or open (Andersson 2007). The grain boundaries can be regarded as the borderlines between adjacent zeolite crystals. The defects in the form of open grain boundaries are thus intercrystalline pores between the grains. The intracrystalline and intercrystalline pathways i.e. different kinds of defects are illustrated in Fig. 3.

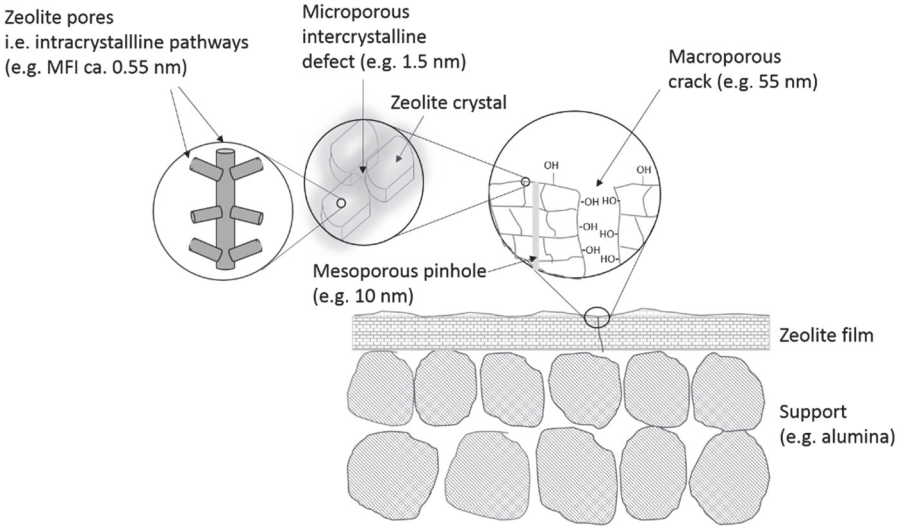

Fig. 3. Schematic representation of zeolite and non-zeolite pores in a composite zeolite membrane.

Another type of defect in zeolite membranes is broken Si-O-Si bonds in the zeolite crystals (Hunger *et al.* 1987), referred to as an intracrystalline defect. In general, the hydrophobicity of zeolite membranes is caused by the Si-O-bonds, resulting in the lack of ionic sites for water adsorption. Hence, hydrophobic zeolite membranes preferentially adsorb organic molecules that are small enough to enter the pore openings. Conventional zeolite synthesis is performed in alkaline conditions. The presence of hydroxide ions causes structural defects which originate from the formation of Si-OH and Si-O^- groups at internal defect sites (Zhou *et al.* 2014), i.e., at sites where Si-O bonds are broken. These intracrystalline defects decrease the hydrophobicity of even a fully siliceous silicalite-1 (Zhang *et al.* 2012a). In addition to intracrystalline defects caused by the broken Si-O bonds in the zeolite lattice, silanol (-OH) groups are present on the external surface of a zeolite where Si-O-Si network is terminated and oxygen atoms cannot be bonded to another Si atom (Özgür Yazaydin & Thompson 2009). These terminal silanol groups are able to interact with guest molecules (Saengsawang *et al.* 2005).

The influence of defects on zeolite membrane performance depends on the selected application e.g. whether the operating conditions are at high or low temperatures or whether the application is gas/vapor/liquid separation (Julbe 2007). Typically defects lower the selectivity of zeolite membranes. As silanol groups are

hydrophilic, the defects increase the local hydrophilicity of zeolite membranes, i.e., water adsorbs in zeolite defects over organics. Due to the hydrophilicity of zeolite defects, the effect of defects in the case of hydrophilic membranes is not necessarily that detrimental to membrane performance as concluded e.g. in the study of Okamoto *et al.* (2001). On the other hand, in the case of hydrophobic membranes, as the zeolite pores favor ethanol transport and defects water transport (Algieri *et al.* 2003, Sebastian *et al.* 2010), the net effect of defects on the organic/water selectivity is larger than in the case of hydrophilic zeolite membranes. Even high-quality zeolite membranes contain intercrystalline defects with sizes smaller than 2 nm, but larger than the zeolite pores (Lin & Duke 2013). A schematic representation of the contribution of zeolite pores and microporous defects for hydrophilic LTA/FAU and hydrophobic high silica MFI zeolite membranes in the pervaporation of water/ethanol is shown in Fig. 4.

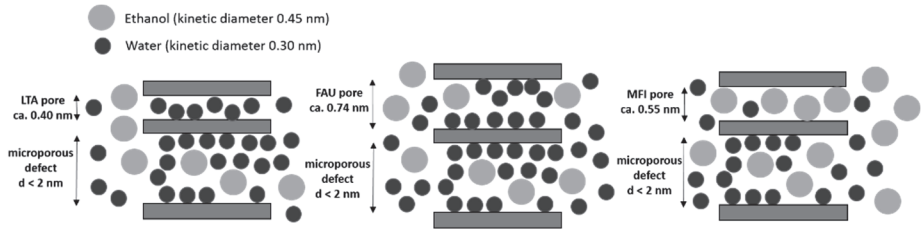

Fig. 4. Contribution of zeolite pores and defects in pervaporation using hydrophilic (LTA, FAU) and hydrophobic (high-silica MFI) zeolite membranes in the pervaporation of water/ethanol mixtures.

Separation in zeolite membranes occurs mostly through adsorption and surface diffusion, as discussed in more detail in Section 2.2. In Fig. 4, it is shown in principle that due to the local polarity and thus hydrophilicity, defects in zeolite membranes favor the transport of water molecules. Small-pore hydrophilic LTA membranes adsorb water rather than ethanol in addition to that transport of ethanol molecules is also inhibited due to size exclusion (molecular sieving effect). Large-pore hydrophilic FAU membranes adsorb water over ethanol, whereas hydrophobic high-silica MFI membranes adsorb ethanol over water.

2.1.4 Characterization

Membrane characterization is essential in order to evaluate the quality of the membranes synthesized. Zeolite membranes can be characterized using several

methods. Zeolite film properties (thickness, uniformity, continuity) can be investigated by imaging zeolite film with scanning electron microscopy (SEM). For example, pinholes and cracks can in principle be observed by characterizing the surface using SEM whereas open grain boundaries in the micropore range are difficult to observe due to the limited resolution (Hedlund *et al.* 2009). Zeolite phase identification, framework structure and degree of crystallinity are usually determined by using X-ray diffraction (XRD).

Minimizing the proportion of defects in the membrane is important in membrane synthesis since defects typically lower the membrane selectivity. As the direct observation of microdefects in zeolite membranes is difficult, indirect methods have been used to characterize membranes. Single gas permeation is a common method used in membrane characterization, and the ratio of single gas permeances (ideal selectivity) is often used as an indication of membrane quality (Funke *et al.* 1996, Kalipçilar & Çulfaz 2002, Sebastian *et al.* 2010). Single-gas permeation is typically measured with small molecules (e.g. H_2, N_2, He) and molecules of the same size range as the membrane pores (e.g. SF_6 for MFI membranes). The assumption behind single gas permeance ratio measurements is that the permeation rate through the zeolite pores for components of the same size as the intracrystalline pores should be very low so that substantial flux of these probe components is an indication of flow-through defects. For example, N_2/SF_6 permeance ratios varying from as low as 4 (Macdougall *et al.* 1999) to as high as 80 (Funke *et al.* 1996) have been claimed to be a criterion of good quality MFI membranes.

However, despite the wide use of single gas permeance ratios as an indication of membrane quality, it does not necessarily correlate with the achieved separation levels or even with whether a membrane can separate certain mixtures or not (Bernal *et al.* 2002, Coronas *et al.* 1998). Single-component permeance ratios also depend on several other parameters besides the defects in the zeolite film (Hedlund *et al.* 2003, Jareman & Hedlund 2005). Nevertheless, notable permeation of molecules much larger than the zeolite pores, can be used as an indicator of the presence of flow-through defects (Bowen *et al.* 2004).

Permporometry is generally used for the characterization of the size and proportion of pores in porous membranes. As permporometry is a simple and non-destructive method, zeolite membrane microstructure has been characterized frequently by permporometry, in the determination of flow-through defects (Hedlund *et al.* 2002, Noack *et al.* 2006, Wang *et al.* 2009a). The basic concept of permporometry is that the permeance of an inert, non-condensable (and non-

adsorbing) gas like helium is measured while the activity (calculated as the ratio of the partial pressure of the component to its saturated vapor pressure) of a highly adsorbing vapor is increased gradually from 0 to 1. Typically, *n*-hexane is used as the condensable component in the case of hydrophobic membranes, and water in the case of hydrophilic membranes (Caro & Noack 2008). As the activity of the highly adsorbing component increases, its occupancy in the pores increases, blocking the flow of the non-condensable component through the pores so that the remaining flux is assumed to occur through the defects above a certain size. The defect size blocked by the condensable vapor can be estimated with appropriate physical equations such as the Horvath-Kawazoe and Kelvin equations (see e.g. Hedlund *et al.* 2009). As a result, the defect distribution of the flow-through defects in a zeolite membrane can be obtained.

2.2 Adsorption and diffusion in zeolite materials

Permeation of components through zeolite membranes is generally explained by adsorption of the components in the zeolite pores and diffusion along the surface of the zeolite pores as a consequence of the chemical potential gradient $\nabla\mu_i$ within the pores. Due to the differences between the adsorption and diffusion properties of the components in the zeolite pores, zeolite membranes can be applied in the separation of certain mixtures. In order to design zeolite membrane based processes, knowledge of adsorption and diffusion behavior is essential.

2.2.1 Pure component adsorption

In the adsorption phenomenon, an adsorbate (sorbate) is accumulated on the surface of a solid adsorbent (sorbent). The adsorbate attaches on the surface by physical adsorption (physisorption) or chemical adsorption (chemisorption). Adsorption on zeolites under pervaporation conditions is mainly physical in nature (Bowen *et al.* 2004). The characteristics of physisorption depend on several factors, e.g. adsorbent porosity, the size and geometry of pores, defects in the adsorbent structure, and interactions between adsorbent-adsorbate and adsorbate-adsorbate pairs.

Although applications of adsorption usually involve mixtures, adsorption equilibrium data is typically measured for single components as pure component adsorption measurements are the most reliable and also the easiest to perform. Mixture adsorption is then predicted by adsorption models, which are discussed in

more detail in Section 2.2.2. In general, pure component adsorption behavior is investigated based on isothermal equilibrium measurements. The adsorption equilibrium data is then used to form an adsorption isotherm. Isotherms typically describe the amount of adsorbate adsorbed for a given mass of adsorbent as a function of adsorbate pressure, relative pressure, fugacity or concentration in the fluid phase at a constant temperature. Adsorption in zeolite crystals have been measured, for example, by gravimetric (Nayak & Moffat 1988, Ryu *et al.* 2001) and volumetric uptake (Wang & LeVan 2009, Yun *et al.* 1998) as well as chromatographic (Sakuth *et al.* 1995) methods.

Adsorption measurements on zeolites are typically performed with zeolite powders, and not with membranes, because the measurement techniques are usually not suitable for measuring adsorption directly from membranes. The main practical reason for this is that the zeolite material constitutes only a minor weight fraction of the whole composite membrane. Hence, the adsorption measurements would include the adsorption behavior of the support material, which is not part of the film transport pathway (Gardner *et al.* 2002b). For example, it has been concluded that alumina supports significantly affect the total amount adsorbed due to its relative thickness (Hammond *et al.* 2007). An alternative method to evaluate the adsorption behavior of a zeolite film is to use computational methods. Hence, molecular simulation techniques have been used to study adsorption in zeolites (Smit & Krishna 2001).

Adsorption equilibrium data can be described with different mathematical models, i.e. adsorption isotherm equations. The adsorption behavior of different adsorbent-adsorbate pairs varies considerably. Therefore, a number of isotherm formulations have been proposed in the literature to describe adsorption on porous adsorbents. Some of the frequently applied isotherms connected to adsorption on zeolites are shown in Table 1. It is characteristic to the isotherm equations presented in Table 1 that they have mostly two or three adjustable parameters, which are determined on the basis of the adsorption equilibrium data.

Table 1. Isotherms for component adsorption on porous adsorbents.

Isotherm	Equation	Adjustable parameters
1. Henry's law	$q_i = K_{H,i}P$	$K_{H,i}(T)$
2. Freundlich	$q_i = K_{F,i}P^{\frac{1}{n}}$	$K_{F,i}(T), n$
3. Langmuir	$q_i = \frac{q_i^{sat} b_i P}{1 + b_i P}$	$q_i^{sat}, b_i(T)$
4. Sips	$q_i = \frac{q_i^{sat} (b_i P)^{1/n}}{1 + (b_i P)^{1/n}}$	$q_i^{sat}, b_i(T), n$
5. Tóth	$q_i = \frac{q_i^{sat} b_i P}{[1 + (b_i P)^n]^{1/n}}$	$q_i^{sat}, b_i(T), n$
6. BET	$q_i = \frac{q_i^{sat} c_i (P/P_i^{sat})}{(1 - P/P_i^{sat})(1 - P/P_i^{sat} + c_i P/P_i^{sat})}$	$q_i^{sat}, c_i(T)$
7. Dubinin- Raduschkevich	$q_i = q_i^{sat} exp\left\{-\left[\frac{RT}{E} ln\left(\frac{P_i^{sat}}{P}\right)\right]^2\right\}$	q_i^{sat}, E

At low pressures (or fugacities), the adsorption loading is directly proportional to pressure, referred to as Henry's law (isotherm 1 in Table 1). The low loading q_i region where the adsorption isotherm is linear is called Henry's law region. At higher pressures, the linear relationship between loading and pressure is no longer valid. Thus, the application of Henry's law should be restricted to the linear region of the isotherm from adsorption equilibrium measurements.

The Langmuir isotherm (isotherm 3 in Table 1) is widely applied in the adsorption of a pure component on zeolite. The Langmuir isotherm is nonlinear at high pressures and shows linearity at low pressures, i.e., it reduces according to Henry's law in low-pressure conditions. On the other hand, at high pressures the Langmuir isotherm approaches asymptotically the maximum adsorption loading (saturation loading) q_i^{sat} i.e., the amount where the zeolite pores are completely filled. The Langmuir isotherm is a frequently used theoretical model for monolayer adsorption (Ruthven 1984). In general, saturation loading can be taken as constant or it can take an empirical functional form of temperature dependency. However, the temperature dependency of saturation loading is not well validated (Malek & Farooq 1996) and the temperature dependency of q_i^{sat} has only a small effect in model predictions (Do & Do 1997). The usage of a constant saturation loading is

widely accepted when describing adsorption on zeolites (Pera-Titus *et al.* 2008, Zhu *et al.* 2006).

The earliest empirical isotherm is the Freundlich isotherm (isotherm 2 in Table 1). The Freundlich isotherm does not approach asymptotically the saturation loading as the pressure increases. Furthermore, as the empirical Freundlich isotherm does not exhibit proper Henry's law behavior at low pressure, i.e., lacking linear proportionality between the adsorbed amount and pressure, it is generally valid in a limited range of adsorption equilibrium data (Do 1998). The same kind of form as in the Freundlich isotherm is found in the Sips isotherm (isotherm 4 in Table 1), but in a finite adsorption loading at high pressure. In addition, an empirical three-parameter Tóth isotherm (isotherm 5 in Table 1) is commonly used to correlate the adsorption equilibrium data of zeolites. The heterogeneity parameter n in isotherms 4 and 5 in Table 1 can be regarded as the parameter characterizing the system heterogeneity, which could stem from the adsorbent or the adsorbate, or both (Do 1998). If the parameter n has the value of one, the Sips and Tóth isotherms reduce to the Langmuir isotherm. Deviations from unity, on the other hand, indicate that the system is heterogeneous.

The temperature dependency of adsorption isotherms (see Table 1) is frequently represented by the adsorption equilibrium parameter b_i. The temperature dependency of b_i is often described using the van't Hoff type equation (Zhu *et al.* 2006)

$$b_i = b_{i,0} e^{\frac{-\Delta H_i^{\text{ads}}}{RT}}, \tag{5}$$

where $b_{i,0}$ is the adsorption equilibrium constant and ΔH_i^{ads} is the heat of adsorption reflecting the degree of adsorption strength in the adsorbent. As adsorption is an exothermic process, adsorption loading q_i decreases as the temperature increases.

As can be seen in Table 1, isotherms 6 and 7 include the ratio of pressure to the saturated vapor pressure of a component, P/P_i^{sat}. The theory of Brunauer-Emmet-Teller (BET, isotherm 6 in Table 1) was developed to describe multilayer adsorption. BET is used mainly in the determination of the surface area of finely-divided and porous materials (Sing *et al.* 1985). The validity range of the BET isotherm is approximately between the relative pressure values of 0.05 and 0.30. In addition to the temperature dependency of the vapor pressure, the affinity coefficient c_i in the BET isothem (isotherm 6 in Table 1) is dependent on the temperature.

The basis for having the P/P_i^{sat} relation in the Dubinin-Radushkevich (D-R) isotherm (isotherm 7 in Table 1) is the adsorption potential theory originally

presented by Polanyi, and further developed by Dubinin. The theory states that the adsorbed amount of a component is a function of the adsorption potential ε (Ruthven 1984, Wood 2001)

$$q_i = f(\varepsilon) = f\left(RT \ln\left[\frac{P_i^{\text{sat}}(T)}{P} \right] \right). \tag{6}$$

The utility of the D-R isotherm is that the temperature dependency is reflected in the adsorption potential, i.e., if the adsorption data at different temperatures are plotted as the logarithm of the amount adsorbed vs. the square of the adsorption potential, all the data points should fall into one curve called the characteristic curve (Nguyen & Do 2001). The D-R isotherm is generally applicable for systems involving only van der Waals forces (non-polar systems), being particularly useful for adsorption on activated carbon (Chen & Yang 1994). However, it does not perform well in solids having fine micropores, such as molecular sieving carbon and zeolites (Do 1998).

2.2.2 Mixture adsorption

Mixture adsorption measurements are much more complicated, tedious and error-prone than single component measurements (Talu 2011). Yet, multi-component adsorption knowledge is crucial as typical industrial applications of adsorption involve mixtures. Thus, typically only single-component isotherms are determined experimentally, and mixture adsorption is then predicted by multicomponent adsorption isotherms or adsorption models based on adsorbed solution theory (AST), for example.

The simplest mathematical function to account for multicomponent adsorption is the extended Langmuir isotherm, which gives the adsorbed amount of species *i* in the multicomponent system as

$$q_i = \frac{q_i^{\text{sat}} b_i p_i}{1 + \sum_{j=1}^{N} b_j p_j}, \quad i, j = 1, 2, \ldots, N. \tag{7}$$

The extended Langmuir isotherm, however, is applicable only when the saturation loadings of the mixture components are identical, as otherwise Eq. (7) is not thermodynamically consistent (Krishna 2001). Thus, for the general case of

unequal saturation loadings, it is better to use models based on the adsorbed solution theory.

Myers and Prausnitz (1965) were the first to propose the usage of AST in the description of multicomponent adsorption. The basis of AST is that the bulk fluid phase and the adsorbed phase are in thermodynamic equilibrium. On the basis of AST, two different approaches have been formulated: the real adsorbed solution theory (RAST) and the ideal adsorbed solution theory (IAST). The main difference between RAST and IAST is that in IAST the adsorbed phase is assumed to be ideal whereas in RAST the deviations of the adsorbed phase from ideal behavior are taken into account. The relationship between the phases can be formulated based on AST as

$$y_i P = \gamma_i^{\text{ads}} x_i^{\text{ads}} P_i^0(\pi)\,, \tag{8}$$

where y_i is the gas phase mole fraction, γ_i^{ads} is the adsorbed phase activity coefficient (in IAST the adsorbed phase is considered ideal, i.e. $\gamma_i^{\text{ads}} = 1$), and x_i^{ads} is the adsorbed phase mole fraction of component i. π is the mixture spreading pressure, and P_i^0 is the hypothetical pressure of the pure component that gives the same spreading pressure on the surface as that of the mixture. The spreading pressure is a thermodynamic variable, which cannot be measured directly. According to AST, the relationship between the spreading pressure and pure component adsorption isotherms can be represented as

$$\frac{\pi A}{RT} = \int_0^{P_1^0} \frac{q_1}{P_1} dP_1 = \int_0^{P_2^0} \frac{q_2}{P_2} dP_2 = \ldots = \int_0^{P_i^0} \frac{q_i}{P_i} dP_i, \tag{9}$$

where A is the specific surface area of the adsorbent. The sum of the mole fractions in the adsorbed phase must naturally equal one:

$$\sum_{i=1}^{N} x_i^{\text{ads}} = 1\,. \tag{10}$$

When the adsorbed phase is considered to behave non-ideally and RAST is applied, the activity coefficients can be estimated, in principle, using correlations with similar mathematical formulation as is used for vapor-liquid equilibrium, e.g., the Wilson activity coefficient model. However, in the estimation of the activity coefficients of the adsorbed phase using correlations for vapor-liquid equilibrium, the spreading pressure is not taken into account (Sochard *et al.* 2010). The application of RAST is limited because of the uncertainty in the activity coefficient calculation of the adsorbed phase (Do 1998).

Based on the knowledge of the pure component adsorption isotherms together with the bulk gas composition and system pressure, the values for P_i^0 and x_i^{ads} for each component in the mixture can be determined using Eqs (8)–(10). When IAST is applied in the description of mixture adsorption, or when RAST is applied assuming that adsorbate-adsorbate interactions prevail with respect to adsorbate-adsorbent interactions, the adsorption loadings can be calculated using

$$\frac{1}{q_{\text{tot}}} = \sum_{i=1}^{N} \frac{x_i^{\text{ads}}}{q_i^0}, \tag{11}$$

where q_{tot} is the total adsorbed amount and q_i^0 is the amount of component i adsorbed at the reference state, and is thus obtained with the pure component adsorption isotherm equation applied to P_i^0.

IAST and RAST are not limited to any particular pure component adsorption isotherm, being suitable also for the description of various adsorbent-adsorbate systems, e.g., an adsorbate mixture having unequal saturation loadings on the adsorbent. The ideal solution concept has been used a lot in predicting mixture adsorption.

2.2.3 Diffusion

Diffusion in micropores is dominated by interactions between the diffusing molecules and the pore wall (Kärger & Ruthven 1992). Diffusion in zeolites takes place mostly in the configurational regime (Xiao & Wei 1992) by configurational diffusion, also often referred to as activated surface diffusion. Physically adsorbed molecules are relatively mobile, and adsorbates can be considered as jumping from site to site in the zeolite pores. Thus, the different diffusion rates of molecules in zeolite pores is based partly on adsorption. The driving force for diffusion through the zeolite membrane is the chemical potential gradient of the component. Jumping from one site to another requires a molecule to surmount an energy barrier, i.e., surface diffusion is an activated process. The temperature dependency of surface diffusion can be represented according to the Arrhenius equation as (Kärger & Ruthven 1992)

$$D_i = D_i^0 \exp\left(\frac{-E_i^{\text{dif}}}{RT}\right), \tag{12}$$

where D_i is the diffusivity of component i, D_i^0 a pre-exponential factor and E_i^{dif} the activation energy of diffusion. Larger molecules generally have larger activation energies of diffusion than smaller molecules (Xiao & Wei 1992).

In addition to adsorption and surface diffusion, separation may, in the case of zeolite membranes, also occur through molecular sieving, where smaller molecules can fit into zeolite pores while larger molecules have difficulties (see Fig. 4).

Diffusivity is a measure of the mobility of individual molecules. Due to the small pore sizes of zeolites, the diffusivities of molecules with different sizes may differ by orders of magnitude (Xiao & Wei 1992). Knowledge of diffusivities is essential in evaluating the mass transfer of components through a zeolite film. However, most diffusion studies have been performed with permanent gases (Bowen *et al.* 2004). Thus, diffusivities have not been measured comprehensively for molecules used in pervaporation.

Different techniques have been employed in determining component diffusivities in zeolites. Mass transfer can result from a concentration gradient and Brownian molecular motion, i.e. transport diffusion and self-diffusion, respectively (Kärger & Ruthven 1992). Therefore, the mobility of molecules can be measured on microscopic scale at equilibrium conditions, that is, without the application of a concentration gradient by either pulsed field gradient nuclear magnetic resonance (PFG NMR) (Bussai *et al.* 2002, Caro *et al.* 1986) or quasi-elastic neutron scattering (QENS) (Demontis *et al.* 2009), yielding self-diffusivities. Microscopic techniques measure the diffusivities on a length scale smaller than the individual crystals. Self-diffusivities can also be obtained from theoretical grounds by molecular dynamics (MD) simulations (Ari *et al.* 2009, Bussai *et al.* 2002).

In contrast to steady-state measurements, transient measurements contain information of both adsorption and diffusion (Gavalas 2008). In powder uptake measurements, for example, where the adsorption equilibrium quantity of the adsorbate on the adsorbent is measured, the uptake rates can be used to estimate the intracrystalline diffusion coefficient (Kärger & Ruthven 1992). Besides uptake-measurements (Nayak & Moffat 1988, Zhang *et al.* 2013), non-equilibrium macroscopic techniques also include e.g. chromatographic techniques (Lin & Ma 1988). Since in macroscopic methods, the whole transport process from the surrounding phase into the porous solid is considered, macroscopic techniques generally measure transport diffusivities. Typically, packed beds are investigated rather than individual particles, or much less membranes. Gardner and coworkers (Gardner *et al.* 2002a, Gardner *et al.* 2004) developed a transient method to estimate simultaneously membrane thickness as well as adsorption and diffusion

parameters in a gas/membrane system with a two-step procedure for thick membranes. Another macroscopic method in determining diffusion coefficients has been the application of Maxwell-Stefan (MS) modeling to steady-state gas permeation through zeolite membranes (Kangas *et al.* 2013, Kapteijn *et al.* 1995).

At zero loading, self-diffusivity, transport-diffusivity and MS diffusivity should equal one another (Paschek & Krishna 2001). Unfortunately, the diffusivities determined by different techniques vary quite considerably. Kapteijn *et al.* (1995), for example, tabulated the reported diffusivities for alkanes and alkenes for silicalite-1, having orders of magnitude differences in the diffusivity values obtained using various techniques. Generally, the component diffusivities determined by the microscopic techniques or MD simulations can be several magnitudes higher than those measured by macroscopic methods.

2.3 Modeling of mass transfer in pervaporation using zeolite membranes

Mathematical modeling is an indispensable tool in process design and optimization, as well as for the purpose of the performance evaluation of process alternatives. Modeling the mass transfer could lead to a better understanding of the phenomena occurring in the pervaporation process, allowing predictions of fluxes and selectivities.

The separation in pervaporation using inorganic membranes is generally based on adsorption and diffusion. Adsorption-diffusion theory basically divides pervaporation into a few consecutive steps: adsorption on the membrane surface, diffusion through the zeolite film, desorption as a vapor on the other side of the membrane, and combined diffusion and bulk flow through the support layer (see also Fig. 2). Modeling of the mass transfer through pervaporation membranes requires the consideration of these steps. Desorption on the permeate side of the membrane is typically fast, and thus generally not considered in modeling (Bettens *et al.* 2005). Moreover, the flow through the support layer is also mostly omitted, and the focus of modeling is on the phenomena occurring in the separation layer.

Both empirical and more theoretical approaches to model pervaporation have been developed, with the empirical models being less complex than the theoretical models (Lipnizki & Trägårdh 2001). The models for mass transfer in pervaporation are mostly semi-empirical, combining features of both the theoretical and empirical approaches. In semi-empirical models, typically the permeation-related effects such as adsorption and diffusion effects are summarized in empirical parameters.

Thus, these types of models rely heavily on experiments as experimental data is required to determine certain parameters for the models. However, often the semi-empirical models may still provide the desired depth especially for process and module design (Lipnizki & Trägårdh 2001).

Wijmans & Baker (1993) showed that, based on a solution-diffusion model for polymeric membranes, a component flux can be described by multiplying the normalized permeation flux or permeance by the driving force, i.e., the fugacity difference across the membrane

$$J_i = Q_i \left(x_i \gamma_i P_i^{\text{sat}} - y_i P_{\text{perm}} \right) = Q_i \left(f_{i,\text{feed}} - f_{i,\text{perm}} \right), \tag{13}$$

where Q_i is the permeance of component i, x_i is the mole fraction, γ_i the activity coefficient of component i in the liquid feed, P_{perm} is the permeate pressure and $f_{i,\text{feed}}$ and $f_{i,\text{perm}}$ are the feed and permeate fugacities. As adsorption-diffusion model for inorganic membranes is analogous to solution-diffusion model for polymeric membranes, similar models can be applied to describe transport through inorganic membranes. The model shown in Eq. (13) has been applied to the description of pure component transport through microporous silica membranes (de Bruijn *et al*. 2007), dehydration of alcohols with LTA-type zeolite membranes (Sommer & Melin 2005) and also for the removal of ethanol from aqueous streams by multi-channel MFI zeolite membranes (Kuhn *et al.* 2009b).

Eq. (13) does not require any additional information about the affinity (adsorption) and diffusivity of permeating species in the membrane film as those effects are combined into a single permeance term. In order to be able to describe the adsorption and diffusion more precisely, information regarding the material properties and adsorption behavior of the components in the material, for instance, should be known. Detailed modeling could offer a good insight into the transport mechanisms, which in turn is crucial in the design and development of membranes, as well as pervaporation-based processes. In detailed models the parameters are generally more fundamental than in semi-empirical models, i.e., the parameters have a physical meaning.

Krishna (1990) proposed the application of a generalized Maxwell-Stefan (GMS) formulation to surface diffusion. Since then, GMS has been successfully applied in modeling gas permeation of both a single component and mixtures through zeolite membranes (Kangas *et al.* 2013, Kapteijn *et al.* 1995, Zhu *et al.* 2006). However, application of Maxwell-Stefan (MS) modeling in pervaporation using zeolite membranes, is not very common; it is generally limited to the

dehydration of alcohols using LTA or DDR zeolite membranes where simplifications to the MS equations are possible on the basis of the assumption that the interactions between the adsorbed molecules are of negligible importance (Kuhn *et al.* 2009a, Pera-Titus *et al.* 2008). It is a little controversial that, despite the active research work in developing alcohol-selective zeolite membranes for alcohol concentration from fermentation broths (Chen *et al.* 2007, Kosinov *et al.* 2014, Negishi *et al.* 2002, Sebastian *et al.* 2010), the pervaporation process using hydrophobic zeolite membranes has not been modeled using the Maxwell-Stefan formulation.

The general form of GMS equations applied to surface diffusion for an *n*-component system is given as (Kapteijn *et al.* 2000)

$$-\rho\frac{\theta_i}{RT}\nabla\mu_i = \sum_{j=1,j\neq i}^{n}\frac{q_j J_i - q_i J_j}{q_i^{sat} q_j^{sat} Đ_{ij}} + \frac{J_i}{q_i^{sat} Đ_{i,z}},\ i = 1,2,\ldots,n. \tag{14}$$

where J_i is the molar flux of component i and ρ is the zeolite density, which is 1760 kg m^{-3} for high-silica MFI zeolite (Farhadpour & Bono 1996). Eq. (14) defines two types of MS diffusivities: $Đ_{i,z}$ and $Đ_{i,j}$. $Đ_{i,z}$ represents single-component surface diffusivity, i.e. adsorbate-adsorbent interactions, whereas $Đ_{i,j}$ represents interexchange diffusivity between species i and j, i.e., adsorbate-adsorbate interactions. Thus, the first term on the right side of Eq. (14) describes the friction from the interaction between the adsorbed molecules and the last term the friction between the molecule and the zeolite.

The chemical potential gradient can be related to the surface coverage by the thermodynamic matrix [Γ] as

$$\frac{\theta_i}{RT}\nabla\mu_i = \sum_{j=1}^{n}\Gamma_{ij}\nabla\theta_j\ , \tag{15}$$

$$\text{where } \Gamma_{ij} = \theta_i\frac{\partial \ln f_i}{\partial\theta_j}\ \ i,j = 1,2,\ldots,n\ . \tag{16}$$

The thermodynamic factor Eq. (16) includes the partial derivative of fugacity f_i with respective to coverage θ_i, i.e., thermodynamic factor is closely related to adsorption. Thus, the thermodynamic factor can be determined on the basis of the adsorption isotherm, which relates the surface coverage to fugacity. The elements of Γ_{ij} can be determined from the models describing mixture adsorption, e.g. IAST. The analytical solution of the thermodynamic factor for some pure component

adsorption isotherms is possible (Lito *et al.* 2011). When the Langmuir isotherm is applied, the thermodynamic factor is reduced to

$$\Gamma_i = \frac{1}{1-\theta_i} . \tag{17}$$

As can be seen in Eq. (17), the thermodynamic factor increases as the coverage increases.

The MS diffusivity $Đ_{i,z}$ has frequently been assumed to be independent of coverage when modeling gas permeation through zeolite membranes (Gardner *et al.* 2002a, Li *et al.* 2005, Nagumo *et al.* 2001, Zhu *et al.* 2006). The assumption of coverage independence has also been used in modeling pervaporation of water and ethanol using hydrophilic LTA membranes (Guo *et al.* 2011). When $Đ_{i,z}$ is assumed to be independent of coverage, it is equal to the limiting value of zero loading as

$$Đ_{i,z} = Đ_{i,z}(0) , \tag{18}$$

where $Đ_{i,z}(0)$ is the zero-loading MS diffusivity of component *i*.

$Đ_{i,z}$ can also be considered dependent on the fractional surface coverage within the zeolite so that a molecule can only migrate from one site when the receiving site is vacant. Several molecular simulation studies (Chempath *et al.* 2004, Krishna & Van Baten 2005, Paschek & Krishna 2000, Skoulidas & Sholl 2002) have been carried out to evaluate the coverage-dependency for a variety of components in various zeolites. It has been shown that the $Đ_{i,z}$ changes as a function of fractional surface coverage. In many studies $Đ_{i,z}$ has been shown to vary linearly with loading, but not necessarily throughout the whole fractional surface coverage area (Chempath *et al.* 2004). Without experimental evidence, however, $Đ_{i,z}$ can be assumed to depend linearly on the vacant sites as

$$Đ_{i,z} = Đ_{i,z}(0)(1-\theta_{tot}) , \tag{19}$$

where the total coverage is

$$\theta_{tot} = \sum_{i=1}^{n} \theta_i . \tag{20}$$

Linearly coverage-dependent MS diffusivity has been applied, e.g., in the modeling of dehydration of water/ethanol mixtures by pervaporation (Pera-Titus *et al.* 2006, Pera-Titus *et al.* 2008).

The MS interexchange coefficient $Đ_{i,j}$ represents the capability of the adsorbed component *i* to replace the adsorbed component *j*. There are no fundamental models to predict $Đ_{i,j}$ (Krishna & Paschek 2000). Krishna (1990) proposed a procedure to estimate binary correlations based on the generalization of the empirical Vignes (1966) relation developed originally for bulk liquid mixture diffusion. For the determination of $Đ_{i,j}$ in the diffusion of adsorbed species the mole fractions are replaced with fractional surface coverages as

$$Đ_{i,j} = \left[Đ_{i,z}\right]^{\theta_i/(\theta_i+\theta_j)} \left[Đ_{j,z}\right]^{\theta_j/(\theta_i+\theta_j)} . \qquad (21)$$

Thus, the value of $Đ_{i,j}$ falls in between the values of $Đ_{i,z}$ and $Đ_{j,z}$.

The strength of Maxwell-Stefan modeling in comparison to semi-empirical modeling (see e.g. Eq. (13)) is that it comprises both intracrystalline diffusion as well as adsorption, and all the parameters applied have a physical meaning. In addition, mixture permeation through zeolite membranes can be predicted by incorporating the following properties in the Maxwell-Stefan formulation:

- single component adsorption isotherms with IAST
- single component surface diffusivities with Eq. (21).

This approach has been applied to gas separation modeling using zeolite membranes (Kapteijn *et al.* 1995, Van De Graaf *et al.* 1999, Zhu *et al.* 2006), and can also be applied to pervaporation modeling using zeolite membranes.

3 Materials and methods

3.1 Synthesis and properties of composite membranes

The zeolite membranes employed in the study were prepared and characterized by Prof. Jonas Hedlund's group at Luleå University of Technology. The high-silica MFI zeolite membranes (film thickness is approximately 0.5 μm as detected by SEM) were prepared using the seeding method and support masking procedure described in detail in Hedlund *et al.* (2002), Hedlund *et al.* (2003), and briefly in Paper I.

The MFI zeolite membranes synthesized similarly to the membranes applied in this study, have a Si/Al ratio of 139 (Sandström *et al.* 2010). Thus, the high-silica MFI membranes considered in this work can be classified as hydrophobic (Zhang *et al.* 2012a). Similar membranes as used in this study have been shown to be reproducible and isomer selective (Hedlund *et al.* 2002), and very efficient in various gas separation applications (Hedlund *et al.* 2009, Lindmark & Hedlund 2010, Sandström *et al.* 2010).

The zeolite membranes prepared by Prof. Jonas Hedlund's group are characterized typically by *n*-hexane/helium permporometry (Hedlund *et al.* 2009). The membranes have low amount of detectable flow-through defects (Hedlund *et al.* 2003, Korelskiy *et al.* 2012). The total amount of defects for membrane M2 used in this study accounted for 0.5% of the total membrane area, and more than 97% of the total relative area of defects consisted of defects smaller than 1 nm. Essentially no defects larger than 4.25 nm were detected by permporometry.

Zeolite X (FAU) membranes (film thickness approximately 1 μm as detected by SEM, crystal phase confirmed with XRD) for ethanol dehydration were prepared using the synthesis method described in Paper VI.

The membranes in this work are referred to as ultra-thin, as in the literature zeolite membranes below 2.5–3 μm are considered ultra-thin membranes (Liu *et al.* 2011b, White *et al.* 2010). Zeolite films were grown on graded α-alumina support discs (Fraunhofer IKTS, Germany) with a diameter of 25 mm. The disc consists of two layers: a thin 30 μm top layer with 100 nm pores and a thicker 3 mm layer with larger 3 μm pores.

As the membrane consists of a microporous selective layer on top of a porous support, the mass transfer through the composite membrane is the overall contribution of both the zeolite film and the support. As discussed in Section 2.2.3,

surface diffusion governed by adsorption controls the transport through the zeolite film. To estimate the mass transfer resistance in the support, the approach presented by de Bruijn *et al.* (2003) was applied, where the Knudsen diffusion and/or viscous flow controls the transport though the zeolite support (see Section 2.1.2). A schematic representation of the composite membrane and the transport mechanisms considered in this work is given in Fig. 5.

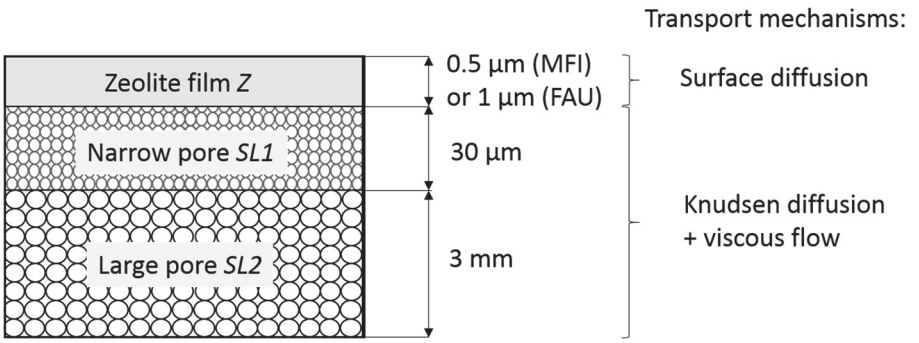

Fig. 5. Zeolite membrane on a graded support. SL1 denotes support layer 1 and SL2 support layer 2.

The Knudsen structural parameters (see Eq. (2)) and the effective permeability for the supporting layers (see Eq. (3) and Paper VI) are shown together with the zeolite film characteristics in Table 2.

Table 2. Characteristics of the composite zeolite (MFI/FAU) membrane.

Parameter	zeolite	α-alumina support	
	film	SL1	SL2
l *(m)*	500 x 10^{-9} (MFI) / 1000 x 10^{-9} (FAU)	30 x 10^{-6}	3 x 10^{-3}
d_{pore} *(m)*	0.55 x 10^{-9} (MFI) / 0.74 x 10^{-9} (FAU)	100 x 10^{-9}	3 x 10^{-6}
K_s *(m)*		2.94 x 10^{-9}	2.04 x 10^{-7}
$B_{0,s}^{eff}$ *(m²)*		1.45 x 10^{-16}	6.46 x 10^{-13}

SL1 denotes support layer 1 and SL2 support layer 2

3.2 Pervaporation experiments

Pervaporation experiments of aqueous solutions of ethanol and *n*-butanol were carried out using the pervaporation experimental set-up presented in Fig. 6.

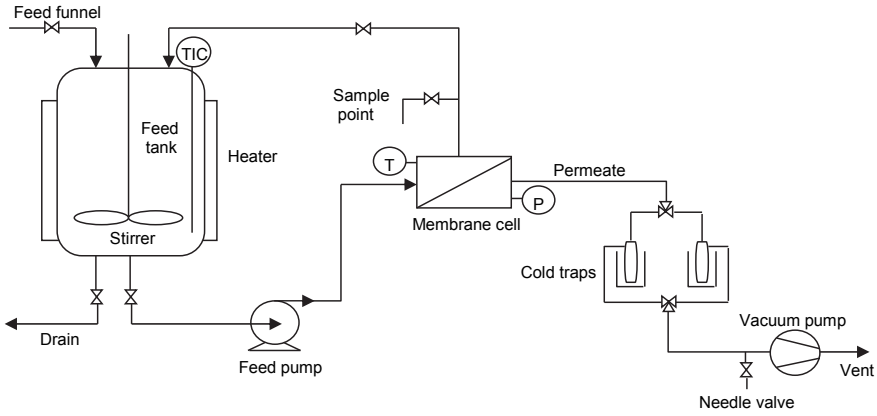

Fig. 6. Pervaporation equipment.

The membrane was sealed in a stainless steel cell with the zeolite film facing the feed side. Liquid feed was pumped to the membrane cell at a flow rate of approximately 0.7 kg min^{-1} from a feed tank containing approximately 3 liters of feed mixture, and the retentate, i.e., the flow retained by the membrane, was recirculated back to the feed tank.

The experiments were carried out at feed temperatures in a range of 30–70 °C. The temperature of the feed tank was kept at the desired value with a heating jacket connected to a temperature control system. The piping as well as the membrane cell was insulated in order to minimize heat losses. The temperature of the cell was monitored by a thermocouple.

Pervaporation deals typically with components of less than 10 wt.% of the liquid mixtures. The feed compositions were selected on the basis of typical alcohol concentrations in fermentation broths in the case of hydrophobic membranes. For hydrophilic membranes the feed composition, on the other hand, was selected on the basis of the typical composition for ethanol dehydration. In the case of MFI membranes, the binary ethanol/water solutions had 5/7.5/10 wt.% of ethanol and the binary *n*-butanol/water solution had 3 wt.% of *n*-butanol (Papers I and II). In the case of hydrophilic zeolite X (FAU) membranes (Paper VI) the feed was 90/10 wt.% ethanol/water mixture. The composition change in the feed was not considered as the permeate flux was insignificant both in comparison to the total feed volume and feed flow rates of individual components.

After start-up, the system was allowed to equilibrate in order to attain steady-state conditions. The permeate side pressure was kept low with a vacuum pump,

the pressure staying below 24 mbar in all the experiments. The permeate samples, i.e., the flow that traverses the membrane, were collected in liquid nitrogen cold traps. There were two condensation loops in order to enable continuous operation. Several samples were taken at each experimental temperature. The samples were defrosted and weighed, and the steady-state pervaporation flux was determined as

$$J = \frac{m}{At}, \tag{22}$$

where m is the mass of the permeate sample, t is the sampling time, and A is the effective membrane area for permeation, which for the membranes studied was 3.14×10^{-4} m^2.

The composition of samples was analyzed off-line by gas chromatography (Agilent Technologies 6890N Network GC System) equipped with a flame ionization detector. In the case of the *n*-butanol experiments, the two-phase permeate sample was diluted with Milli-Q water prior to the analysis in order to obtain a homogeneous sample. The separation factor was determined as the ratio of component weight fractions in the permeate to those in the feed as

$$\alpha_{i/j} = \frac{w_{i,\text{perm}} / w_{j,\text{perm}}}{w_{i,\text{feed}} / w_{j,\text{feed}}}, \tag{23}$$

where $w_{i,\text{perm}}$ and $w_{j,\text{perm}}$ are the weight fractions of components i and j in the permeate, and $w_{i,\text{feed}}$ and $w_{j,\text{feed}}$ are the weight fractions of components i and j in the feed, respectively.

Both the separation factor and the pervaporation flux are generally applied to evaluate the membrane performance. However, both factors yield only a partial view of the membrane overall performance. Therefore, Huang & Yeom (1990) introduced pervaporation separation index PSI (kg m^{-2} h^{-1}) to facilitate simultaneous evaluation of the effects of both the flux and separation factor. PSI was originally defined as the total flux multiplied by separation factor. Later, to exclude the effects of a membrane with no separation ($\propto = 1$), PSI has been modified to

$$\text{PSI} = J(\alpha - 1). \tag{24}$$

However, PSI is can be considered only as a pragmatic attempt to evaluate flux and separation factor simultaneously. Nevertheless, PSI is usable, e.g., when similar membranes are compared. For adequate process evaluation, however, modeling of the pervaporation process is needed.

3.3 Modeling

The present work includes both experimental work and modeling. The Antoine equation, with parameters from Poling *et al.* (2001), was used to determine the saturated vapor pressures of ethanol, *n*-butanol and water. Other equations and corresponding parameters for calculating the saturated vapor pressures were also used in Papers III and IV. The choice of P_i^{sat} representation was done on the basis of the validity-range of P_i^{sat} formulation and its parameters with respect to temperature.

The viscosity for the permeate vapor and the activity coefficients of the components in the feed mixture were obtained with Aspen Plus, a commercial simulation software. The Wilson property package was used for ethanol/water mixtures as the Wilson activity coefficient model is suitable for liquid-phase non-idealities. For the *n*-butanol/water mixtures, the NRTL model (LLE-Aspen) was used, as it is also suitable for immiscible systems.

The parameters for the semi-empirical mass transfer models (Paper II, Section 4.3), pure component adsorption isotherms (Papers III and IV, Section 4.4) and diffusion parameters (Paper V, Section 4.5) were determined by non-linear regression minimizing the sum of squares of the difference between the model and experimental data, using the optimization routine *lsqcurvefit* of Matlab. The non-linear equation set formed for IAST calculations by Eqs. (8)–(10) was solved using the Matlab *fsolve* routine (Paper IV, Section 4.4.2).

4 Results

4.1 Performance of ultra-thin zeolite membranes in alcohol/water separations

In Papers I and VI the pervaporation performance of ultra-thin MFI and FAU membranes are evaluated for the first time for the separation of aqueous mixtures of ethanol and *n*-butanol. Ethanol/water pervaporation using hydrophobic high-silica MFI membranes is discussed in Section 4.1.1 and dehydration by pervaporation using hydrophilic zeolite X (FAU) membranes in Section 4.1.2. *n*-Butanol recovery using hydrophobic MFI membranes is discussed in Section 4.1.3.

4.1.1 Ethanol/water pervaporation using high-silica MFI membranes (Papers I and II)

During the past decades, efforts have been made to develop various membrane materials for separating ethanol from fermentation broths. The reported fluxes for ethanol/water separation by pervaporation using the most common polymeric membranes, poly(dimethyl siloxane) (PDMS) membranes, are mostly below 1 kg m^{-2} h^{-1} (Beaumelle *et al.* 1993, Chovau *et al.* 2011, Gaykawad *et al.* 2013, Li *et al.* 2004, Rozicka *et al.* 2014); the ethanol/water separation factor ($\alpha_{EtOH/water}$) often being a little above or below 10 (Lee *et al.* 2012, Vane 2005). The modification of PDMS membranes with fillers (e.g. hydrophobic zeolites), referred to as mixed matrix membranes, has also been studied. Typically the ethanol/water separation factors of hydrophobic polymer/zeolite mixed matrix membranes are somewhat higher than those of polymer membranes, with the fluxes remaining mostly below 1 kg m^{-2} h^{-1} (Peng *et al.* 2011, Shirazi *et al.* 2012, Vane *et al.* 2008).

For organic removal from aqueous streams by pervaporation using zeolite membranes, high silica MFI membranes have been studied the most due to their hydrophobic properties and well-defined pore size. The performance of the MFI membranes used in this study in ethanol/water separation are reported in Table 3 together with other reported ethanol/water pervaporation performances using high-silica MFI membranes for comparison. M1 and M2 in Table 3 refer to the membranes used in Paper I and M3 to the membrane used in Paper II.

Table 3. Pervaporation performance of high-silica MFI zeolite membranes in the separation of ethanol/water mixtures (results from this study bolded).

T (°C)	Feed EtOH (wt.%)	Flux (kg $m^{-2}h^{-1}$)	Separation factor ($EtOH/H_2O$)	PSI (kg $m^{-2}h^{-1}$)	Membrane thickness (μm)	Support	Reference
25	5	0.07	10	0.6	80–90	SS-tube	Tuan *et al.* 2002
30:M1	**10**	**1.9**	**4.4**	**6.5**	**0.5**	**α-disc**	**this study, Paper I**
30:M2	**10**	**2.4**	**4.4**	**8.2**	**0.5**	**α-disc**	**this study, Paper I**
30:M3	**10**	**2.0**	**4.4**	**6.8**	**0.5**	**α-disc**	**this study, Paper II**
30:M3	**5**	**2.0**	**5.8**	**9.6**	**0.5**	**α-disc**	**this study, Paper II**
30	4	0.24 (ave)	39 (ave)	9.1	-	SS-support	Matsuda *et al.* 2002
30	4	0.55 (ave)	28 (ave)	14.9	-	SS-support	Ikegami *et al.* 1997
30	4	0.6	63	37.2	460	SS-disc	Sano *et al.* 1995b
30	4.65	ca. 0.6	64	37.8	400	SS-support	Nomura *et al.* 1998
30	4	0.22	59	12.8	-	SS-disc	Sano *et al.* 1997
30	4	0.19	4.2	0.6	-	α-disc	Sano *et al.* 1997
32	9.7	0.1	11.5	1.1	-	γ-tube	Liu *et al.* 1996
40	5	0.81	99.8	80.0	50	titania-tube	Weyd *et al.* 2008
45	5	1.5	54	79.5	~5[a](2-sided)	α-capillary	Sebastian *et al.* 2010
60:M1	**10**	**8.5**	**4.8**	**32.3**	**0.5**	**α-disc**	**this study, Paper I**
60:M2	**10**	**10.7**	**4.2**	**34.2**	**0.5**	**α-disc**	**this study, Paper I**
60:M3	**10**	**9.6**	**4.8**	**36.5**	**0.5**	**α-disc**	**this study, Paper II**
60:M3	**5**	**8.7**	**6.6**	**48.7**	**0.5**	**α-disc**	**this study, Paper II**
60	5	4.02	30	116.6	10–30	SS-tube	Lin *et al.* 2001
60	5	1.81	89	159.3	10–30	α-tube	Lin *et al.* 2001
60	5	0.93	106	97.7	10–30	mullite tube	Lin *et al.* 2003
60	5	1.51	39	57.4	10	α-tube	Shen *et al.* 2011
60	5	2.9 (ave)	12.3 (ave)	32.8	0.5–5	α-HF	Kosinov *et al.* 2014
60	5	1.91	66	124.2	10	mullite tube	Zhang *et al.* 2012b
60	3	2.9	66	188.5	12	α-HF	Shan *et al.* 2011
60	5	7.4	47	340.4	3	YSZ-HF	Shu *et al.* 2012
60	5	4.0	11	40.0	5	α-HF	Shu *et al.* 2012
60	5	1.82	62	111.0	3.5	α-tube	Peng *et al.* 2013
60	5	~1.3	~85	109.2	~5	α-tube	Peng *et al.* 2014
70	9.4	2.1	1.3	0.6	2	α-tube	Algieri *et al.* 2003
70:M3	**10**	**14.0**	**5.8**	**67.8**	**0.5**	**α-disc**	**this study, Paper II**
75	5	5.4	54	286.2	12	α-HF	Shan *et al.* 2011
75	5	1.2	43	50.4	-	SS-tube	Stoeger *et al.* 2011
80	3	1.35 (ave)	69 (ave)	91.8	30	silica tube	Chen *et al.* 2007

Where ave is average; SS is stainless steel; α is α-alumina; γ is γ-alumina; YSZ is yttria stabilized zirconia; HF is hollow fiber; [a] denotes the total thickness of membrane on both support sides

M1 and M2 denotes membranes used in Paper I and M3 the membrane used in Paper II

As shown in Table 3, the reported ethanol/water separation factors range from 1.3 to 106. High separation factors are often accompanied by rather low flux, as the membranes having a separation factor above 40 display mostly fluxes of below 0.5 kg m^{-2} h^{-1} at 30 °C, and typically below 2 kg m^{-2} h^{-1} at higher temperatures as shown in Table 3.

The high-silica MFI membranes studied in this work display a higher pervaporation flux than that previously reported. The high flux of the studied membranes is attributed to the lower zeolite film thickness of the synthesized membranes compared to the other reported fluxes for thicker high-silica MFI membranes. However, the ethanol/water separation factors of this work are mostly poorer than those reported for other high-silica MFI membranes. Fig. 7 shows the flux and separation factor for ethanol/water mixtures using the studied membranes as a function of temperature at different feed compositions (5/7.5/10 wt.% ethanol). The data points in Fig. 7 are the mean values of the samples with the same experimental conditions; the error bars represent the standard deviations between the replicates.

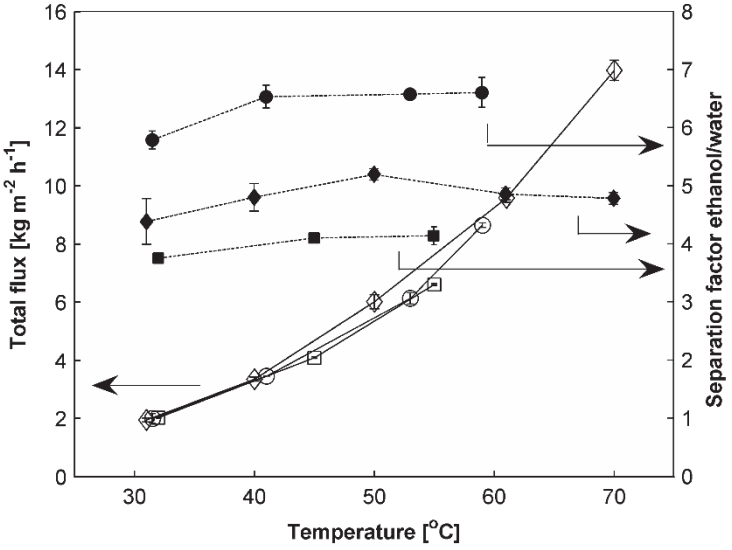

Fig. 7. Total flux (open symbols) and ethanol/water separation factor (filled symbols) as a function of temperature for ethanol/water pervaporation experiments at different feed compositions: (o) 5 wt.% ethanol, (□) 7.5 wt.% ethanol, and (◊) 10 wt.% ethanol. The lines are guidance for the eye. (Paper II)

Typically, the permeation flux through the membrane increases exponentially with increasing temperature (Sommer & Melin 2005), as can also be seen in Fig. 7. This is due to the strong influence of temperature on the saturated vapor pressure P_i^{sat}, and thus on the feed side fugacity (see Eq. (13)).

As shown in Fig. 7, there is a slight temperature-dependency of the separation factor for each feed composition: the selectivity first slightly increases as the temperature increases and then rather stabilizes as the temperature is further increased. However, the temperature-effect is so minor that the ethanol/water separation factor can be considered basically independent of temperature in the investigated conditions. In pervaporation, the adsorption and diffusion of the components in the zeolite film as well as the driving force for mass transfer are influenced by temperature. Thus, the overall effect of temperature on membrane separation is a result of the combination of all these factors.

As ethanol is a larger molecule than water, it should have a lower diffusivity in zeolites than water. Thus, in pervaporation using zeolite membranes, diffusion favors water permeation. Larger molecules typically have a larger activation energy of diffusion than small molecules (Bowen *et al.* 2003). This implies that the ethanol diffusivity should increase more with temperature than water diffusivity (see Eq. (12)). Hence, the diffusion rate of ethanol should increase more with increasing temperature than the diffusion rate of water.

Components in feed mixtures compete for occupation of vacant adsorption sites. Hydrophobic zeolites preferentially adsorb organics over water. The analysis of adsorption selectivity as a function of temperature is difficult without valid experimental data. This is apparent, as for example the data for heat of adsorption $-\Delta H_i^{ads}$ on high-silica MFI zeolite varies for ethanol from 18 kJ mol^{-1} (Chandak & Lin 1998) to 70 kJ mol^{-1} (Lee *et al.* 1997) and for water from 25.1 kJ mol^{-1} to 50.6 kJ mol^{-1} (Bordat *et al.* 2010).

In contrast to the present study, the ethanol/water separation factor using similar MFI membranes to this study often decreases, even substantially, with increasing temperature, such as in the studies of Lin *et al.* (2001), Matsuda *et al.* (2002), Sano *et al.* (1994), and Kuhn *et al.* (2009b). This type of behavior could be attributed to the defects in the membrane structure (Pera-Titus *et al.* 2006, Tuan *et al.* 2002).

The membranes used have a low proportion of defects of the overall membrane surface, characterized by permporometry (see Section 3.1), the defect distribution being similar to previously reported as-synthesized high-quality MFI membranes (Korelskiy *et al.* 2012). Due to the high quality of the studied membranes, the

ethanol/water separation factors were originally anticipated to be higher. In the absence of larger defects, the explanation for the modest separation factors achieved may basically be caused by the combination of three factors, all of which become significant when the zeolite film is ultra-thin:

- aluminum incorporated from the α-alumina support into the zeolite framework makes the zeolite film less hydrophobic (Geus *et al.* 1992, Shu *et al.* 2012),
- directly undetectable open grain boundaries in the zeolite film (see Fig. 3) serve as water selective pathways (Algieri *et al.* 2003, Sebastian *et al.* 2010),
- the support of the membrane considerably reduces the chemical potential gradient across the zeolite layer (analyzed in Section 4.2).

Despite the masking of the support in zeolite synthesis of the studied membranes, some aluminum is incorporated in the ultra-thin zeolite film (see Section 3.1). Water adsorption in particular has been observed to depend strongly on the Si/Al ratio of the zeolite, although the Si/Al ratio of 140 (approximately the same as the ratio in the membranes studied) is considered to be fairly hydrophobic (Zhang *et al.* 2012a). As it is seen in Table 3, many of the separation factors above 40 have been prepared on aluminum-free substrates. For example, by using an inert YSZ (yttria stabilized zirconia) support, and thus eliminating Al contamination, a relatively high separation factor of 47 for a thin 3 μm zeolite film was obtained (Shu *et al.* 2012). Thicker alumina-supported membranes also have high separation factors (see Table 3). The increased thickness of the membrane reduces the effect of Al incorporation in the membrane (Shu *et al.* 2012).

Achieving high flux, as with the studied membranes, is an advantageous property of a membrane. The potential of the high-flux membranes originates from the fact that the increase of flux, assuming that the separation factor stays on the same level, reduces the capital investment and processing costs. PSI (see Eq. (24)) can be used to roughly compare similar membranes for a certain separation target in comparable conditions. As it can be observed from Table 3, the membranes of this study fall in the middle range in terms of PSI in separating ethanol from aqueous mixtures by pervaporation using high-silica MFI membranes. Although PSI is a decent attempt to compare the membrane performance including the effects of permeation flux and selectivity simultaneously, just selecting a membrane with the highest PSI may not be the optimal choice for the pervaporation process (Chapman *et al.* 2008). In fact, recently Van der Bruggen & Luis (2014) stated that a high-performance membrane in the case of bioethanol purification is a high-flux membrane rather than a highly selective membrane, and that PSI might

underestimate the significance of flux. With the combination of high flux and a decent separation factor, the membranes studied in this work have potential in bioethanol purification. Nevertheless, for adequate process evaluation, proper modeling of the pervaporation process is inevitably needed.

4.1.2 Ethanol dehydration by pervaporation using zeolite X (FAU) membranes (Paper VI)

Anhydrous ethanol is used as a gasoline extender. Pervaporation is considered as a viable, energy-efficient separation method for ethanol dehydration (Cardona Alzate & Sánchez Toro 2006). Although the small-pore LTA zeolite membranes are very well suited for organics dehydration, and have already found industrial application (Morigami *et al.* 2001), they are unstable in high water concentrations (>20 wt.%) due to the dealumination of the zeolite framework (Li *et al.* 2007, Zhang *et al.* 2014). FAU membranes are more hydrothermally stable than LTA membranes (Zhang *et al.* 2014). The separation factors achieved with FAU membranes are not as high as with LTA membranes, but the permeation fluxes are higher with FAU membranes due to the larger pore size of a FAU zeolite (Zhu *et al.* 2009), which makes them attractive for the dehydration of relatively water-rich solutions. However, the pervaporation dehydration using FAU membranes has not been studied extensively. The performance of the ultra-thin zeolite X (FAU) membranes considered in this study in ethanol dehydration by pervaporation are reported in Table 4 together with other reported ethanol-water pervaporation performances with similar membranes for comparison.

As the pervaporation temperature was increased, the pervaporation flux was increased as expected due to the increase in driving force. As shown in Table 4, the performance of the membranes in this study in terms of flux, separation factor, and PSI is rather similar to that of the thicker membranes reported in the literature.

Table 4. Pervaporation performance of zeolite X membranes in the dehydration of aqueous ethanol (results from this study bolded).

T (°C)	Feed EtOH (wt.%)	Flux (kg $m^{-2}h^{-1}$)	Separation factor (H_2O/EtOH)	PSI (kg $m^{-2}h^{-1}$)	Membrane thickness (μm)	Support	Reference
40–M4	**90**	**1.3**	**256**	**332**	**1**	**α-disc**	**this study, Paper VI**
50–M5	**90**	**1.5**	**410**	**614**	**1**	**α-disc**	**this study, Paper VI**
65–M6	**90**	**3.4**	**296**	**1003**	**1**	**α-disc**	**this study, Paper VI**
65	90	1.48	380	561	7	α-tube	Zhu *et al.* 2008
65	90	1.70	10 000[a]	16998	4–5	α-tube	Zhu *et al.* 2009
75	90	5.5	230	1260	10	α-tube	Sato *et al.* 2007
75	90	1.91	170	323	20–30	cer-tube	Kita *et al.* 2001

Where α is α-alumina; cer is ceramic; M4–M6 are membranes used in Paper VI

[a] denotes being beyond the detection limit of GC

In the case of hydrophilic membranes, the effect of aluminum incorporated in the zeolite structure and the intercrystalline grain boundaries should not have as detrimental effect on pervaporation performance as in the case of hydrophobic membranes (see Section 4.1.1). On the other hand, the contribution of the support may decrease the membrane performance significantly. The effect of the support on membrane performance is analyzed in Section 4.2.

4.1.3 Butanol/water pervaporation using high-silica MFI membranes (Paper I)

Several research groups have focused on butanol recovery from aqueous solutions using polymeric or mixed matrix membranes in pervaporation (Liu *et al.* 2011a, Päkkilä *et al.* 2012, Qureshi *et al.* 2001). The fluxes using polymeric membranes are typically below 0.5 kg m^{-2} h^{-1} with separation factors below 40 (Dong *et al.* 2014). For mixed matrix membranes, the fluxes remain mostly below 1 kg m^{-2} h^{-1} and the separation factor below 50 (Huang *et al.* 2014), although a high butanol/water separation factor of 465 was reported by Negishi *et al.* (2010) for a silicone rubber-coated silicalite membrane, with a low flux of 0.04 kg m^{-2} h^{-1}.

Butanol recovery by pervaporation from dilute solutions using zeolite membranes, on the other hand, had not been studied much before Paper I. The performance of the ultra-thin MFI membranes used in this study in butanol/water separation are reported in Table 5, together with other reported butanol/water pervaporation performances using similar membranes for comparison.

As shown in Table 5, the *n*-butanol/water separation factors in this work are similar to the work of Stoeger *et al.* (2011), although the fluxes of the studied membranes are considerably higher. In general, the earlier reported fluxes of butanol separation in pervaporation using zeolite membranes are considerably lower compared to the studied membranes, which in turn leads to the PSI being higher with the membranes used in this work (see Table 5). Low flux is a limiting factor considering industrial application due to the need for a high membrane area, and because the costs of pervaporation are dominated by membrane units and membrane replacements (Srinivasan *et al.* 2007).

Table 5. Pervaporation performance of MFI zeolite membranes in the separation of *n*-butanol/water mixtures (results from this study bolded).

T (°C)	Feed BuOH (wt.%)	Flux (kg $m^{-2}h^{-1}$)	Separation factor ($BuOH/H_2O$)	PSI (kg m^{-2} h^{-1})	Membrane thickness (μm)	Support	Reference
25	5	0.09	4	0.3	-	SS-tube	Stoeger *et al.* 2011
30:M1	**3**	**1.1**	**4.7**	**4.1**	**0.5**	**α-disc**	**this study, Paper I**
30:M2	**3**	**1.4**	**4.0**	**4.2**	**0.5**	**α-disc**	**this study, Paper I**
30	5	0.02	19	0.4	30	SS	Li *et al.* 2003
60:M1	**3**	**3.6**	**10.2**	**33.1**	**0.5**	**α-disc**	**this study, Paper I**
60:M2	**3**	**6.3**	**7.0**	**37.8**	**0.5**	**α-disc**	**this study, Paper I**
60	5	0.10	8	0.7	-	SS-tube	Stoeger *et al.* 2011
70	2	0.10	150	14.9	>10	α-tube	Shen *et al.* 2011
90	5	0.11	21	2.0	-	SS-tube	Stoeger *et al.* 2011

Where SS is stainless steel; α is α-alumina; γ is γ-alumina; M1and M2 are membranes used in Paper I

In the present work, the *n*-butanol/water separation factor increases noticeably as the temperature increases. This is partly due to the fugacity difference of the feed and permeate of *n*-butanol increasing more relative to that of water and partly due to the increase in the relative permeance of *n*-butanol to water in MFI zeolite with increasing temperature (see e.g. Tables 4 and 5 in Paper I).

As dilute alcohol mixtures cannot be concentrated in a one-step pervaporation unit to anhydrous alcohol, further treatment is required. Yet, even small changes in concentration may lead to high changes in process costs, e.g., when butanol concentration is increased from approximately 1 wt.% to 4 wt.%, considerable energy savings can be achieved in butanol recovery by distillation (Ezeji *et al.* 2004).

Cost-effective butanol recovery is critical for the successful commercialization of biobutanol production. In fact, in the case of butanol separation, phase separation by decantation can be utilized as the binary *n*-butanol/water system exhibits partial miscibility. For example, at 30 °C (in atmospheric pressure), *n*-butanol/water mixture with *n*-butanol concentration of more than 7 wt.% separates into two phases: an organic concentrated phase with a composition of 80/20 wt.% *n*-butanol/water, and a low organic concentration in the aqueous phase with a concentration of 7/93 wt.% *n*-butanol/water.

Thus, if the permeate falls into the immiscible region, the organic phase in the permeate will have a high *n*-butanol concentration and the aqueous phase a low *n*-butanol concentration. As an example, in order to produce 80 wt.% *n*-butanol at 30 °C from 3 wt.% *n*-butanol solution (corresponding to a separation factor of 130), it would be sufficient to shift the concentration to the immiscible region by pervaporation with membranes displaying a separation factor of above 3. In this case the pervaporation unit should be followed by a settler to carry out the phase separation. After the phase separation, the aqueous phase could be recycled to the feed stream to increase the butanol recovery. The *n*-butanol-rich phase can be further dehydrated, for instance, by pervaporation using hydrophilic membranes (e.g. FAU or LTA). In this type of process the relative amount of the two phases depends on the membrane separation factor. Thus, separation factors of higher than 3 would definitely be desired. The utilization of phase separation in combination with pervaporation has not been studied extensively. Only recently Zhou *et al.* (2014b) analyzed the phase separation of the permeate during the pervaporation of ABE-water solution, and concluded that it is possible to obtain a high permeate organic concentration under proper conditions.

The fluxes in *n*-butanol/water separation by pervaporation in this work are very high, while the separation factors are reasonable. Thus, the membranes in this study may have a potential for *n*-butanol recovery from dilute aqueous solutions, especially if phase separation is utilized in the process. The effect of support resistance is discussed in Section 4.2.

4.2 Mass transfer resistance caused by the support when using ultra-thin membranes in pervaporation of binary alcohol/water mixtures (Papers I, II and VI)

In essence, a decrease in zeolite film thickness, while assuming that the permeation properties of the film stay the same, should increase the permeation flux in

proportion to the change in the film thickness. Indeed, the membranes of this study with ultra-thin selective layer, have a higher flux than similar, thicker membranes studied in the literature. However, when comparing the fluxes achieved in this study to the ones obtained with thicker membranes (see Tables 3–5), the fluxes of the ultra-thin zeolite membranes in the present work do not increase in proportion to the membrane thickness. The most probable explanation for the smaller fluxes is the flux limitation caused by the membrane support, as the support has been concluded to also decrease the fluxes when using membranes with thicker selective zeolite layers (de Bruijn *et al.* 2003, Sato *et al.* 2008b, Weyd *et al.* 2008, Zah *et al*. 2006).

The effect of the support on the mass transfer of the composite membrane used in this study is depicted in Fig. 8. As Fig. 8 illustrates, the effective driving force over the membrane is reduced due to the fugacity drop in the supporting layers. The feed-side fugacities can be determined based on the feed-side bulk liquid properties (see Eq. (13)) whereas the component fugacities from the zeolite film-support layer interface downstream can be determined from the gas phase properties. Due to the low pressure, the ideal gas assumption is reasonable. Thus, the component fugacities can be expressed as partial pressures in the support layers.

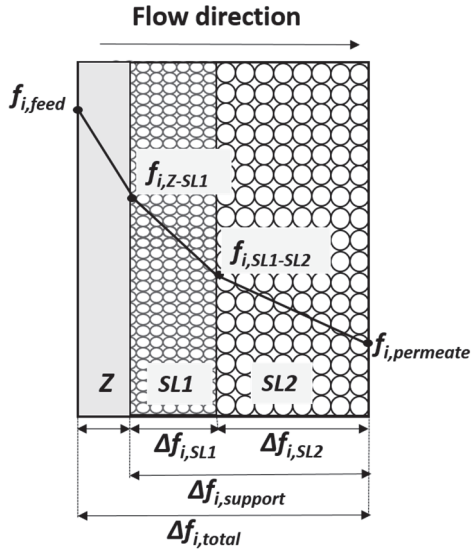

Fig. 8. Composite zeolite membrane and fugacity profile over the zeolite film (Z) and support layers 1 and 2 (SL1 and SL2).

As the total pressure and composition at the interfaces between the zeolite film and SL1 as well as between SL1 and SL2 cannot be measured directly, some means to calculate the fugacity drop across the support layers is needed, i.e., to describe the mass transfer in the support. As outlined in Section 3.1, in this work it was assumed that both Knudsen diffusion and viscous flow have significance in the transport through the composite support. Thus, the transport in the support layer can be written out as a combination of Knudsen diffusion Eq. (1) and viscous flow Eq. (3) as

$$J_{i,\mathrm{SL1}} = 97 K_{\mathrm{SL1}} \sqrt{\frac{T}{M_i}} \frac{\Delta p_{i,\mathrm{SL1}}}{l_{\mathrm{SL1}} RT} + \left(\frac{B_{0,SL1}^{\mathrm{eff}} \left(p_{i,Z-\mathrm{SL1}} + p_{i,\mathrm{SL1-SL2}} \right)}{RT 2\eta} \right) \frac{\Delta p_{\mathrm{SL1}}}{l_{\mathrm{SL1}}}, \tag{25}$$

$$J_{i,\mathrm{SL2}} = 97 K_{\mathrm{SL2}} \sqrt{\frac{T}{M_i}} \frac{\Delta p_{i,\mathrm{SL2}}}{l_{\mathrm{SL2}} RT} + \left(\frac{B_{0,SL2}^{\mathrm{eff}} \left(p_{i,\mathrm{SL1-SL2}} + p_{i,\mathrm{perm}} \right)}{RT 2\eta} \right) \frac{\Delta p_{\mathrm{SL2}}}{l_{\mathrm{SL2}}}. \tag{26}$$

As can be seen in Eqs. (25) and (26), the Knudsen diffusion and viscous flow parameters of the individual support layers are needed. These can be determined on the basis of suitable permeation experiments. With the parameters (see Table 2) and having knowledge of the fluxes from the pervaporation experiments, pressures and compositions at the interfaces can be determined on the basis of Eqs. (25) and (26). The contribution of the support to the mass transfer resistance can be expressed as the relative fugacity drop across the entire support as

$$\text{the relative fugacity (pressure) drop (\%)} = \frac{f_{i,\mathrm{Z-SL1}} - f_{i,\mathrm{perm}}}{f_{i,\mathrm{feed}} - f_{i,\mathrm{perm}}} \times 100\%. \tag{27}$$

The relative contributions of Knudsen diffusion and viscous flow can be calculated; e.g., the Knudsen share can be determined as

$$\text{Knudsen share (\%)} = \frac{J_{\mathrm{Kn},i,\mathrm{s}}}{J_{\mathrm{Kn},i,\mathrm{s}} + J_{\mathrm{Vis},i,\mathrm{s}}} \times 100\%. \tag{28}$$

4.2.1 High-silica MFI zeolite membranes (Papers I and II)

The relative fugacity drop for each component is determined by Knudsen diffusion and viscous flow on the basis of Eqs. (25)–(28) for different conditions. The effect of the support on the mass transfer for ethanol/water mixture using MFI membranes is introduced in Table 6 and for *n*-butanol/water in Table 7.

Table 6. Effect of support on the mass transfer in ethanol/water pervaporation experiments (modified from Paper I, published by permission of Elsevier).

Membrane	T (°C)	Water			Ethanol		
		Fugacity drop (%)	Knudsen share (%)		Fugacity drop (%)	Knudsen share (%)	
			SL1	SL2		SL1	SL2
M1	30	58.6	96.8	49.4	39.3	95.7	41.7
	60	42.7	91.6	31.1	31.8	89.1	23.7
M2	30	78.8	96.0	42.9	47.0	94.8	35.8
	60	56.7	89.9	26.3	32.9	86.9	19.8

Where SL1 is support layer 1; SL2 is support layer 2; M1 and M2 are membranes used in Paper I

Table 7. Effect of support on the mass transfer in *n*-butanol/water pervaporation experiments (modified from Paper I, published by permission of Elsevier).

Membrane	T (°C)	Water			*n*-Butanol		
		Fugacity drop (%)	Knudsen share (%)		Fugacity drop (%)	Knudsen share (%)	
			SL1	SL2		SL1	SL2
M1	30	46.0	97.7	55.3	32.7	96.5	44.4
	60	24.5	95.2	41.9	24.4	92.7	29.6
M2	30	59.5	97.1	49.6	38.6	95.7	38.9
	60	41.0	92.7	32.1	31.9	89.2	21.5

Where SL1 is support layer 1; SL2 is support layer 2; M1 and M2 are membranes used in Paper I

As can be observed from Table 6 and Table 7 (see also Table 3 in Paper II), the relative fugacity drop over the support for alcohol and water fluxes is substantial, thus limiting the component fluxes considerably. The effect of the support can be reduced by increasing the operating temperature as the relative fugacity drop decreases with increasing temperature. Mass transfer, especially in the narrow-pore support layer SL1, is governed by Knudsen diffusion. Knudsen diffusion favors the permeation of water over ethanol or *n*-butanol, resulting in lower alcohol/water selectivity. Thus, besides affecting the pervaporation flux, the support affects the separation factor of the pervaporation process. As the composition of the mixture in zeolite film–support layer 1 can be determined on the basis of Eqs. (25) and (26), the separation factor for the zeolite film can be determined from

$$\alpha_{i/j} = \frac{w_{i,\mathrm{Z-SL1}} / w_{j,\mathrm{Z-SL1}}}{w_{i,\mathrm{feed}} / w_{j,\mathrm{feed}}}. \qquad (29)$$

The separation factor for the zeolite film alone (Eq. (29)) is shown for ethanol/water (10/90 wt.% feed) and *n*-butanol/water (3/97 wt.% feed) mixtures in

Fig. 9 together with the actual measured separation factors, i.e. including the effect of the support from the experiments at 30 °C and 60 °C (see Tables 3 and 5).

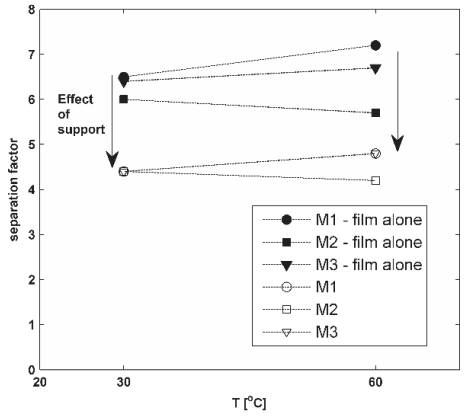

a)

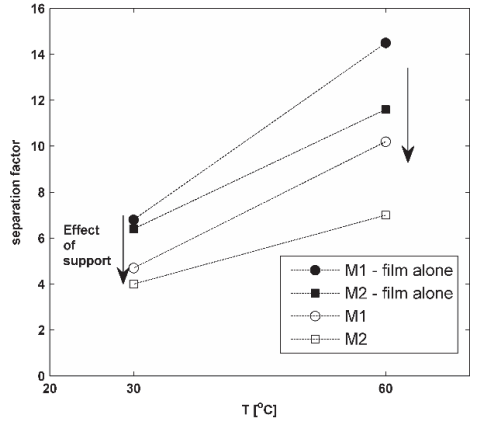

b)

Fig. 9. Effect of the support used on the alcohol/water separation factor in the pervaporation of a) ethanol/water (10/90 wt.%) and b) *n*-butanol/water (3/97 wt.%) feed solutions using membranes M1 and M2 (Paper I) for both solutions and M3 for ethanol/water (Paper II). The lines are just guidance for the eye.

As it is seen in Fig. 9, the support lowers the separation factors of both ethanol/water and *n*-butanol/water pervaporation. The decreased effective driving force caused by support resistance is taken into account later in Sections 4.3 and 4.5 where the pervaporation of ethanol/water mixtures and pure component pervaporation through MFI membranes is modeled.

Thus, in addition to membrane thickness affecting the membrane performance, the mass transfer resistance of the support has a significant effect on the flux and selectivity of the supported zeolite membranes. The options for reducing the resistance caused by the support are to reduce the thickness of the support layers, and to increase the size of the support pores and porosity.

An example of supports having a very thin wall thickness is porous ceramic hollow fibers, which have recently been successfully adopted to support zeolite membranes (Pera-Titus *et al.* 2009, Wang *et al.* 2009b). Due to the thin wall thickness, hollow fiber supports are claimed to be superior in low transport resistance, and also have other advantages such as high packing density and cost-effectiveness (Dong *et al.* 2014, Liu *et al.* 2014, Wang *et al.* 2009b).

In fact, besides the effect of membrane thickness, the effect of the support can also be roughly evaluated on the basis of the reported support properties in combination with the reported pervaporation performance of MFI membranes in ethanol/water separation. The support properties of the thinnest (film thickness < 5 μm) MFI membranes from Table 3 are collected in Table 8 together with the pervaporation performance of ethanol separation from aqueous streams.

Table 8. Pervaporation performance of very thin MFI zeolite membranes on different supports in ethanol/water separation.

Support				Membrane thickness	Pervaporation conditions		Membrane performance		Reference
Material - geometry	*l* (mm)	d_{pore} (μm)	ε (%)	(μm)	Feed (wt.%)	T (°C)	Flux (kg m^{-2} h^{-1})	Sep factor	
α[a]: SL1	0.03	0.1	34[b]	0.5	5	60	8.7	6.6	this study, Paper II
α[a]: SL2	3	3	34[b]						
α-HF	1	0.2	25	0.5	5	60	3.7	7.9	Kosinov *et al.* 2014
α-HF	1	0.2	25	5	5	60	1.8	21	Kosinov *et al.* 2014
YSZ-HF	< 0.5	0.67	57	3	5	60	7.4	47	Shu *et al.* 2012
α-HF	< 0.5	0.63	58	5	5	60	4.0	11	Shu *et al.* 2012
α-tube	4	1–3	–	3.5	5	60	1.82	62	Peng *et al.* 2013
α-tube	4	1–3	–	~5	5	60	1.3	85	Peng *et al.* 2014
α-capillary	1	0.2	–	2.5	5	45	0.9	35	Sebastian *et al.* 2010
α-capillary	1	0.8	–	2.5	5	45	1.5	37	Sebastian *et al.* 2010
α-tube	3	0.06	–	2	9.4	70	2.1	1.3	Algieri *et al.* 2003

Where HF is hollow fiber; YSZ is yttria stabilized zirconia

[a] Membrane used in this study has two α-alumina support layers SL1 and SL2

[b] see structural parameters in Table 2

The highest flux after the ultra-thin membranes used in this study have been achieved with membranes synthesized on hollow fiber supports (see Table 8, Kosinov *et al.* 2014 and Shu *et al.* 2012). Even though the pervaporation conditions, zeolite film thickness and support geometry are similar, the flux in the study of Shu *et al.* (2012) is approximately twice as high as that in the study of Kosinov *et al.* (2014). This is most probably due to the reduced support resistance of the thinner hollow fiber support wall with larger pore sizes and porosity in the study of Shu *et al.* (2012) in comparison to Kosinov *et al.* (2014) (see Table 8).

The MFI membranes with a membrane thickness of below 5 μm synthesized on α-alumina tubes (tube wall thickness of 3–4 mm, Table 8), on the other hand, exhibit a noticeably lower pervaporation flux in similar pervaporation conditions when compared to membranes synthesized on hollow fiber supports. This is an indirect indication of the lower support resistance of hollow fiber supports. On the other hand, in the study of Sebastian *et al.* (2010) (see Table 8) the fluxes increased considerably with basically no contribution to the separation factor when only the support pore size of otherwise similar membranes was increased. This is due to the decreased flux limitation caused by the support resistance. Although a quantitative analysis is difficult to make from different sources due to insufficient information especially of support properties, based on the above analysis the support plays an important role in determining the membrane performance. Thus, as well as optimizing the membrane film properties of very thin membranes in particular, optimization of the support properties is crucial.

4.2.2 Zeolite X membranes (Paper VI)

In the case of zeolite X membranes, the water/ethanol separation factor is very high (Table 4). Thus, it would be justified to assume water as the only permeating species when calculating the contribution of the support using Eqs. (25) and (26), as it is done in Paper VI and, for instance, in the studies of de Bruijn *et al.* (2003) and Sato *et al.* (2008). When including both the components in the calculations, it is shown in Table 9 that for water the fugacity drop (Eq. (27)) is almost 90%, and still more than 50% at higher temperatures, limiting the water flux. On the other hand, the generally low ethanol flux is not limited by the support (Table 9) as it was assumed in Paper VI.

Table 9. Effect of support on the mass transfer in ethanol dehydration by pervaporation.

	T	Water					Ethanol				
	(°C)	Q	Fugacity drop (%)		Knudsen share (%)		Q	Fugacity drop (%)		Knudsen share (%)	
		(x 10^{-5} mol m^{-2} s^{-1} Pa^{-1})	SL1	SL2	SL1	SL2	(x 10^{-8} mol m^{-2} s^{-1} Pa^{-1})	SL1	SL2	SL1	SL2
M4	40	4.85	48	37	97	52	1.86	0.19	0.13	96	45
M5	50	1.08	31	31	97	50	0.83	0.09	0.05	96	43
M6	65	1.05	32	32	95	40	1.27	0.13	0.06	94	32

Where M4–M6 are membranes used in Paper VI

Besides optimizing the membrane synthesis to obtain ultra-thin membranes with high selectivity, optimizing the support mass transfer properties is also very important, so that the fluxes would not become significantly limited by the support. Thinner support layers (see Eqs. (25) and (26)), for example, decrease the resistance caused by the support. In addition, the support resistance can be decreased by using supports with less tortuosity and larger porosity and pores (see Eqs. (2) and (4)).

In this study, the majority of the fugacity drop using zeolite X membranes occurs in the thin supporting layer SL1 (see Table 9), which is why reducing the resistance in SL1 affects the flux relatively more than the thicker layer SL2. The effect of the support on the flux can be demonstrated by changing the support properties while retaining the membrane properties. In addition to the experimental flux using zeolite X membranes M4–M6 with the support used, the predicted flux and separation factor using changed support properties can be viewed in Fig. 10 for the following cases:

- Case 1: Decreasing the SL1 thickness from 30 μm to 10 μm since the ceramic microfiltration membrane used as zeolite membrane supports are typically prepared with layers of between 10–50 μm thick (Purchas & Sutherland 2002).
- Case 2: Decreasing both the SL1 and SL2 thicknesses to one third (SL1 from 30 μm to 10 μm and SL2 from 3 mm to 1 mm). The wall thickness of typical hollow fiber supports is below 1 mm (see Table 8).
- Case 3: Decreasing both the supporting layer thicknesses to one third, and additionally increasing the Knudsen structural parameter K_{SL1} approximately 3-fold from 2.94×10^{-9} to 10×10^{-9} (almost all the transport in SL1 occurs by Knudsen diffusion, Table 9). The structural parameter K can be affected by pore size, porosity and tortuosity (see Eq. (2)). A threefold increase of, for example, the pore size is very realistic (see e.g. Sebastian *et al.* 2010).

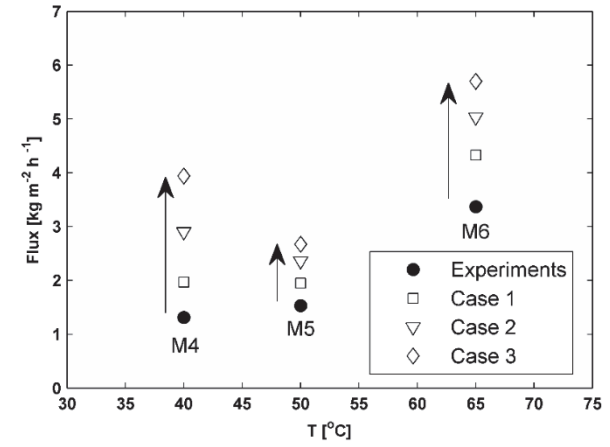

a)

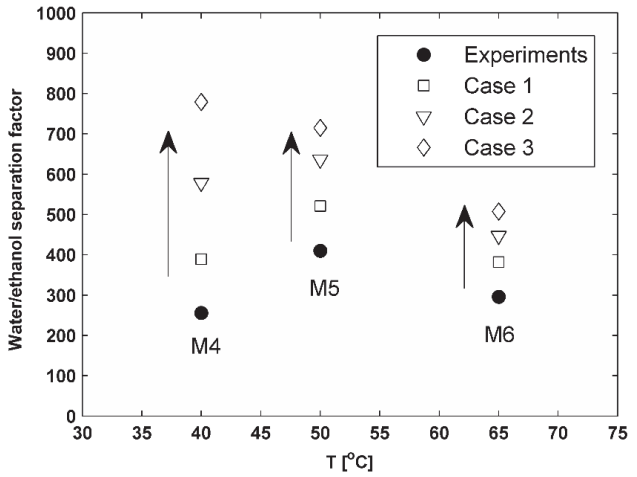

b)

Fig. 10. Estimated a) fluxes and b) water/ethanol separation factors for membranes M4–M6 prepared on graded support with tailored support properties.

As can be seen from Fig. 10a, the flux could be increased substantially by tailoring the support properties. Furthermore, as shown in Fig 10b, also the water/ethanol separation factor would increase as a result of tailored support properties. The increase of the separation factor (Eq. (23)) from for example 256 (M4 experiment at 30 °C) to 779 (Case 3 for M4) means an increase of permeate water content from 96.6 wt.% to 98.9 wt.%. Optimizing the support properties is essential in order to

make pervaporation through zeolite membranes an attractive alternative for industrial application.

4.3 Modeling of ethanol/water mixture pervaporation using MFI membranes (Paper II)

As discussed in Section 1, the mass-transfer modeling of pervaporation using hydrophobic zeolite membranes in particular, has been somewhat neglected, even though a lot of laboratory work has been conducted on using hydrophobic zeolite membranes in pervaporation (see Tables 3 and 5). Nevertheless, a semi-empirical model (see Eq. (13)) based on solution-diffusion has been applied, e.g., in the study of Kuhn *et al.* (2009b) in the removal of ethanol from an aqueous mixture using MFI zeolite membranes.

Although the influence of the support has been analyzed to reduce the driving force through the zeolite layer (Weyd *et al.* 2008, Zah *et al.* 2006), the contribution of the support layer is generally omitted when modeling pervaporation in various conditions. As concluded in Section 4.2, the contribution of the support to the mass transfer resistance is substantial in pervaporation using the ultra-thin zeolite membranes. The influence of the support should thus be included in model describing membrane mass transfer, as it reduces the driving force. The reduced fugacity difference can be used as a driving force in modeling the mass transfer of pervaporation of ethanol/water mixtures using high-silica MFI membranes by replacing the permeate side fugacity determined from bulk conditions in Eq. (13) with the fugacity between the zeolite layer and support layer 1 (see Table 5 and Fig. 8) as

$$J_i = Q_i \left(x_i \gamma_i P_i^{\text{sat}} - y_{i,\text{Z-SL1}} P_{\text{Z-SL1}} \right), \tag{30}$$

The temperature-dependency of permeance Q_i can be described as

$$Q_i = Q_i^{\text{ref}} \exp\left[\frac{-E_i^{\text{p}}}{R} \left(\frac{1}{T} - \frac{1}{T_{\text{ref}}} \right) \right], \tag{31}$$

where Q_i^{ref} is the permeance of component i at a reference temperature T_{ref}, which in this study is the mean temperature of the experiments, and E_i^{p} is the activation energy of permeance for component i, characterizing the temperature effect of adsorption and diffusion in the zeolite layer.

The model based on reduced fugacity in Eq. (30) has not been used earlier in modeling the mass transfer in pervaporation using hydrophobic zeolite membranes. As shown in Section 4.2, the total pressure and the composition and thus the fugacity between the zeolite film and support layer 1 is determined on the basis of the mass transfer model for the support. The model parameters were fitted based on all the available experimental data points, and are shown in Table 10.

Table 10. Parameters for transport model (Eqs. (30) and (31), T_{ref} = 50.5 °C).

component	Q_i^{ref} (kg m^{-2} h^{-1} Pa^{-1})	E_i^p (kJ mol^{-1})
ethanol	6.28 x 10^{-4}	-5.35
water	7.74 x 10^{-4}	-14.59

The fit of the model to the experimental partial fluxes can be seen in Fig. 11. The experimental data points are the mean values of the samples from the same experimental conditions; the error bars represent the standard deviation.

As can be observed in Table 10, the activation energy of both water and ethanol is negative. This implies that the membrane permeance decreases with increasing temperature. Nevertheless, overall, the flux still increases with increasing temperature (see Fig. 11), because the temperature effect on saturated vapor pressure and thus feed side fugacity is so significant. Although the water activation energy of permeance is more negative than that of ethanol leading to water permeance decreasing more with increasing temperature in comparison to ethanol, the effect of the driving force is the opposite (see e.g. Tables 7 and 8 in Paper I). Therefore, the separation factor is relatively independent of temperature.

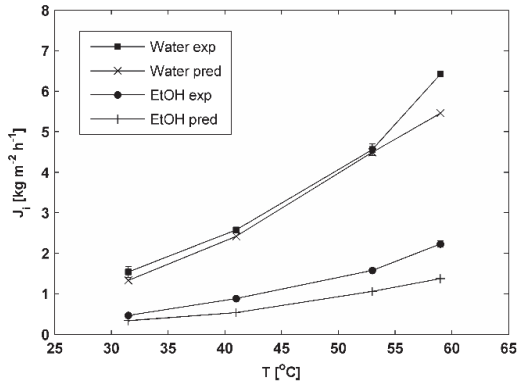

a)

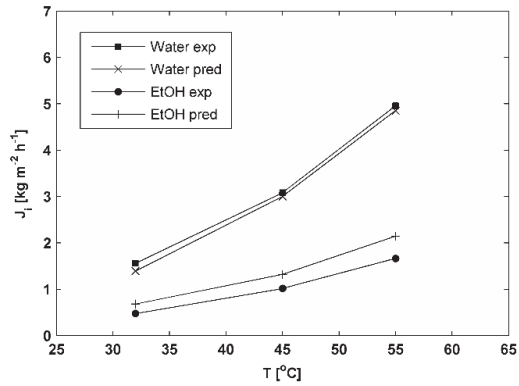

b)

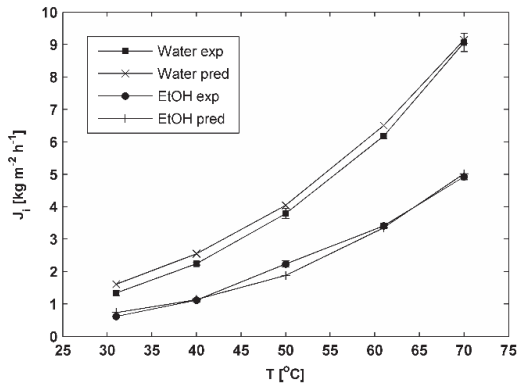

c)

Fig. 11. Experimental and modelled fluxes for ethanol and water for a) 5 wt.% EtOH, b) 7.5 wt.% EtOH and c) 10 wt.% EtOH mixture as feed. The lines are guidance for the eye. (Paper II)

As shown in Section 4.2, the reduction of the driving force is substantial with the ultra-thin membranes studied in this work. For comparison, Weyd *et al.* (2008) reported a support pressure drop of approximately 450 Pa for 5 wt.% aqueous ethanol feed at 40 °C (see also Table 3), corresponding to approximately 5% of the total mass transfer resistance with a thicker 50 μm high-silica MFI membrane. If the membranes studied in this work had a similar relative pressure drop (retaining the membrane properties), the predicted total flux for 5 wt.% ethanol feed at 40 °C, using the parameters in Table 10 would be doubled to about 7 kg m^{-2} h^{-1} (the corresponding experimental value with a supported membrane is 3.5 kg m^{-2} h^{-1}, see Table 3 and Fig. 7).

Although the model applied performs satisfactorily, it does not take into account, for example, the variation of feed concentration in the permeance, which causes some error in the model predictions. Furthermore, any error in the Knudsen diffusion and viscous flow parameters used to model the support mass transfer behavior (Table 2) propagates additional error in the model predictions.

The semi-empirical model applied in Paper II relies heavily on experiments. Therefore, extrapolation into regions beyond the measurement range can lead to clear errors in the model predictions. It is notable, however, that semi-empirical models have been used in the simulation of hybrid distillation-pervaporation systems in the dehydration of alcohols using polymeric membranes (see e.g. Koczka *et al.* 2007 and Valentínyi & Mizsey 2014). The main shortcoming of the model applied in Koczka *et al.* (2007) and Valentínyi & Mizsey (2014) is that a higher number of parameters needs to be estimated than in the model of this work. The higher number of parameters enables model flexibility and better prediction of membrane behavior in varying feed conditions, but the model application requires more extensive experimental work to obtain credible values for the parameters. Thus, due to the satisfactory performance of the model applied in the present work, the model of this work is applicable in the initial stages of conceptual design of an ethanol recovery process that applies pervaporation.

4.4 Predicting adsorption on zeolites (Papers III and IV)

In Section 4.3, the applied pervaporation model did not require specification of the adsorption behavior of components in the zeolite or their diffusion behavior in the membrane. However, both of these phenomena have significance in pervaporation. In addition, the usability of the model in varying process conditions increases considerably by the proper description of the prevailing phenomena. Thus, a

description of the adsorption and diffusion behavior should be included in a detailed membrane model. As discussed in Section 2.2.1, the adsorption data is typically obtained for zeolite powders, and zeolite membranes are assumed to have similar properties to the powders. The tools for modeling the adsorption of pure components and mixtures are studied in Paper III and Paper IV.

4.4.1 Modeling pure component adsorption (Paper III)

Usually the adsorption isotherms of gases and vapors on zeolites are expressed as a function of pressure. An example of this is illustrated in Fig. 12a for methanol adsorption at three temperatures on a hydrophobic high-silica MFI zeolite. When the same adsorption data is presented as a function of P/P_i^{sat} as in Fig. 12b, it can be seen that the data points at different temperatures form a uniform temperature dependency.

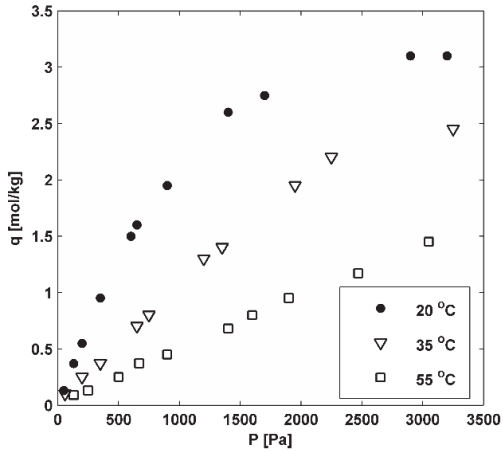

a)

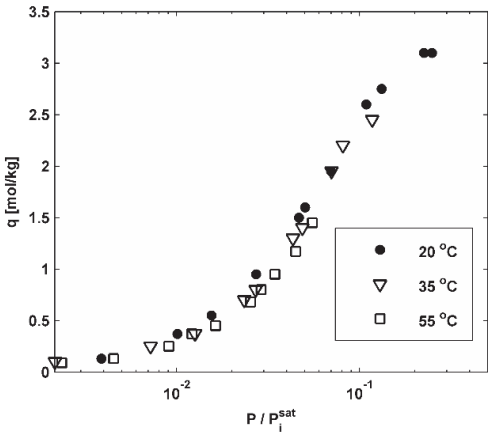

b)

Fig. 12. Methanol adsorption a) as a function of pressure and b) as a function of P/P_i^{sat} on high-silica MFI (Si/Al=990). Data taken from Nayak and Moffat (1988).

The unique relationship between the methanol loadings and P/P_i^{sat} (Fig. 12b) means that the temperature dependency of methanol adsorption on a hydrophobic high-silica zeolite can be represented by pure component saturated vapor pressure P_i^{sat}. The overlapping behavior of the adsorption of various components on various types of zeolites is studied in Paper III with the conclusion that the temperature dependency especially of water and short straight-chain alcohol adsorption on zeolites can be covered with the temperature dependency of saturated vapor pressure. Additionally, as concluded in Paper IV, the temperature dependency of

short-chain condensable aliphatic hydrocarbons adsorption on zeolites can be described with the temperature-dependency of pure component saturated vapor pressure. On the other hand, the temperature dependency of the adsorption of aromatics on zeolites could not be represented by saturated vapor pressure alone. An example of water adsorption as a function of P/P_i^{sat} on hydrophilic NaA zeolite (LTA) is illustrated in Fig. 13.

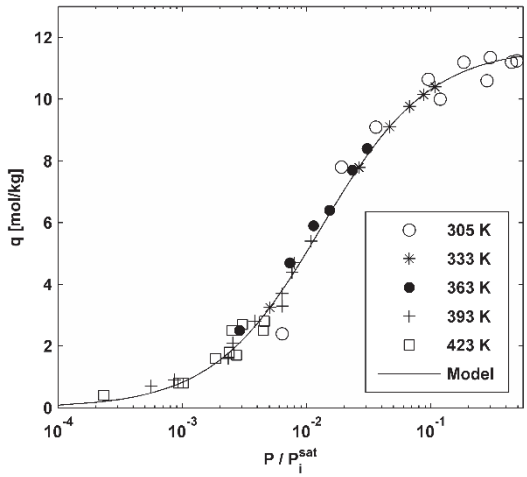

Fig. 13. Water adsorption on a NaA zeolite at different temperatures. Symbols refer to experimental data from Pera-Titus *et al.* (2008) and solid lines to modified Langmuir model predictions (see Table 11).

The P/P_i^{sat} approach can be used in the context with existing adsorption models by adopting the mathematical form of the existing isotherms and replacing the pressure P term with P/P_i^{sat}, which makes the approach flexible and not bound to a certain adsorption isotherm. Instead, the adsorption behavior of pure components on zeolites can be modeled as a function of P/P_i^{sat} with an adsorption model that is able to describe the adsorption data well. In the case of the Langmuir isotherm (isotherm 3 in Table 1), the modified Langmuir model is presented as

$$q_i = \frac{q_i^{sat} b_i^* \dfrac{P}{P_i^{sat}}}{1 + b_i^* \dfrac{P}{P_i^{sat}}}, \tag{32}$$

where b_i^* is a dimensionless and temperature-independent adsorption equilibrium parameter. The application of the proposed P_i^{sat} temperature-dependency approach is straightforward as parameters for P_i^{sat} are available in numerous textbooks and databanks. The solid line in Fig. 13 refers to the modified Langmuir model prediction, based only on the adsorption data derived at 305 K (see Table 11).

Traditionally the temperature dependency of adsorption is represented e.g., with Eq. (5). Thus, to include the temperature dependency of adsorption, at least data on the heat of adsorption is required. The determination of the heat of adsorption requires experimental data at several temperatures. In the literature, on the other hand, it is common to report the measured adsorption data at only one temperature. The usage of this data (or isotherm) to predict adsorption behavior at another temperature is difficult without heat of adsorption values. Performing adsorption equilibrium measurements at different temperatures may not be a feasible alternative due to limitations of the time and experimental facilities. Hence, due to the lack of applicable adsorption data, the temperature dependency has to be estimated based on the literature values, which can differ substantially even though the adsorption isotherm shape and also the measured adsorption amount on the same type of zeolite at different pressures would otherwise be quite similar. Therefore, sometimes the temperature dependency of adsorption may even have to be neglected in order to estimate the adsorption behavior (see e.g. Bettens *et al.* 2010). At least the approaches presented in Fig. 14 can be applied to predict adsorption at different temperatures.

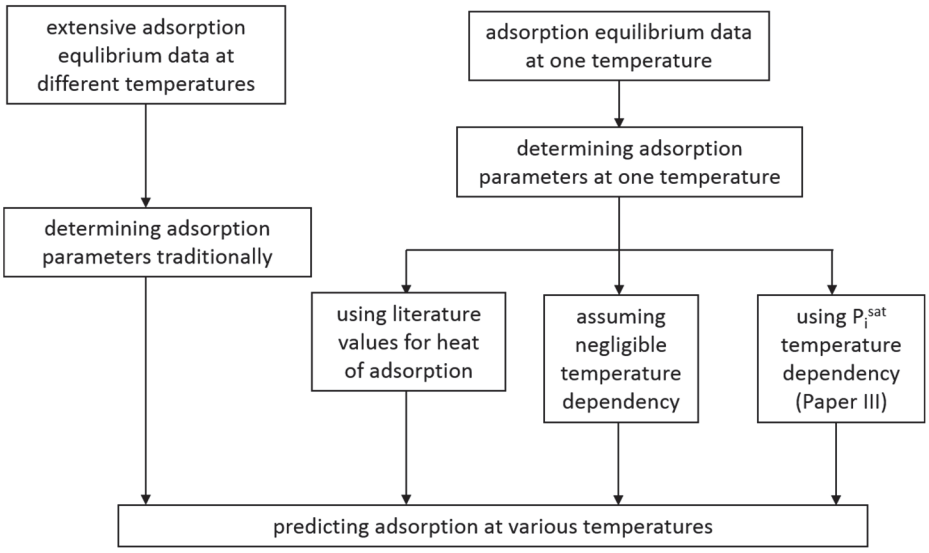

Fig. 14. Routes to predicting adsorption at various temperatures.

When the approach presented in Paper III is used, instead of Eq. (5), the temperature-dependency of the equilibrium parameter can be represented as

$$b_i = \frac{b_i^*}{P_i^{\text{sat}}} . \tag{33}$$

The dimensionless parameter b_i^* in Eq. (33) can be determined on the basis of extensive pure component adsorption data at only one temperature, and then the adsorption behavior can be predicted at other temperatures.

The fruitful area of predicting the temperature dependency of adsorption on microporous materials on the basis of a minimum amount of adsorption data has also been realized recently in other studies (Krishna 2015, Whittaker *et al.* 2013). Whittaker *et al.* (2013) introduced a method to predict the temperature dependency of gas adsorption on solid materials on the basis of one adsorption equilibrium data set at one temperature. Krishna (2015) evaluated the procedure of Whittaker *et al.* (2013) in the estimation of the heat of adsorption, and also analyzed the applicability of the P/P_i^{sat} approach developed in this work (Paper III) in the adsorption of components on microporous materials, also other than zeolites. Using the P_i^{sat} temperature-dependency approach or the method of Whittaker *et al.* (2013) both have applicability, but they cannot predict the temperature-dependency of adsorption of all adsorbate-adsorbent combinations (Krishna 2015).

Predicting temperature dependency of adsorption using different approaches

Case examples to elucidate the differences between different approaches (see Fig. 14) to predict adsorption behavior are presented below for the adsorption of water on NaA zeolite (see Fig. 13). In modeling adsorption, the Langmuir isotherm (isotherm 3 in Table 1) for Cases 1–4 and the modified Langmuir isotherm Eq. (32) for Case 5 were applied as a Langmuir-type isotherm can describe the applied adsorption data well. In all the cases, the adsorption is predicted at 423 K. The following cases are included:

- Case 1: The adsorption parameters are determined traditionally for the Langmuir isotherm based on all the adsorption experiments at various temperatures, parameters obtained from Pera-Titus *et al.* (2008).

In all the other cases it is assumed that adsorption data is available at only 305 K, and thus the adsorption parameters are fitted based on data at that temperature. The temperature dependency is predicted in some other way, or totally omitted as it is sometimes done when there is a lack of adsorption data (Bettens *et al.* 2010).

- Case 2: The temperature dependency is estimated by the value of lower limit of heat of adsorption from the literature, which ranges for water adsorption in NaA zeolite from approximately 20 to 120 kJ mol^{-1} as reviewed by Loughlin (2009) and Murdmaa & Serpinskii (1972).
- Case 3: The temperature dependency is estimated similarly to Case 2, except that the higher limit of heat of adsorption value is used.
- Case 4: The temperature-dependency is totally omitted.
- Case 5: The P/P_i^{sat} approach (Paper III) is used where the temperature dependency of pure component saturated vapor pressure alone is used to describe the temperature dependency of adsorption.

Table 11 shows the adsorption parameters for the different cases and Fig. 15 the adsorption prediction of different cases as a function of pressure at 423 K, together with the experimental data points at that temperature, from Pera-Titus *et al.* (2008).

Table 11. Langmuir isotherm (Cases 1–4) and modified Langmuir isotherm parameters (Case 5) for water adsorption on a NaA zeolite.

Case	T (K)	b_i (Pa^{-1})	b_i* (-)	q_i^{sat} (mol kg^{-1})	$-\Delta H_i^{ads}$ (kJ mol^{-1})
1[a]	363.4	0.0014	-	11.4	45
2	305	0.0162	-	11.67	20[b]
3	305	0.0162	-	11.67	120[c]
4	305	0.0162	-	11.67	0
5	305	-	76.46	11.67	

[a] From Pera-Titus *et al.* (2008)

[b] The lower and [c] the higher limit of heat of adsorption values

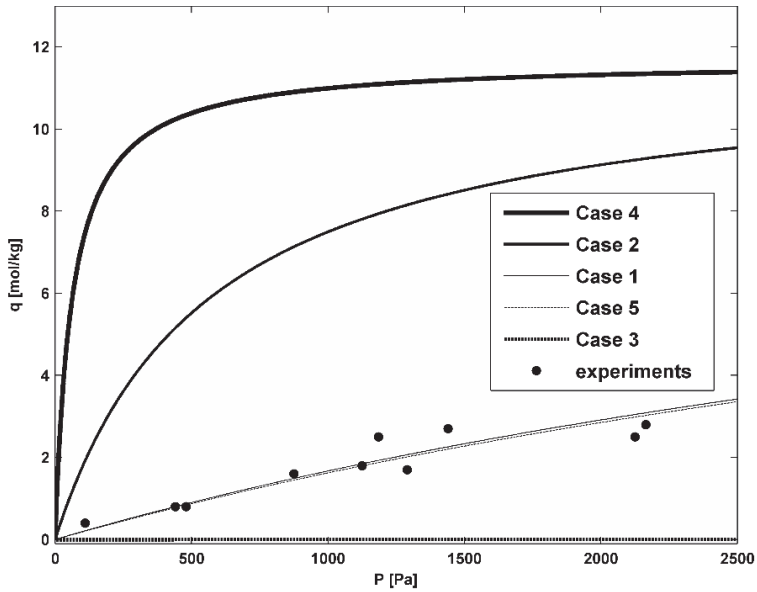

Fig. 15. Water adsorption loadings on NaA zeolite at 423 K predicted using different temperature-dependency approaches (Table 11). Experimental data from Pera-Titus *et al.* (2008).

The average percentage deviation for adsorption Δq_i (%) was determined as

$$\Delta q_i = \frac{100}{C}\sum_{j=1}^{C}\left|\frac{q_i^{\exp} - q_i^{\text{pred}}}{q_i^{\exp}}\right|, \tag{34}$$

where C is the number of data points. The average percentage deviation for water adsorption on NaA zeolite in different cases is presented in Table 12.

Table 12. Average percentage deviation Δq_i for different cases of adsorption prediction of water on the NaA zeolite at 423 K.

Case 1	Case 2	Case 3	Case 4	Case 5
15.8	349.0	100.0	692.1	15.6

As shown in Table 12 and the observed overlapping behavior in Fig. 15, the accuracy provided by the P/P_i^{sat} approach (Case 5) is very similar to that obtained using the traditional approach (Case 1) of having extensive adsorption equilibrium data at various temperatures to determine the adsorption parameters. When the traditional case of fitting the adsorption parameters at one temperature (305 K), and using the lower limit literature heat of adsorption value (Case 2), the adsorption at 423 K is clearly overestimated. On the other hand, if the higher limit literature heat of adsorption value (Case 3) is used, the adsorption is severely underestimated. When temperature dependency is omitted (Case 4), the adsorption is severely overestimated at a substantially higher temperature than where the adsorption parameters were obtained.

If adsorption equilibrium data are abundantly available at several temperatures, it is natural to use the traditional approach (Case 1) to model adsorption. However, based on Fig. 15 and Table 12 it can be concluded that with adsorption data at one temperature, the largely varying literature $-\Delta H_i^{ads}$ values cause uncertainty in predicting adsorption. Selecting an inappropriate literature value for the heat of adsorption may cause the traditional approach to fail. Thus, with a lack of adsorption data as a function of temperature, by applying the pure component saturated vapor pressure temperature dependency, adsorption can be predicted in a straightforward manner having a theoretical base, which is particularly valuable for engineers for process design purposes. The main limit of the approach with respect to temperature is the validity range of the vapor pressure, i.e., the proposed approach is only suitable for components in subcritical conditions. For instance, the approach can be used as a modeling tool in mass-transfer modeling of pervaporation using zeolite membranes, where knowledge of adsorption is essential.

Moreover, the studies of P/P_i^{sat} behavior of multiple cases in Paper III support the conception that saturation loading is essentially independent of temperature. However, occasionally in the literature, saturation loading is also estimated for each temperature separately as in the studies of Kim *et al.* (2003), Loughlin (2009), and Ryu *et al.* (2002). This leads typically to a decline in the saturation loading with increasing temperature, which in general may be merely a result of the lack of adsorption data over a sufficiently wide pressure range. The approach may even

lead to changes of an order of magnitude in the q_i^{sat} value (Kim *et al.* 2005), which is highly unlikely in the given context. The need for estimating saturation loading separately can be avoided when using the P_i^{sat} temperature-dependency approach (Paper III).

A summary of the systematic and engineering-friendly procedure to model pure component adsorption on zeolites developed in this work is introduced in Fig. 16.

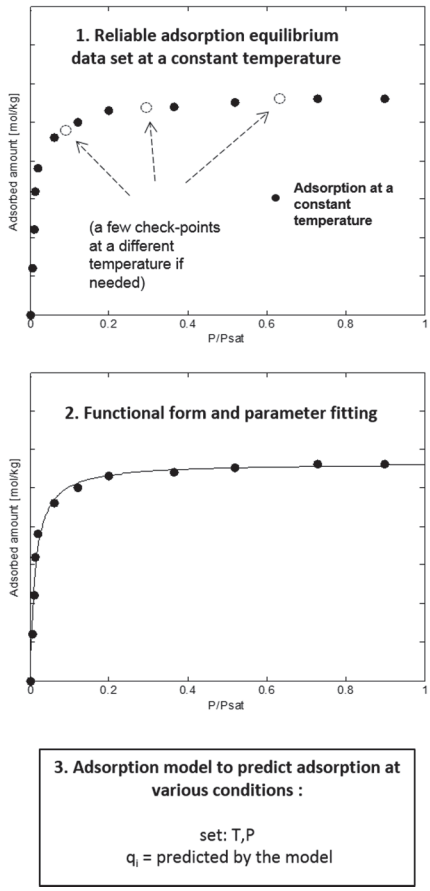

Fig. 16. P_i^{sat} temperature-dependency approach to model pure component adsorption on zeolites. (Paper III, published by permission of Elsevier)

4.4.2 Predicting mixture adsorption (Paper IV)

Mixture adsorption data is scarce in the literature, which is natural due to the considerable number of different types of adsorbents and adsorbate combinations. In addition, mixture adsorption measurements are more prone to error than pure component adsorption. Hence, there is a clear need to predict mixture adsorption based on pure component adsorption.

In Paper IV the P/P_i^{sat} approach investigated in Paper III and Section 4.4.1 is applied to predict mixture adsorption on zeolites. The basic idea is to fit pure component adsorption parameters at one temperature for each component (the temperatures do not have to be the same), using the P_i^{sat} temperature dependency (Fig. 16). Then the mixture adsorption is predicted at a different temperature than where the pure component data was obtained, with a suitable mixture adsorption model discussed in Section 2.2.2.

The application of the P/P_i^{sat} approach together with IAST to predict mixture adsorption is demonstrated for water/ethanol mixture adsorption on a NaA zeolite, which was investigated in Paper IV. The fitted water adsorption parameters of water adsorption on the NaA zeolite at 305 K, using the modified Langmuir model Eq. (32), is shown in Section 4.4.1 (see Case 5 in Table 11 and Fig. 13). For ethanol, the parameters and fit of the model are presented in Table 4 and Fig. 3b in Paper IV.

Fig. 17 shows the water/ethanol mixture adsorption loading predictions at a higher temperature (333 K) than where the pure component adsorption parameters had been fitted (305 K). For comparison, as well as using the P_i^{sat} temperature dependency, a case of IAST prediction with no temperature dependency of adsorption is shown in Fig. 17. In order to be able to evaluate the predictions, mixture experimental data points (taken from Pera-Titus *et al.* (2008)) are also included in Fig. 17. The error bars indicate the uncertainty of the measured mixture data points given in Pera-Titus *et al.* (2008).

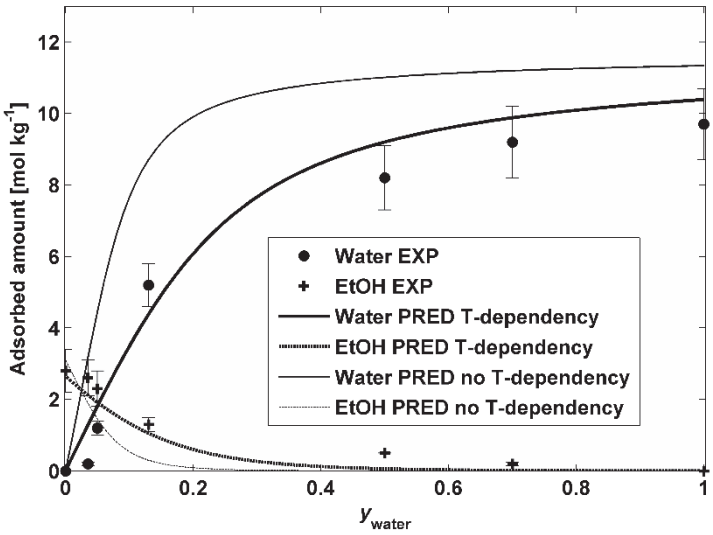

Fig. 17. Water and ethanol mixture adsorption loadings on NaA zeolite at 333 K and 2.1 kPa based on the experiments (Pera-Titus *et al.* 2008) and IAST model predictions both with the P_i^{sat} temperature-dependency approach and without any temperature dependency. (Paper IV, published by permission of Elsevier)

As shown in Fig. 17, using the P_i^{sat} temperature-dependency approach with IAST is a feasible method in predicting water/ethanol mixture adsorption on NaA zeolite. When the temperature dependency is omitted, IAST clearly overestimates water adsorption loading and underestimates that of ethanol, as illustrated in Fig. 17.

As shown in Fig. 17 and concluded in Paper IV, reasonably good mixture adsorption predictions can be achieved using the P_i^{sat} temperature-dependency approach (presented in Paper III and Section 4.4.1) in conjunction with a suitable mixture adsorption model. The approach is not restricted to the vapor phase as it is also applicable in the modeling of liquid phase adsorption (Paper IV). Adsorption isotherms in the literature are typically presented as a function of pressure P as shown in Table 1, but they can also be expressed as a function of fugacity f to emphasize the non-idealities of the bulk phase, by replacing pressure with fugacity. Thus, e.g. the modified Langmuir model (see Eq. (32)) can be expressed as

$$q_i = \frac{q_i^{sat} b_i^* \dfrac{f_i}{P_i^{sat}}}{1 + b_i^* \dfrac{f_i}{P_i^{sat}}}. \tag{35}$$

The gas phase can be considered ideal at low or moderate pressures. Thus, the fugacity of a component can be expressed as partial pressure in the conditions. Instead, for the liquid phase fugacities, activity coefficients are applied if the liquid mixture contains polar components like water, see Eq. (13).

Hence, it can be concluded that the P_i^{sat} temperature-dependency approach with IAST is a versatile method of predicting both liquid mixture and vapor mixture adsorption on zeolites. The approach could be used in e.g., in modeling the mass transfer in pervaporation or vapor permeation, where both adsorption and diffusion phenomena are important.

4.5 Modeling ethanol and water unary pervaporation using MFI membranes (Paper V)

Mass transfer models for pervaporation are based on the phenomena occurring in the process. In Paper V, the Maxwell-Stefan formalism (see Section 2.3) was used to model the mass transfer of pure ethanol and water through an ultra-thin supported high-silica MFI membrane. Together with pure component adsorption isotherms and pervaporation flux measurements, Maxwell-Stefan modeling allows the estimation of component diffusivities in zeolites.

For single-component diffusion, inserting Eq. (15) into Eq. (14), and considering mass transfer only in the z direction perpendicular to the membrane surface, the molar flux of component i across the membrane can be expressed as

$$J_i = -\rho q_i^{sat} \Gamma Đ_{i,z} \frac{d\theta_i}{dz} . \tag{36}$$

The steady-state single-component molar flux can be obtained by integrating Eq. (36) in combination with the modified Langmuir model Eq. (32), assuming adsorption equilibrium on both sides of the membrane as

$$J_i = -\frac{\rho q_i^{sat}}{l} \int_{\theta_i^f}^{\theta_i^p} \frac{Đ_{i,z}(\theta)}{1-\theta_i} d\theta_i . \tag{37}$$

The coverage dependency of MS surface diffusivity $Đ_{i,z}$ of ethanol and water in MFI zeolites has not been studied experimentally in the literature. The simplest scenario is to consider $Đ_{i,z}$ to be independent of the occupancy fraction of component i according to Eq. (18). Guo *et al.* (2011) assumed a coverage-independent MS diffusivity in modeling the pervaporation of water and ethanol through hydrophilic NaA zeolite membranes. The study of Krishna & van Baten

(2010), using configurational-bias Monte Carlo (CBMC) and MD simulations, shows that the MS diffusivities of water and alcohols may have several types of coverage dependencies, depending on the investigated adsorbate-adsorbent combination. Without experimental evidence, the use of coverage-independent MS surface diffusivity is a good first step approximation. With this approximation, the MS surface diffusivity can be assumed to present the average diffusivity value across the membrane, including all the pathways to mass transfer. With coverage-independent $Đ_{i,z}$, i.e. $Đ_{i,z}(\theta) = Đ_{i,z}(0)$, the permeation flux Eq. (37) is reduced to

$$J_i = \frac{\rho q_i^{\mathrm{sat}} Đ_{i,z}(0)}{l} \ln\left(\frac{1 + b_i^* \dfrac{f_i^{\mathrm{f}}}{P_i^{\mathrm{sat}}}}{1 + b_i^* \dfrac{f_i^{\mathrm{Z-SLI}}}{P_i^{\mathrm{sat}}}} \right). \tag{38}$$

The MS diffusivity follows the Arrhenius-type temperature dependency (see Eq. (12)). To enable efficient parameter estimation, typically the MS diffusivity value is estimated at the reference temperature T_{ref}. Hence, the MS surface diffusivities at zero loading are expressed as

$$Đ_{i,\mathrm{z}}(0) = Đ_{i,\mathrm{z}}^{0}(T_{\mathrm{ref}}) \exp\left[\frac{-E_i^{\mathrm{dif}}}{R} \left(\frac{1}{T} - \frac{1}{T_{\mathrm{ref}}} \right) \right]. \tag{39}$$

The Maxwell-Stefan model, Eq. (11), does not in principle take into account the effect of support. However, when the permeate-side fugacity is considered from the zeolite-support interface in Eq. (38) (estimated similarly to Section 4.2, details in Paper V), the driving force is corrected by the resistance in the support.

As it can be seen in Eq. (38), the evaluation of the flux requires knowledge of the physical properties of the film and adsorption behavior of the components under investigation. As the measurement of adsorption straight from ultra-thin zeolite membranes is not possible, the adsorption data were taken from the literature. The selected data sets were obtained from adsorption measurements on similar high-silica MFI zeolites to those used in the pervaporation studies of this work. However, it is worth noting that there are discrepancies between the available adsorption data sets. Ethanol adsorption has been shown to present relatively comparable results with zeolites of different Si/Al ratios, whereas water uptake can differ considerably (Zhang *et al.* 2012a).

The adsorption data for ethanol was acquired from the study of Nayak & Moffat (1988) and for water from Li *et al.* (2001). The data from Li *et al.* (2001) is

very similar to the water adsorption data on silicalite-1 from Flanigen *et al.* (1978), and also qualitatively similar (same shape of the isotherm) as, e.g., the water adsorption reported by Ohlin *et al.* (2013) in a Na-ZSM-5 zeolite film with a similar Si/Al ratio compared to the zeolite membranes used in this study. The saturation loadings of both pure ethanol and water in high-silica MFI are approximately 2.8 mol kg^{-1} (Farhadpour & Bono 1996). This value was given for q_i^{sat} of both the components. The modified Langmuir isotherm Eq. (32) is used as the adsorption model. The dimensionless parameter b_i^* was determined for ethanol on the basis of data at 293 K and for water at 298 K, being 75.872 for ethanol and 5.891 for water. The fit of the models to experimental data is shown in Fig. 18.

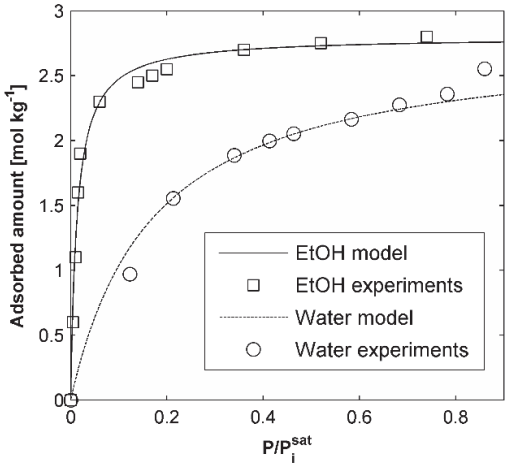

Fig. 18. Ethanol and water adsorption on high-silica MFI zeolite. Open symbols refer to experimental adsorption data (ethanol from Nayak and Moffat (1988) and water from Li *et al.* (2001)). Lines refer to modified Langmuir model predictions. (Paper V, reprinted with permission from ACS)

The fitted adsorption models were used to predict adsorption of ethanol and water in a high-silica MFI zeolite membrane at 30–70 °C. The temperature dependency of adsorption was accounted for through P_i^{sat} as described in Paper III and Section 4.4.1.

The relative fugacity drop (see Eq. (27)) across the support for water was calculated to be 70 % at 31°C, decreasing at higher temperatures, thus affecting the driving force considerably. In fact, although the fugacity drop for ethanol was below 10 % at each experimental temperature, it also has a considerable effect on the ethanol coverage at the permeate side of the membrane due to the Langmuirian-

type adsorption behavior characterized by the steep increase in loading with increasing fugacity (see Fig. 18). Thus, even a minor increase in the fugacity at low pressures typical of the permeate side of the membrane leads to appreciable changes in the surface coverage. Thus, it is important to include the effect of the support, as otherwise the derived diffusivities would be reduced in value.

The parameters for Eq. (38) along with Eq. (39) for the temperature-dependency were fitted on the basis of all the experimental data points. The parameters are shown in Table 13.

Table 13. Parameters for ethanol and water mass-transfer models (Eqs. (38) and (39), T_{ref} = 322 K), 95 % Confidence interval, t distribution assumed.

component	$Đ_{i,z}^{0}(T_{ref})$ (x 10^{-11} m^2 s^{-1})	E_i^{dif} (kJ mol^{-1})
ethanol	0.046±0.0043	40.7±6.0
water	1.68±0.083	30.3±2.8

The fit of the formed Maxwell-Stefan based model to the experimental fluxes is illustrated in Fig. 19. The experimental data points in Fig. 19 are the mean values of the samples at the same experimental conditions; error bars represent the standard deviation. For water, the predicted flux fits within the standard deviation of the experiments, and for the flux of ethanol the average percentage of deviation (Eq. (34)) for the flux is approximately 15%.

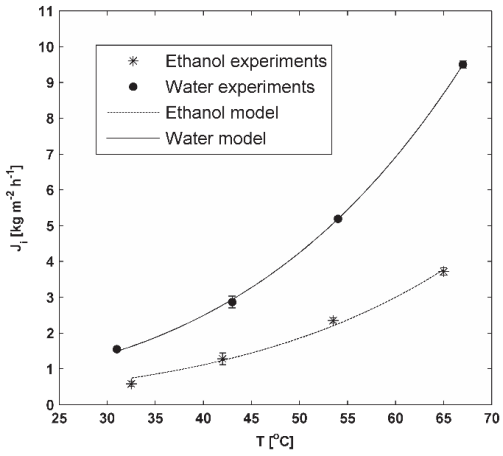

Fig. 19. Experimental and predicted ethanol and water fluxes in the unary permeation experiments as a function of temperature.

The water MS diffusivity (see Table 13, and Tables 4 and 5 in Paper V) is larger than that of ethanol. That is at least partly due to the larger kinetic diameter of ethanol (0.43 nm) compared to that of water (0.30 nm), which causes ethanol to have more trouble jumping from one adsorption site to another site in the zeolite pores than water. The activation energy of diffusion for a larger ethanol molecule is as expected larger than that of water. Maxwell-Stefan modeling comprises both intracrystalline diffusion as well as adsorption, but real zeolite membranes consist of complexly intergrown zeolite crystals with defects. The application of MS modeling to steady-state permeation through zeolite membranes includes all the pathways involved in mass transfer. Thus, the diffusivities determined in this work are generally a little higher than those transport diffusivities determined by other macroscopic measurement methods using zeolite powder (see Tables 4 and 5 in Paper V).

Ethanol and water self-diffusivities in MFI type zeolites determined either by microscopic methods or by MD simulations are several orders of magnitude higher than those obtained in this study or by other macroscopic measurement techniques (see Tables 4 and 5 in Paper V). Although consistent with the results typically obtained with macroscopic vs. microscopic methods, the extent of deviation is considerable. Yang *et al.* (2007), for example, computed self-diffusivity coefficients by molecular dynamics simulation for water as 26×10^{-10} m^2 s^{-1} and for ethanol 1.2×10^{-10} m^2 s^{-1} at 303 K. If these diffusivity values were used in predicting ethanol and water transport at 30 °C under the same reduced fugacity and zeolite film properties as in this study (Eq. (38)), the predicted ethanol flux would be approximately 500 kg m^{-2} h^{-1} (experimental value 0.5 kg m^{-2} h^{-1}), and water flux approximately 400 kg m^{-2} h^{-1} (experimental value 1.5 kg m^{-2} h^{-1}). Thus, the predicted fluxes would be severely overestimated, in proportion to the difference in the diffusion coefficients. Considerable overestimation of unary pervaporation fluxes can be found e.g. in the study of Guo *et al.* (2011). According to Guo *et al.* (2011), the overestimation of pervaporation flux is caused probably by the combination of the resistance of the support layer, defects and the multi-crystalline zeolite film structure. However, it is also highly likely that the simulated high diffusivity values have an effect on the overestimation of the unary fluxes.

Molecular simulations in general do not take into account the polycrystalline nature of the membrane. Thus, the quantitative prediction of membrane permeation by molecular simulations is still facing challenges. On the basis of this work, it is recommended that the diffusivities should be determined from pervaporation flux

measurements rather than the other methods due to the real zeolite membrane properties differ from those of individual crystals.

The quantitative prediction of mixture pervaporation using MS modeling would ideally be possible on the basis of pure component adsorption isotherms and pervaporation data (see Section 2.3). As analyzed in Sections 4.2 and 4.5, including the description of the support is important in membrane models, but also the incorporation of defects, for example, into the detailed mass transfer model would be important. Thus, further work is required on the development of reliable prediction procedures for mixture pervaporation using zeolite membranes.

5 Conclusions

Pervaporation is seen as a viable separation alternative in the purification of bio-based alcohols. Especially bioethanol upgrading is actively studied on laboratory scale. The main constraint of hydrophobic membranes in e.g., ethanol/water pervaporation has been the low flux, although the achieved separation factors especially in the case of zeolite membranes are reasonably high. The increase of pervaporation flux, while the separation factor stays the same, reduces the required membrane area, and size of the membrane unit. This in turn means that a high pervaporation flux is highly beneficial in industrial applications as the costs of pervaporation are determined by the size and number of membrane units.

The flux through a membrane can be increased by decreasing the membrane thickness. In this work, ultra-thin (0.5–1 μm) alumina-supported MFI and FAU zeolite membranes were studied in the pervaporation of aqueous ethanol/*n*-butanol solutions. Due to the low zeolite film thickness, the fluxes achieved in this work are generally higher than those reported earlier. Use of thin zeolite membranes in pervaporation, however, constitutes another challenge as the relative resistance caused by the support becomes significant, affecting membrane performance negatively. As analyzed in Section 4.2, the support used reduces both the separation factor and the flux in this work considerably. Thus, besides optimizing the operating conditions, the support resistance should be minimized by optimizing the support properties. This is important as otherwise the benefit of the thinner selective zeolite layer is partly lost.

Based on the experimental results, it can be concluded that the membranes studied in this work have potential in the recovery of products in bioethanol and biobutanol production. The design of pervaporation-based processes for the applications requires tools to evaluate the process feasibility. Mass-transfer models for the applied membranes can be used as a tool in the feasibility studies. An example of mass-transfer models is semi-empirical models, which can be used when there is empirical permeation data available for the investigated mixtures. In this work, this type of a model, based originally on the solution-diffusion theory of polymeric membranes, was applied in describing the mass transfer of ethanol/water mixtures in pervaporation using MFI zeolite membranes, based on experiments of several feed compositions at various temperatures. In the semi-empirical model used, the phenomena occurring in the zeolite film were combined into one permeance term, which can be considered as a significant simplification in

comparison to the phenomena occurring in reality. The effect of support resistance was also taken into account in modeling the mass transfer in pervaporation.

The correlation between the experiments and the semi-empirical model used was acceptable. Although performing relatively well in the experimental range, the model relies heavily on the experiments due to the semi-empirical nature of the model. Thus, it should be used with caution if extrapolating outside the experimental area. This type of model is still sufficient for the early stages of process design, i.e. when the operating conditions of the pervaporation unit have not yet been fixed or alternatively when the purpose is to compare different type of membranes in a given separation task.

The semi-empirical pervaporation model in this work did not require any additional information about the adsorption of components on the zeolite or the diffusion in the membrane. However, as both of these phenomena are considered important in pervaporation, including them in the membrane model is desirable.

Single-component adsorption isotherms on zeolites can be found in the literature, although typically they are reported at only one temperature. The large variation in heat of adsorption values causes uncertainty in predicting the temperature-dependency of adsorption, as it was demonstrated in Section 4.4.1. In this work, a simple tool was developed to utilize pure component saturated vapor pressure in representing the temperature-dependency of adsorption on zeolites. The application of the P_i^{sat} temperature-dependency approach is straightforward, as temperature-dependency parameters for P_i^{sat} are abundantly available. The proposed approach, however, can be used only in subcritical conditions. As shown in Section 4.4.2, reasonably good mixture adsorption predictions can be achieved using the developed approach in conjunction with a suitable mixture adsorption model. As a result of this work, vapor and also liquid adsorption can be predicted in various conditions on the basis of extensive pure component adsorption equilibrium data at one temperature. The approach can be applied in modeling zeolite-membrane based processes, for instance, pervaporation.

Besides adsorption, knowledge of diffusion behavior, and diffusivities, is essential in evaluating transport through zeolite films. Both phenomena are taken into account in Maxwell-Stefan modeling of pervaporative transport using zeolite membranes. In the present work, Maxwell-Stefan modeling was applied for unary permeation, together with pure component adsorption isotherms and pervaporation flux measurements, in the estimation of component diffusivities in zeolites. The diffusivities determined by different techniques differ considerably, which unfortunately can result in large deviations in predicted fluxes using zeolite

membranes, as demonstrated in Section 4.5. Thus, when the defects and zeolite pores are not considered separately in the model describing membrane mass-transfer, it is recommended to estimate the diffusivities from real membranes as it is done in the present work. As the direct measurement of the adsorption properties of the ultra-thin zeolite membranes studied is not possible, the adsorption data for unary permeation modeling were taken from the literature. The P_i^{sat} temperature-dependency approach developed in this work was used to describe the temperature dependency of adsorption in unary pervaporation modeling.

6 Future perspectives

The ultra-thin membranes studied in this work exhibit a high membrane flux with a modest separation factor. The influence of the support is concluded in the present work to significantly reduce the membrane performance. However, in case of hydrophobic MFI membranes, even after eliminating the contribution of the support, the alcohol/water separation factors of the zeolite film in this study remain lower than reported in most literature studies. Further studies are needed to better understand the microstructure of the membranes. With this knowledge, the main factors affecting membrane separation can be identified, and the means of increasing the separation factor of ultra-thin membranes can be developed.

The membranes used in this work were characterized as having a small amount of flow-through defects, which are detectable by permporometry and SEM. However, some of the defects, in the form of open grain boundaries cannot be detected with those methods. These defects may have significance in relation to the membrane separation performance. In the case of ethanol or *n*-butanol separation from aqueous solutions with zeolite membranes, the open grain boundaries are assumed to be water-selective pathways. Hence, the grain boundaries have a negative effect on membrane performance. The low film thickness may result in a greater negative effect of directly undetectable open grain boundaries than in the case of thicker membranes. This is because, with increasing film thickness, the crystal grains most probably have the chance to inter-grow better i.e. the proportion of flow-through defects decreases.

For future research, due to the lack of direct analysis methods, the effect of grain boundaries should be studied indirectly e.g. by testing similarly synthesized thicker pervaporation membranes. However, as concluded in Section 4.1.1, aluminum incorporated from the α-alumina support into the zeolite framework reduces the membrane hydrophobicity. Hence, the increase of film thickness could reduce the possible negative effects of aluminum. Thus, it would be difficult to separate the effects of grain boundaries and aluminum incorporation from each other, when alumina supports are used. Therefore, whether or not aluminum has a negative effect on the performance of thin zeolite membranes in pervaporation, should be studied using aluminum-free supports, e.g., other metal oxides like titania or zirconia.

Similarly to the membranes in this work, MFI zeolites are commonly synthesized in basic media with OH^- ions as the mineralizing agent. However, as discussed in Section 2.1.3, OH^- ions result in zeolite intracrystalline defects, which

decrease the hydrophobicity. Using fluoride ions as the mineralizing agent at near neutral conditions instead of OH^- in zeolite synthesis, results in silicalite-1 with the lowest water adsorption reported in the literature (Zhang *et al.* 2012a). Therefore, synthesis via a fluoride-mediated route has also attracted recently zeolite membrane fabrication research. In fact, the fluoride-mediated zeolite membrane synthesis route has been noticed to decrease the amount of intercrystalline defects considerably in addition to intracrystalline defects (Zhou *et al.* 2014). This could have a profound effect on pervaporation performance, and thus using ultra-thin MFI membranes prepared via the fluoride-route (Zhou *et al.* 2014) should be studied in pervaporation.

As concluded, the membranes studied in this work have potential in the product recovery of bioethanol and biobutanol production. The potential should be investigated in more detail in the future. Typically the most attention in zeolite membrane research is paid to preparing more selective membranes. As discussed in Section 4.1.1, it is not that straightforward, however, to conclude which kind of membrane is the best for each separation case. The optimal membrane might not be the highly selective membrane if it is accompanied with low flux, but rather a membrane with a high flux with acceptable selectivity. In the future, more effort should be targeted to evaluating the performance and feasibility of processes based on the use of pervaporation. Complete replacement of distillation as the most typical separation process with pervaporation units might be difficult, but more research, development and collaborative efforts should be targeted to consideration of distillation-pervaporation hybrid processes.

The adsorption parameters used in zeolite membrane modeling, including this work, are typically obtained from zeolite powder measurements, although zeolite membrane adsorption properties are not necessarily similar to those of powders. The distinctive features between adsorption on zeolite powders and membranes has not been sufficiently investigated. Further development of adsorption measurement methods is needed to enable investigation of the adsorption on thin zeolite membranes. In addition, the P_i^{sat} temperature-dependency approach applied in this study was concluded to cover at least the temperature dependency of water, short straight-chain alcohols and short-chain condensable aliphatic hydrocarbons adsorption on zeolites, but not of aromatics adsorption on zeolites. In the future the temperature dependency of adsorption of also other adsorbates on zeolites as well as on other adsorbents using the P_i^{sat} temperature-dependency approach could be studied.

Maxwell-Stefan modeling, as performed in this work, as such does not take the defects in the membrane structure into account. Thus, the diffusivities determined in this work include the effects of non-idealities in the structure of the membrane. The incorporation of defects into a detailed mass-transfer model would be important as zeolite membranes even with reasonable separation performance have nanometer-sized grain boundary defects. The adsorption-diffusion mechanism is also considered to be the prevailing transport mechanism in these grain boundary defects (Yu *et al.* 2011). The adsorption and diffusion parameters of defects, however, are difficult to quantify due to the different sizes of non-zeolite pores. Hence, there is still work to be done in the detailed modeling of the pervaporation process in the future. The inclusion of defects in the membrane model could be started by relating the permporometry data to pervaporation similarly to what has been done previously for gas permeation applications (Jareman *et al.* 2004, Kangas *et al.* 2013).

Zeolite membranes are stated to be stable, but most often the pervaporation experiments on laboratory scale are performed within short periods of time. Thus, more long-term stability tests are required. Moreover, similar to this work, typically most studies in pervaporation using hydrophobic zeolite membranes are conducted on binary water/alcohol solutions, although the actual process stream, e.g., the fermentation broth in bioethanol or biobutanol production is generally a multi-component mixture containing a variety of by-products. Naturally, the by-products have an influence on the separation process, e.g., succinic acid has been found to decrease the pervaporation performance of high-silica MFI membranes in ethanol fermentation (Ikegami *et al.* 2002). As the understanding and modeling of the pervaporation process of aqueous alcohol solutions were the objectives in this thesis, only binary mixtures were studied. However, the effects of fermentation by-products and thus multi-component mixtures certainly have to be addressed in the future.

Active laboratory-scale pervaporation research should be complemented with more efforts in scaling up the process from laboratory to industry. There are still many challenges to enable the usage of especially hydrophobic zeolite membranes in pervaporation separations in the industry. Nevertheless, despite the challenges, in terms of the unique microporous structure and properties of zeolites, zeolite membranes are currently suitable for multiple applications, and are likely to remain potential alternatives for pervaporation separation in the future.

References

Abdehagh N, Tezel FH & Thibault J (2014) Separation techniques in butanol production: Challenges and developments. Biomass Bioenergy 60: 222–246.

Algieri G, Barbieri G & Drioli E (2011) Zeolite membranes for gas separations. In: Drioli E, Barbieri G & Peter L (eds) Membrane Engineering for the Treatment of Gases: Gas-Separation Problems Combined with Membrane Reactors. Great Britain, Royal Society of Chemistry: 223–252.

Algieri C, Bernardo P, Golemme G, Barbieri G & Drioli E (2003) Permeation properties of a thin silicalite-1 (MFI) membrane. J Membr Sci 222(1–2): 181–190.

Andersson C (2007) Factors affecting MFI membrane quality. PhD thesis. Luleå University of Technology, Division of Chemical Technology.

Ari MU, Göktuğ Ahunbay M, Yurtsever M & Erdem-Şenatalar A (2009) Molecular dynamics simulation of water diffusion in MFI-Type zeolites. J Phys Chem B 113(23): 8073–8079.

Baker RW (2012) Membrane technology and applications. John Wiley & Sons, Inc.

Bankar SB, Survase SA, Ojamo H & Granström T (2013) Biobutanol: The outlook of an academic and industrialist. RSC Advances 3(47): 24734–24757.

Beaumelle D, Marin M & Gibert H (1993) Pervaporation with organophilic membranes: State of the art. Trans Inst Chem Eng 71(C): 77–89.

Bernal MP, Coronas J, Menéndez M & Santamaría J (2002) Characterization of zeolite membranes by measurement of permeation fluxes in the presence of adsorbable species. Ind Eng Chem Res 41(20): 5071–5078.

Bettens B, Dekeyzer S, Van Der Bruggen B, Degrève J & Vandecasteele C (2005) Transport of pure components in pervaporation through a microporous silica membrane. J Phys Chem B 109(11): 5216–5222.

Bettens B, Verhoef A, van Veen HM, Vandecasteele C, Degrève J & Van der Bruggen B (2010) Pervaporation of binary water-alcohol and methanol-alcohol mixtures through microporous methylated silica membranes: Maxwell-Stefan modeling. Comput Chem Eng 34(11): 1775–1788.

Bordat P, Cazade P-, Baraille I & Brown R (2010) Host and adsorbate dynamics in silicates with flexible frameworks: Empirical force field simulation of water in silicalite. J Chem Phys 132(9).

Bowen TC, Li S, Noble RD & Falconer JL (2003) Driving force for pervaporation through zeolite membranes. J Membr Sci 225(1–2): 165–176.

Bowen TC, Noble RD & Falconer JL (2004) Fundamentals and applications of pervaporation through zeolite membranes. J Membr Sci 245(1–2): 1–33.

Bussai C, Vasenkov S, Liu H, Böhlmann W, Fritzsche S, Hannongbua S, Haberlandt R & Kärger J (2002) On the diffusion of water in silicalite-1: MD simulations using ab initio fitted potential and PFG NMR measurements. Appl Catal A: General 232(1–2): 59–66.

Cardona Alzate CA & Sánchez Toro OJ (2006) Energy consumption analysis of integrated flowsheets for production of fuel ethanol from lignocellulosic biomass. Energy 31(13): 2111–2123.

Caro J, Hŏcevar S, Kärger J & Riekert L (1986) Intracrystalline self-diffusion of H_2O and CH_4 in ZSM-5 zeolites. Zeolites 6(3): 213–216.

Caro J & Noack M (2008) Zeolite membranes – Recent developments and progress. Micropor Mesopor Mat 115(3): 215–233.

Caro J, Noack M, Kölsch P & Schäfer R (2000) Zeolite membranes - state of their development and perspective. Micropor Mesopor Mat 38(1): 3–24.

Chandak MV & Lin YS (1998) Hydrophobic zeolites as adsorbents for removal of volatile organic compounds from air. Environ Technol 19(9): 941–948.

Chapman PD, Oliveira T, Livingston AG & Li K (2008) Membranes for the dehydration of solvents by pervaporation. J Membr Sci 318(1–2): 5–37.

Chempath S, Krishna R & Snurr RQ (2004) Nonequilibrium molecular dynamics simulations of diffusion of binary mixtures containing short *n*-alkanes in faujasite. J Phys Chem B 108(35): 13481–13491.

Chen H, Li Y & Yang W (2007) Preparation of silicalite-1 membrane by solution-filling method and its alcohol extraction properties. J Membr Sci 296(1–2): 122–130.

Chen SG & Yang RT (1994) Theoretical basis for the potential theory adsorption isotherms. The Dubinin-Radushkevich and Dubinin-Astakhov equations. Langmuir 10(11): 4244–4249.

Chovau S, Gaykawad S, Straathof AJJ & Van der Bruggen B (2011) Influence of fermentation by-products on the purification of ethanol from water using pervaporation. Bioresour Technol 102(2): 1669–1674.

Coronas J, Noble RD & Falconer JL (1998) Separations of C4 and C6 Isomers in ZSM-5 Tubular Membranes. Ind Eng Chem Res 37(1): 166–176.

Cot L, Ayral A, Durand J, Guizard C, Hovnanian N, Julbe A & Larbot A (2000) Inorganic membranes and solid state sciences. Solid State Sci 2(3): 313–334.

de Bruijn F, Gross J, Olujić Ž, Jansens P & Kapteijn F (2007) On the driving force of methanol pervaporation through a microporous methylated silica membrane. Ind Eng Chem Res 46(12): 4091–4099.

de Bruijn FT, Sun L, Olujić Ž, Jansens PJ & Kapteijn F (2003) Influence of the support layer on the flux limitation in pervaporation. J Membr Sci 223(1–2): 141–156.

Demontis P, Jobic H, Gonzalez MA & Suffritti GB (2009) Diffusion of water in zeolites NaX and NaY studied by quasi-elastic neutron scattering and computer simulation. J Phys Chem C 113(28): 12373–12379.

Do DD (1998) Adsorption analysis: equilibria and kinetics. London, Imperial College Press.

Do DD & Do HD (1997) A new adsorption isotherm for heterogeneous adsorbent based on the isosteric heat as a function of loading. Chem Eng Sci 52(2): 297–310.

Dong Z, Liu G, Liu S, Liu Z & Jin W (2014) High performance ceramic hollow fiber supported PDMS composite pervaporation membrane for bio-butanol recovery. J Membr Sci 450: 38–47.

Ezeji TC, Qureshi N & Blaschek HP (2004) Butanol fermentation research: Upstream and downstream manipulations. Chemical Record 4(5): 305–314.

Farhadpour FA & Bono A (1996) Sorptive separation of ethanol-water mixtures with a bi-dispersed hydrophobic molecular sieve, silicalite: Determination of the controlling mass transfer mechanism. Chem Eng Process Process Intensif 35(2): 141–155.

Flanigen EM, Bennett JM, Grose RW, Cohen JP, Patton RL, Kirchner RM & Smith JV (1978) Silicalite, a new hydrophobic crystalline silica molecular sieve. Nature 271(5645): 512–516.

Funke HH, Kovalchick MG, Falconer JL & Noble RD (1996) Separation of hydrocarbon isomer vapors with silicalite zeolite membranes. Ind Eng Chem Res 35(5): 1575–1582.

Gardner TQ, Flores AI, Noble RD & Falconer JL (2002a) Transient measurements of adsorption and diffusion in H-ZSM-5 membranes. AIChE J 48(6): 1155–1167.

Gardner TQ, Falconer JL & Noble RD (2002b) Adsorption and diffusion properties of zeolite membranes by transient permeation. Desalination 149(1–3): 435–440.

Gardner TQ, Falconer JL & Noble RD (2004) Transient permeation of butanes through ZSM-5 and ZSM-11 zeolite membranes. AIChE J 50(11): 2816–2834.

Gavalas GR (2006) Zeolite membranes for gas and liquid separations. In: Freeman B, Yampolskii Y & Pinnau I (eds) Materials Science of Membranes. England, John Wiley & Sons: 307-336.

Gavalas GR (2008) Diffusion in microporous membranes: Measurements and modeling. Ind Eng Chem Res 47(16): 5797–5811.

Gaykawad SS, Zha Y, Punt PJ, van Groenestijn JW, van der Wielen LAM & Straathof AJJ (2013) Pervaporation of ethanol from lignocellulosic fermentation broth. Bioresour Technol 129: 469–476.

Geus ER, den Exter MJ & van Bekkum H (1992) Synthesis and characterization of zeolite (MFI) membranes on porous ceramic supports. J Chem Soc, Faraday Trans 88(20): 3101–3109.

Geus ER & van Bekkum H (1995) Calcination of large MFI-type single crystals, Part 2: Crack formation and thermomechanical properties in view of the preparation of zeolite membranes. Zeolites 15(4): 333–341.

Guo M, Song W, Buhain J (2015) Bioenergy and biofuels: History, status and perspective. Renew Sust Energ Rev 42: 712–725.

Guo S, Yu C, Gu X, Jin W, Zhong J & Chen C-l (2011) Simulation of adsorption, diffusion, and permeability of water and ethanol in NaA zeolite membranes. J Membr Sci 376(1–2): 40–49.

Hammond KD, Tompsett GA, Auerbach SM & Conner Jr. WC (2007) Physical adsorption analysis of intact supported MFI zeolite membranes. Langmuir 23(16): 8371–8384.

Hang Chau JL, Tellez C, Yeung KL & Ho K (2000) The role of surface chemistry in zeolite membrane formation. J Membr Sci 164(1–2): 257–275.

Hedlund J, Jareman F, Bons A-J & Anthonis M (2003) A masking technique for high quality MFI membranes. J Membr Sci 222(1–2): 163–179.

Hedlund J, Sterte J, Anthonis M, Bons A-J, Carstensen B, Corcoran N, Cox D, Deckman H, De Gijnst W, De Moor P-P, Lai F, McHenry J, Mortier W, Reinoso J & Peters J (2002) High-flux MFI membranes. Micropor Mesopor Mat 52(3): 179–189.

Hedlund J, Korelskiy D, Sandström L & Lindmark J (2009) Permporometry analysis of zeolite membranes. J Membr Sci 345(1–2): 276–287.

Huang H-J, Ramaswamy S & Liu Y (2014) Separation and purification of biobutanol during bioconversion of biomass. Sep Purif Technol 132: 513–540.

Huang H-J, Ramaswamy S, Tschirner UW & Ramarao BV (2008) A review of separation technologies in current and future biorefineries. Sep Purif Technol 62(1): 1–21.

Huang, RYM & Yeom CK (1990) Pervaporation separation of aqueous mixtures using crosslinked poly(vinyl alcohol) (pva). II. Permearion of ethanol-water mixtures. J Membr Sci 51(3): 273–292.

Huang Z, Guan H, Tan Wl, Qiao X & Kulprathipanja S (2006) Pervaporation study of aqueous ethanol solution through zeolite-incorporated multilayer poly(vinyl alcohol) membranes: Effect of zeolites. J Membr Sci 276(1–2): 260–271.

Hunger M, Kärger J, Pfeifer H, Caro J, Zibrowius B, Bülow M & Mostowicz R (1987) Investigation of internal silanol groups as structural defects in ZSM-5-type zeolites. J Chem Soc, Faraday Trans 1 F 83(11): 3459–3468.

Ikegami T, Yanagishita H, Kitamoto D, Haraya K, Nakane T, Matsuda H, Koura N & Sano T (1997) Production of highly concentrated ethanol in a coupled fermentation/pervaporation process using silicalite membranes. Biotechnol Tech 11(12): 921–924.

Ikegami T, Yanagishita H, Kitamoto D, Negishi H, Haraya K & Sano T (2002) Concentration of fermented ethanol by pervaporation using silicalite membranes coated with silicone rubber. Desalination 149(1–3): 49–54.

Jareman F & Hedlund J (2005) Single gas permeance ratios in MFI membranes: Effects of material properties and experimental conditions. Micropor Mesopor Mat 82(1–2): 201–207.

Jareman F, Hedlund J, Creaser D & Sterte J (2004) Modelling of single gas permeation in real MFI membranes. J Membr Sci 236(1–2): 81–89.

Ji M, Liu G, Chen C, Wang L & Zhang X (2012). Synthesis of highly b-oriented ZSM-5 membrane on a rough surface modified simply with TiO_2 in situ crystallization. Micropor Mesopor Mat 155: 117–123.

Julbe A (2007) Zeolite membranes - synthesis, characterization and application. In: Cejka J, van Bekkum H, Corma A & Schueth F (eds) Introduction to zeolite molecular sieves. Amsterdam, Elsevier: 181–219.

Kalipçilar H & Çulfaz A (2002) Role of the water content of clear synthesis solutions on the thickness of silicalite layers grown on porous α-alumina supports. Micropor Mesopor Mat 52(1): 39–54.

Kangas J, Sandström L, Malinen I, Hedlund J & Tanskanen J (2013) Maxwell-Stefan modeling of the separation of H_2 and CO_2 at high pressure in an MFI membrane. J Membr Sci 435: 186–206.

Kapteijn F, Bakker WJW, Zheng G, Poppe J & Moulijn JA (1995) Permeation and separation of light hydrocarbons through a silicalite-1 membrane. Application of the generalized Maxwell-Stefan equations. Chem Eng J Bioch Eng J 57(2): 145–153.

Kapteijn F, Moulijn JA & Krishna R (2000) The generalized Maxwell-Stefan model for diffusion in zeolites: Sorbate molecules with different saturation loadings. Chem Eng Sci 55(15): 2923–2930.

Kärger J & Ruthven RM (1992) Diffusion in zeolites. New York, John Wiley & Sons, Inc.

Kim J-H, Lee C-H, Kim W-S, Lee J-S, Kim J-T, Suh J-K & Lee J-M (2003) Adsorption equilibria of water vapor on alumina, zeolite 13X, and a zeolite X/activated carbon composite. J Chem Eng Data 48(1): 137–141.

Kim M-B, Ryu Y-K & Lee C-H (2005) Adsorption equilibria of water vapor on activated carbon and DAY zeolite. J Chem Eng Data 50(3): 951–955.

Kita H, Fuchida K, Horita T, Asamura H & Okamoto K (2001) Preparation of Faujasite membranes and their permeation properties. Sep Purif Technol 25(1–3): 261–268.

Koczka K, Mizsey P & Fonyo Z (2007) Rigorous modelling and optimization of hybrid separation processes based on pervaporation. Central European Journal of Chemistry 5(4): 1124–1147.

Korelskiy D, Grahn M, Mouzon J & Hedlund J (2012) Characterization of flow-through micropores in MFI membranes by permporometry. J Membr Sci 417–418: 183–192.

Kosinov N, Sripathi VGP & Hensen EJM (2014) Improving separation performance of high-silica zeolite membranes by surface modification with triethoxyfluorosilane. Micropor Mesopor Mat 194: 24–30.

Krishna R (2001) Diffusion of binary mixtures across zeolite membranes: Entropy effects on permeation selectivity. Int Commun Heat Mass Transfer 28(3): 337–346.

Krishna R (2015) Evaluation of procedures for estimation of the isosteric heat of adsorption in microporous materials. Chem Eng Sci 123: 191–196.

Krishna R (1990) Multicomponent surface diffusion of adsorbed species: a description based on the generalized Maxwell–Stefan equations. Chem Eng Sci 45(7): 1779–1791.

Krishna R & Paschek D (2000) Separation of hydrocarbon mixtures using zeolite membranes: A modelling approach combining molecular simulations with the Maxwell-Stefan theory. Sep Purif Technol 21(1–2): 111–136.

Krishna R & van Baten JM (2005) Diffusion of alkane mixtures in zeolites: Validating the Maxwell-Stefan formulation using MD simulations. J Phys Chem B 109(13): 6386–6396.

Krishna R & van Baten JM (2010) Hydrogen bonding effects in adsorption of water-alcohol mixtures in zeolites and the consequences for the characteristics of the Maxwell-Stefan diffusivities. Langmuir 26(13): 10854–10867.

Kuhn J, Castillo-Sanchez JM, Gascon J, Calero S, Dubbeldam D, Vlugt TJH, Kapteijn F & Gross J (2009a) Adsorption and diffusion of water, methanol, and ethanol in all-silica DD3R: Experiments and simulation. J Phys Chem C 113(32): 14290–14301.

Kuhn J, Sutanto S, Gascon J, Gross J & Kapteijn F (2009b) Performance and stability of multi-channel MFI zeolite membranes detemplated by calcination and ozonication in ethanol/water pervaporation. J Membr Sci 339(1–2): 261–274.

Kujawski W (2000) Application of Pervaporation and Vapor Permeation in Environmental Protection. Pol J Environ Stud 9(1): 13–26.

Lee C-C, Gorte RJ & Farneth WE (1997) Calorimetric study of alcohol and nitrile adsorption complexes in H-ZSM-5. J Phys Chem B 101(19): 3811–3817.
Lee H-J, Cho EJ, Kim Y-G, Choi IS & Bae H-J (2012) Pervaporative separation of bioethanol using a polydimethylsiloxane/polyetherimide composite hollow-fiber membrane. Bioresour Technol 109: 110–115.
Li L, Xiao Z, Tan S, Pu L & Zhang Z (2004) Composite PDMS membrane with high flux for the separation of organics from water by pervaporation. J Membr Sci 243(1–2): 177–187.
Li S, Martinek JG, Falconer JL, Noble RD & Gardner TQ (2005) High-pressure CO_2 /CH_4 separation using SAPO-34 membranes. Ind Eng Chem Res 44(9): 3220–3228.
Li S, Tuan VA, Falconer JL & Noble RD (2003) Properties and separation performance of Ge-ZSM-5 membranes. Micropor Mesopor Mat 58(2): 137–154.
Li S, Tuan VA, Noble RD & Falconer JL (2001) A Ge-substituted ZSM-5 zeolite membrane for the separation of acetic acid from water. Ind Eng Chem Res 40(26): 6165–6171.
Li Y, Zhou H, Zhu G, Liu J & Yang W (2007) Hydrothermal stability of LTA zeolite membranes in pervaporation. J Membr Sci 297(1–2): 10–15.
Lin X, Chen X, Kita H & Okamoto K (2003) Synthesis of silicalite tubular membranes by in situ crystallization. AIChE J 49(1): 237–247.
Lin X, Kita H & Okamoto K-I (2001) Silicalite membrane preparation, characterization, and separation performance. Ind Eng Chem Res 40(19): 4069–4078.
Lin Y & Duke MC (2013) Recent progress in polycrystalline zeolite membrane research. Curr Opin Chem Eng 2(2): 209–216.
Lin YS & Ma YH (1988) Liquid diffusion and adsorption of aqueous ethanol, propanols, and butanols in silicalite by HPLC. ACS Sym Ser (368): 452–466.
Lindmark J & Hedlund J (2010) Carbon dioxide removal from synthesis gas using MFI membranes. J Membr Sci 360(1–2): 284–291.
Lipnizki F & Trägårdh G (2001) Modelling of pervaporation: Models to analyze and predict the mass transport in pervaporation. Sep Purif Methods 30(1): 49–125.
Lito PF, Santiago AS, Cardoso SP, Figueiredo BR & Silva CM (2011) New expressions for single and binary permeation through zeolite membranes for different isotherm models. J Membr Sci 367(1–2): 21–32.
Liu G, Hou D, Wei W, Xiangli F & Jin W (2011a) Pervaporation separation of butanol-water mixtures using polydimethylsiloxane/ceramic composite membrane. Chin J Chem Eng 19(1): 40–44.
Liu W, Zhang J, Canfield N & Saraf L (2011b) Preparation of robust, thin zeolite membrane sheet for molecular separation. Ind Eng Chem Res 50(20): 11677–11689.
Liu G, Wei W & Jin W (2014) Pervaporation membranes for biobutanol production. ACS Sustainable Chem Eng 2(4): 546–560.
Liu Q, Noble RD, Falconer JL & Funke HH (1996) Organics/water separation by pervaporation with a zeolite membrane. J Membr Sci 117(1–2): 163–174.
Loughlin KF (2009) Water isotherm models for 4A (NaA) zeolite. Adsorption 15(4): 337–353.

Macdougall H, Ruthven DM & Brandani S (1999) Sorption and diffusion of SF_6 in silicalite crystals. Adsorption 5(4): 369–372.
Malek A & Farooq S (1996) Comparison of Isotherm Models for Hydrocarbon Adsorption on Activated Carbon. AIChE J 42(11): 3191–3201.
Mariano AP & Filho RM. Improvements in biobutanol fermentation and their impacts on distillation energy consumption and wastewater generation. Bioener Res 5(2): 504–514.
Matsuda H, Yanagishita H, Negishi H, Kitamoto D, Ikegami T, Haraya K, Nakane T, Idemoto Y, Koura N & Sano T (2002) Improvement of ethanol selectivity of silicalite membrane in pervaporation by silicone rubber coating. J Membr Sci 210(2): 433–437.
McLeary EE, Jansen JC & Kapteijn F (2006) Zeolite based films, membranes and membrane reactors: Progress and prospects. Micropor Mesopor Mat 90(1–3): 198–220.
Morigami Y, Kondo M, Abe J, Kita H & Okamoto K (2001) The first large-scale pervaporation plant using tubular-type module with zeolite NaA membrane. Sep Purif Technol 25(1–3): 251–260.
Murdmaa KO & Serpinskii VV (1972) Thermodynamics of adsorption of water vapor on zeolites. Bulletin of the Academy of Sciences of the USSR Division of Chemical Science 21(2): 417–420.
Myers AL & Prausnitz JM (1965) Thermodynamics of mixed-gas adsorption. AIChE J 11(1): 121–127.
Nagumo R, Takaba H, Suzuki S & Nakao S-I (2001) Estimation of inorganic gas permeability through an MFI-type silicalite membrane by a molecular simulation technique combined with permeation theory. Micropor Mesopor Mat 48(1–3): 247–254.
Nayak VS & Moffat JB (1988) Sorption and diffusion of alcohols in heteropoly oxometalates and ZSM-5 zeolite. J Phys Chem 92(25): 7097–7102.
Negishi H, Mizuno R, Yanagishita H, Kitamoto D, Ikegami T, Matsuda H, Haraya K & Sano T (2002) Preparation of the silicalite membranes using a seeding technique under various hydrothermal conditions. Desalination 144(1–3): 47–52.
Negishi H, Sakaki K & Ikegami T (2010) Silicalite pervaporation membrane exhibiting a separation factor of over 400 for butanol. Chem Lett 39(12): 1312–1314.
Nguyen C & Do DD (2001) The Dubinin-Radushkevich equation and the underlying microscopic adsorption description. Carbon 39(9): 1327–1336.
Noack M, Kölsch P, Dittmar A, Stöhr M, Georgi G, Eckelt R & Caro J (2006) Effect of crystal intergrowth supporting substances (ISS) on the permeation properties of MFI membranes with enhanced Al-content. Micropor Mesopor Mat 97(1–3): 88–96.
Nomura M, Yamaguchi T & Nakao S-i (1998) Ethanol/water transport through silicalite membranes. J Membr Sci 144(1–2): 161–171.
Ohlin L, Bazin P, Thibault-Starzyk F, Hedlund J & Grahn M (2013) Adsorption of CO_2, CH_4, and H_2O in zeolite ZSM-5 studied using in situ ATR-FTIR spectroscopy. J Phys Chem Chem C 117(33): 16972–16982.
Okamoto K-I, Kita H, Horii K, Tanaka K & Kondo M (2001) Zeolite NaA membrane: Preparation, single-gas permeation, and pervaporation and vapor permeation of water/organic liquid mixtures. Ind Eng Chem Res 40(1): 163–175.

Oudshoorn A, van der Wielen LAM & Straathof AJJ (2009) Assessment of options for selective 1-butanol recovery from aqueous solution. Ind Eng Chem Res 48(15): 7325–7336.

Özgür Yazaydin A & Thompson RW (2009) Molecular simulation of water adsorption in silicalite: Effect of silanol groups and different cations. Micropor Mesopor Mat 123(1–3): 169–176.

Päkkilä JM, Kujawski W & Keiski RL (2012) Pervaporation performance of composite PDMS membrane for butanol production. Procedia Engineering 44: 1486–1487.

Paschek D & Krishna R (2000) Monte Carlo simulations of self- and transport-diffusivities of 2- methylhexane in silicalite. Phys Chem Chem Phys 2(10): 2389–2394.

Paschek D & Krishna R (2001) Diffusion of binary mixtures in zeolites: Kinetic Monte Carlo versus molecular dynamics simulations. Langmuir 17(1): 247–254.

Peng P, Shi B & Lan Y (2011) Preparation of PDMS-silica nanocomposite membranes with silane coupling for recovering ethanol by pervaporation. Sep Sci Technol 46(3): 420–427.

Peng Y, Lu H, Wang Z & Yan Y (2014) Microstructural optimization of MFI-type zeolite membranes for ethanol-water separation. J Mater Chem A 2(38): 16093–16100.

Peng Y, Zhan Z, Shan L, Li X, Wang Z & Yan Y (2013) Preparation of zeolite MFI membranes on defective macroporous alumina supports by a novel wetting-rubbing seeding method: Role of wetting agent. J Membr Sci 444: 60–69.

Pera-Titus M, Alshebani A, Nicolas C-H, Roumégoux J-P, Miachon S & Dalmon J-A (2009) Nanocomposite MFI-alumina membranes: High-flux hollow fibers for CO_2 capture from internal combustion vehicles. Ind Eng Chem Res 48(20): 9215–9223.

Pera-Titus M, Fité C, Sebastián V, Lorente E, Llorens J & Cunill F (2008) Modeling pervaporation of ethanol/water mixtures within 'real' zeolite NaA membranes. Ind Eng Chem Res 47(9): 3213–3224.

Pera-Titus M, Llorens J, Tejero J & Cunill F (2006) Description of the pervaporation dehydration performance of A-type zeolite membranes: A modeling approach based on the Maxwell-Stefan theory. Catal Today 118(1–2): 73–84.

Poling BE, Prausnitz JM & O'Connell JP (2001) Properties of Gases and Liquids (5th Edition). New York, McGraw-Hill.

Purchas DB & Sutherland K (2002) Handbook of filter media (2nd Edition). UK, Elsevier.

Qureshi N, Meagher MM, Huang J & Hutkins RW (2001) Acetone butanol ethanol (ABE) recovery by pervaporation using silicalite-silicone composite membrane from fed-batch reactor of Clostridium acetobutylicum. J Membr Sci 187(1–2): 93–102.

REN 21 (2014) Renewables Global Status Report. Paris, Renewable Energy Policy Network for the 21st Century, Secretariat.

Rozicka A, Niemistö J, Keiski RL & Kujawski W (2014) Apparent and intrinsic properties of commercial PDMS based membranes in pervaporative removal of acetone, butanol and ethanol from binary aqueous mixtures. J Membr Sci 453: 108–118.

Ruthven DM (1984) Principles of adsorption and adsorption processes. New York, John Wiley & Sons, Inc.

Ryu Y-K, Chang J-W, Jung S-Y & Lee C-H (2002) Adsorption isotherms of toluene and gasoline vapors on DAY zeolite. J Chem Eng Data 47(2): 363–366.

Ryu YK, Lee SJ, Kim JW & Lee C-H (2001) Adsorption Equilibrium and Kinetics of H2O on Zeolite 13X. Korean J Chem Eng 18(4): 525–530.

Saengsawang O, Remsungnen T, Fritzsche S, Haberlandt R & Hannongbua S (2005) Structure and energetics of water-silanol binding on the surface of silicalite-1: Quantum chemical calculations. J Phys Chem B 109(12): 5684–5690.

Sakuth M, Meyer J & Gmehling J (1995) Vapor phase adsorption equilibria of toluene + 1-propanol mixtures on Y-zeolites with different silicon to aluminum ratios. Journal of Chemical & Engineering Data 40(4): 895–899.

Sandström L, Lindmark J & Hedlund J (2010) Separation of methanol and ethanol from synthesis gas using MFI membranes. J Membr Sci 360(1–2): 265–275.

Sano T, Ejiri S, Yamada K, Kawakami Y & Yanagishita H (1997) Separation of acetic acid-water mixtures by pervaporation through silicalite membrane. J Membr Sci 123(2): 225–233.

Sano T, Hasegawa M, Ejiri S, Kawakami Y & Yanagishita H (1995a) Improvement of the pervaporation performance of silicalite membranes by modification with a silane coupling reagent. Microporous Mater 5(3): 179–184.

Sano T, Hasegawa M, Kawakami Y & Yanagishita H (1995b) Separation of methanol rmmethyl-tert-butyl ether mixture by pervaporation using silicalite membrane. J Membr Sci 107(1–2): 193–196.

Sano T, Hasegawa M, Kawakami Y, Kiyozumi Y, Yanagishita H, Kitamoto D & Mizukami F (1994) Potentials of silicalite membranes for the separation of alcohol/water mixtures. Stud Surf Sci Catal 84: 1175–1182.

Sato K, Sugimoto K & Nakane T (2008a) Mass-production of tubular NaY zeolite membranes for industrial purpose and their application to ethanol dehydration by vapor permeation. J Membr Sci 319(1–2): 244–255.

Sato K, Sugimoto K & Nakane T (2008b) Preparation of higher flux NaA zeolite membrane on asymmetric porous support and permeation behavior at higher temperatures up to 145 °C in vapor permeation. J Membr Sci 307(2): 181–195.

Sato K, Sugimoto K, Sekine Y, Takada M, Matsukata M & Nakane T (2007) Application of FAU-type zeolite membranes to vapor/gas separation under high pressure and high temperature up to 5 MPa and 180°C. Micropor Mesopor Mat 101(1–2): 312–318.

Schiel-Bengelsdorf B, Montoya J, Linder S & Dürre P (2013) Butanol fermentation. EnvironTechnol 34(13–14): 1691–1710.

Sebastian V, Mallada R, Coronas J, Julbe A, Terpstra RA & Dirrix RWJ (2010) Microwave-assisted hydrothermal rapid synthesis of capillary MFI-type zeolite-ceramic membranes for pervaporation application. J Membr Sci 355(1–2): 28–35.

Shan L, Shao J, Wang Z & Yan Y (2011) Preparation of zeolite MFI membranes on alumina hollow fibers with high flux for pervaporation. J Membr Sci 378(1–2): 319–329.

Shen D, Xiao W, Yang J, Chu N, Lu J, Yin D & Wang J (2011) Synthesis of silicalite-1 membrane with two silicon source by secondary growth method and its pervaporation performance. Sep Purif Technol 76(3): 308–315.

Shirazi Y, Ghadimi A & Mohammadi T (2012) Recovery of alcohols from water using polydimethylsiloxane-silica nanocomposite membranes: Characterization and pervaporation performance. J Appl Polym Sci 124(4): 2871–2882.

Shu X, Wang X, Kong Q, Gu X & Xu N (2012) High-flux MFI zeolite membrane supported on YSZ hollow fiber for separation of ethanol/water. Ind Eng Chem Res 51(37): 12073–12080.

Sing KSW, Everett SH, Haul RA, Moscou L, Pierotti RA, Rouquérol J & Sieminiewska T (1985) Reporting physisorption data for gas/solid systems with special reference to the determination of surface area and porosity (Recommendations 1984). Pure Appl Chem 57: 603–619.

Skoulidas AI & Sholl DS (2002) Transport diffusivities of CH_4, CF_4, He, Ne, Ar, Xe, and SF_6 in silicalite from atomistic simulations. J Phys Chem B 106(19): 5058–5067.

Smit B & Krishna R (2001) Monte Carlo simulations in zeolites. Curr Opin Solid St M 5(5): 455–461.

Sochard S, Fernandes N & Reneaume J (2010) Modeling of adsorption isotherm of a binary mixture with real adsorbed solution theory and nonrandom two-liquid model. AIChE J 56(12): 3109–3119.

Sommer S & Melin T (2005) Influence of operation parameters on the separation of mixtures by pervaporation and vapor permeation with inorganic membranes. Part 1: Dehydration of solvents. Chem Eng Sci 60(16): 4509–4523.

Srinivasan K, Palanivelu K & Navaneetha Gopalakrishnan A (2007) Recovery of 1-butanol from a model pharmaceutical aqueous waste by pervaporation. Chem Eng Sci 62(11): 2905–2914.

Stoeger JA, Choi J & Tsapatsis M (2011) Rapid thermal processing and separation performance of columnar MFI membranes on porous stainless steel tubes. Energ Environ Sci 4(9): 3479–3486.

Talu O (2011) Measurement and analysis of mixture adsorption equilibrium in porous solids. Chemie-Ingenieur-Technik 83(1–2): 67–82.

Tavolaro A & Drioli E (1999) Zeolite membranes. Adv Mater 11(12): 975–996.

Thomas S, Schäfer R, Caro J & Seidel-Morgenstern A (2001) Investigation of mass transfer through inorganic membranes with several layers. Catal Today 67(1–3): 205–216.

Tuan VA, Li S, Falconer JL & Noble RD (2002) Separating organics from water by pervaporation with isomorphously-substituted MFI zeolite membranes. J Membr Sci 196(1): 111–123.

Valentínyi N & Mizsey P (2014) Comparison of pervaporation models with simulation of hybrid separation processes. Period Polytech Chem 58(1): 7–14.

van de Graaf JM, Kapteijn F & Moulijn JA (1999) Modeling permeation of binary mixtures through zeolite membranes. AIChE J 45(3): 497–511.

Van der Bruggen B & Luis P (2014) Pervaporation as a tool in chemical engineering: A new era? Curr Opin Chem Eng 4: 47–53.

Vane LM (2005) A review of pervaporation for product recovery from biomass fermentation processes. J Chem Technol Biot 80(6): 603–629.

Vane LM, Namboodiri VV & Bowen TC (2008) Hydrophobic zeolite-silicone rubber mixed matrix membranes for ethanol-water separation: Effect of zeolite and silicone component selection on pervaporation performance. J Membr Sci 308(1–2): 230–241.

Vignes A (1966) Diffusion in binary solutions: Variation of diffusion coefficient with composition. Ind Eng Chem Fund 5(2): 189–199.

Vroon ZAEP, Keizer K, Burggraaf AJ & Verweij H (1998) Preparation and characterization of thin zeolite MFI membranes on porous supports. J Membr Sci 144(1–2): 65–76.

Wang C, Liu X, Cui R & Zhang B (2009a) In situ evaluation of defect size distribution for supported zeolite membranes. J Membr Sci 330(1–2): 259–266.

Wang Z, Ge Q, Saho J & Yan Y (2009b) High performance zeolite LTA pervaporation membranes on ceramic hollow fibers by dipcoating-wiping seed deposition. J Am Chem Soc 131(20): 6910–6911.

Wang Y & LeVan MD (2009) Adsorption equilibrium of carbon dioxide and water vapor on zeolites 5A and 13X and silica gel: Pure components. J Chem Eng Data 54(10): 2839–2844.

Wee S-L, Tye C-T & Bhatia S (2008) Membrane separation process-Pervaporation through zeolite membrane. Sep Purif Technol 63(3): 500–516.

Weyd M, Richter H, Puhlfürß P, Voigt I, Hamel C & Seidel-Morgenstern A (2008) Transport of binary water-ethanol mixtures through a multilayer hydrophobic zeolite membrane. J Membr Sci 307(2): 239–248.

White JC, Dutta PK, Shqau K & Verweij H (2010) Synthesis of ultrathin zeolite y membranes and their application for separation of carbon dioxide and nitrogen gases. Langmuir 26(12): 10287–10293.

Whittaker PB, Wang X, Regenauer-Lieb K & Chua HT (2013) Predicting isosteric heats for gas adsorption. Physical Chemistry Chemical Physics 15(2): 473–482.

Wijmans JG & Baker RW (1993) A simple predictive treatment of the permeation process in pervaporation. J Membr Sci 79(1): 101–113.

Wood GO (2001) Affinity coefficients of the Polanyi/Dubinin adsorption isotherm equations. A review with compilations and correlations. Carbon 39(3): 343–356.

Xiao J & Wei J (1992) Diffusion mechanism of hydrocarbons in zeolites-I. Theory. Chem Eng Sci 47(5): 1123–1141.

Yang JZ, Liu QL & Wang HT (2007) Analyzing adsorption and diffusion behaviors of ethanol/water through silicalite membranes by molecular simulation. J Membr Sci 291(1–2): 1–9.

Yu M, Noble RD & Falconer JL (2011) Zeolite membranes: Microstructure characterization and permeation mechanism. Accounts Chem Res 44(11): 1196–1206.

Yun J-H, Choi D-K & Kim S-H (1998) Adsorption of organic solvent vapors on hydrophobic Y-type zeolite. AIChE J 44(6): 1344–1350.

Zah J, Krieg HM & Breytenbach JC (2006) Pervaporation and related properties of time-dependent growth layers of zeolite NaA on structured ceramic supports. J Membr Sci 284(1–2): 276–290.

Zhang F, Xu L, Hu N, Bu N, Zhou R & Chen X (2014) Preparation of NaY zeolite membranes in fluoride media and their application in dehydration of bio-alcohols. Sep Purif Technol 129: 9–17.

Zhang K, Lively RP, Dose ME, Li L, Koros WJ, Ruthven DM, McCool BA & Chance RR (2013) Diffusion of water and ethanol in silicalite crystals synthesized in fluoride media. Micropor Mesopor Mat 170: 259–265.

Zhang K, Lively RP, Noel JD, Dose ME, McCool BA, Chance RR & Koros WJ (2012a) Adsorption of water and ethanol in MFI-type zeolites. Langmuir 28(23): 8664–8673.

Zhang X-L, Zhu M-H, Zhou R-F, Chen X-S & Kita H (2012b) Synthesis of a silicalite zeolite membrane in ultradilute solution and its highly selective separation of organic/water mixtures. Ind Eng Chem Res 51(35): 11499–11508.

Zhou H, Korelskiy D, Sjöberg E & Hedlund J (2014a) Ultrathin hydrophobic MFI membranes. Micropor Mesopor Mat 192: 76–81.

Zhou H, Su Y & Wan Y (2014b) Phase separation of an acetone-butanol-ethanol (ABE)-water mixture in the permeate during pervaporation of a dilute ABE solution. Sep Purif Technol 132: 354–361.

Zhu G, Li Y, Chen H, Liu J & Yang W (2008) An in situ approach to synthesize pure phase FAU-type zeolite membranes: Effect of aging and formation mechanism. J Mater Sci 43(9): 3279–3288.

Zhu G, Li Y, Zhou H, Liu J & Yang W (2009) Microwave synthesis of high performance FAU-type zeolite membranes: Optimization, characterization and pervaporation dehydration of alcohols. J Membr Sci 337(1–2): 47–54.

Zhu W, Hrabanek P, Gora L, Kapteijn F & Moulijn JA (2006) Role of adsorption in the permeation of CH_4 and CO_2 through a silicalite-1 membrane. Ind Eng Chem Res 45(2): 767–776.

Original papers

I Korelskiy D, Leppäjärvi T, Zhou H, Grahn M, Tanskanen J & Hedlund J (2013) High flux MFI membranes for pervaporation. Journal of Membrane Science 427: 381–389.

II Leppäjärvi T, Malinen I, Korelskiy D, Kangas J, Hedlund J & Tanskanen J (2015) Pervaporation of ethanol/water mixtures through a high-silica MFI membrane: Comparison of different semi-empirical mass transfer models. Periodica Polytechnica: Chemical Engineering 59(2): 111–123.

III Leppäjärvi T, Malinen I, Kangas J & Tanskanen J (2012) Utilization of P_i^{sat} temperature-dependency in modelling adsorption on zeolites. Chemical Engineering Science 69: 503–513.

IV Leppäjärvi T, Kangas J, Malinen I & Tanskanen J (2013) Mixture adsorption on zeolites applying the P_i^{sat} temperature-dependency approach. Chemical Engineering Science 89: 89–101.

V Leppäjärvi T, Malinen I, Korelskiy D, Hedlund J & Tanskanen J (2014) Maxwell-Stefan modeling of ethanol and water unary pervaporation through a high-silica MFI zeolite membrane. Industrial & Engineering Chemistry Research 53: 323–332.

VI Zhou H, Korelskiy D, Leppäjärvi T, Grahn M, Tanskanen J & Hedlund J (2012) Ultrathin zeolite X membranes for pervaporation dehydration of ethanol. Journal of Membrane Science 399–400: 106–111.

515. Kulju, Timo (2014) Utilization of phenomena-based modeling in unit operation design

516. Karinkanta, Pasi (2014) Dry fine grinding of Norway spruce (*Picea abies*) wood in impact-based fine grinding mills

517. Tervo, Valtteri (2015) Joint multiuser power allocation and iterative multi-antenna receiver design

518. Jayasinghe, Laddu Keeth Saliya (2015) Analysis on MIMO relaying scenarios in wireless communication systems

519. Partala, Juha (2015) Algebraic methods for cryptographic key exhange

520. Karvonen, Heikki (2015) Energy efficiency improvements for wireless sensor networks by using cross-layer analysis

521. Putaala, Jussi (2015) Reliability and prognostic monitoring methods of electronics interconnections in advanced SMD applications

522. Pirilä, Minna (2015) Adsorption and photocatalysis in water treatment : active, abundant and inexpensive materials and methods

523. Alves, Hirley (2015) On the performance analysis of full-duplex networks

524. Siirtola, Pekka (2015) Recognizing human activities based on wearable inertial measurements : methods and applications

525. Lu, Pen-Shun (2015) Decoding and lossy forwarding based multiple access relaying

526. Suopajärvi, Terhi (2015) Functionalized nanocelluloses in wastewater treatment applications

527. Pekuri, Aki (2015) The role of business models in construction business management

528. Mantere, Matti (2015) Network security monitoring and anomaly detection in industrial control system networks

529. Piri, Esa (2015) Improving heterogeneous wireless networking with cross-layer information services

530. Leppänen, Kimmo (2015) Sample preparation method and synchronized thermography to characterize uniformity of conductive thin films

Book orders:
Granum: Virtual book store
http://granum.uta.fi/granum/

UNIVERSITY OF OULU P.O. Box 8000 FI-90014 UNIVERSITY OF OULU FINLAND

ACTA UNIVERSITATIS OULUENSIS

UNIVERSITY of OULU
OULUN YLIOPISTO

ISBN 978-952-62-0841-1 (Paperback)
ISBN 978-952-62-0842-8 (PDF)
ISSN 0355-3213 (Print)
ISSN 1796-2226 (Online)